NASA
Reference
Publication
1154

October 1985

Design of Traction Drives

Stuart H. Loewenthal
and Erwin V. Zaretsky

NASA

NASA
Reference
Publication
1154

1985

Design of Traction Drives

Stuart H. Loewenthal
and Erwin V. Zaretsky

Lewis Research Center
Cleveland, Ohio

National Aeronautics
and Space Administration

**Scientific and Technical
Information Branch**

Contents

page

Summary 1
Symbols 1
1.0 Introduction 2
2.0 Traction Drive Types and Applications 3
  2.1 Automotive Applications 4
  2.2 Industrial Applications 6
  2.3 Fixed-Ratio Traction Drives 7
3.0 Elastohydrodynamic Film Thickness 8
4.0 Traction Drive Capacity and Durability 10
  4.1 Contact Stress 11
  4.2 Fatigue Life Model 12
  4.3 Effects of Size, Traction Coefficient, and Contact Shape 16
  4.4 Effects of Multiple Contacts 18
  4.5 Other Durability Considerations 19
5.0 Traction Phenomena 22
  5.1 Traction Curve 22
  5.2 Creep 23
  5.3 Traction Coefficient 23
6.0 Performance Predictions 24
  6.1 Traction Experiments 24
  6.2 Theory 25
  6.3 Traction Contact Kinematics 25
  6.4 Dimensionless Traction Parameters 26
  6.5 Effects of Slip, Side Slip, and Spin on Traction 28
  6.6 Traction Contact Power Loss 28
  6.7 Other Contact and Drive Losses 32
7.0 Fluid Traction Properties 33
  7.1 Traction Fluids 33
  7.2 Traction Fluid Data 34
  7.3 Effect of Operating Conditions 35
8.0 Performance Calculation Example 35
  8.1 Contact Stress, Shape, and Size 36
  8.2 Traction/Slip Characteristics 37
  8.3 Power Loss 37
9.0 Loading Mechanism Design 38
  9.1 Constant Loading 39
  9.2 Variable Loading 39
10.0 Friction Wheels and Rings 40
  10.1 Rubber Friction Wheels Against Steel or Cast Iron 41
  10.2 Rubber Friction Rings Against Steel or Cast Iron 42
  10.3 Arrangements 42
References 43

Summary

The analytical methods required for the design, selection, and evaluation of traction drives are summarized. The introductory sections provide background information as to the types and applications of traction drives from their use in early woodworking machinery and vintage automobiles to future applications such as high-powered helicopter transmissions. Lubrication principles, sizing criteria, material selection, and means of estimating service life are treated in sections 3.0 and 4.0. The next three sections are devoted to the fundamental principles of power transfer through traction. Here the importance of the traction-versus-slip curve, the effects of the lubricant's traction coefficient, and the concept of creep are introduced. Also, both theoretical and experimental efforts leading to a comprehensive model for predicting traction contact performance are reviewed. In section 8.0 the model is used to predict power loss. Section 9.0 discusses the considerations associated with the design of a mechanism to automatically regulate the normal load between rollers. The final section deals with the design of nonlubricated friction contacts such as a rubber wheel against a metal drum or ring. Dry friction drives are excellent, inexpensive solutions for low-speed and low-power-transmission applications.

Symbols

A	coefficient in equation (53)
a	contact ellipse radius transverse to rolling direction, m
a^*	dimensionless contact ellipse factor
b	contact ellipse radius in rolling direction, m
b^*	dimensionless contact ellipse factor
C	traction contact parameter
c	orthogonal shear stress exponent
D	diameter of mating friction wheel or ring, m
d_i	inside diameter of friction ring, m
d_m	equivalent diameter of friction wheel or ring, m
d_o	outside diameter of friction wheel, m
E	modulus of elasticity parameter, Pa
E'	material elasticity parameter, Pa
e	Weibull exponent
F	relative curvature difference
F_a	axial thrust force, N
F_h	hysteresis drag force, N
F_r	rolling traction drag force, N
F_t	tangential force, N
F_x,F_y	traction force, N
f	coefficient of friction
G	dimensionless EHD materials parameter
$\bar{G}$	apparent elastic shear modulus of contact, Pa
G'	weight of friction drive assembly, N
g	auxiliary elliptical contact parameter, m
H_c	dimensionless central EHD film thickness, m
H_i	life of ith body, hr
H_{min}	dimensionless minimum EHD film thickness, m
H_s	drive system life, hr
h	depth to critical stress exponent
h_c	central EHD film thickness, m
h_{min}	minimum EHD film thickness, m
J_1	dimensionless slip parameter
J_2	dimensionless side-slip parameter
J_3	dimensionless spin parameter
J_4	dimensionless traction parameter in x direction
J_5	dimensionless side traction parameter in y direction
J_6	dimensionless torque parameter
J_7	dimensionless total power loss parameter
J^*	dimensionless traction coefficient parameter
K	empirical stress parameter for friction material, N/mm^2
K_s	loading mechanism spring rate, N/m
$K_1,\ldots,K_6$	constants for life equations
k	contact ellipse ratio, a/b
L	life, millions of stress cycles
LF	loss factor
l	length of line contact, m

m	initial slope of traction curve
m_f	friction ring size correction factor, N/mm
N	normal force, N
n_i	speed of rotation, rpm
P_f	frictional power intensity, W/mm^2
P_h	hysteresis loss
P_r	rolling traction power loss, W
Q	rolling body normal load, N
Q_0	preload for friction drive
R_A,R_B	rolling radius, m
R_c	cone rolling radius, m
R_p	pitch radius of ball-cam contact, m
R_x	equivalent radius in rolling direction, m
R_y	equivalent radius transverse to rolling direction, m
r	radius of body, m
S	slip parameter
S_r	factor to ensure against slip
S_0	spring load, N
T	traction force, N
T_0	torque, N-m
$\tilde{T}$	lubricant inlet temperature, °C
$\Delta\tilde{T}$	flash temperature, °C
U	average surface velocity in x direction, m/sec
U_D	dimensionless EHD speed parameter
ΔU	velocity difference (slip) in x direction, m/sec
u_A,u_B	surface velocity of body in x direction, m/sec
V	average surface velocity in y direction, m/sec
V_s	stressed volume, m^3
ΔV	velocity difference (side slip) in y direction, m/sec
v	number of stress cycles per revolution
W	dimensionless EHD load parameter
x	rolling direction coordinate
y	transverse direction coordinate
z_o	depth to critical shear stress, m
α	spin angle, deg
α_p	pressure-viscosity coefficient, Pa^{-1}
α'	friction drive loading mechanism angle, deg
β	misalignment angle, deg
β_t	Blok's thermal coefficient, N/°C m sec$^{1/2}$
β'	cam mechanism ramp angle, deg
γ	included angle between rotation axes, deg
Δ	preload-spring deflection, m
δ	normal load angle relative to contact surface, deg
ϵ	friction ring power per unit width, W/m
η_0	absolute viscosity of fluid at ambient pressure, N sec/m^2
θ	included angle between rotation of axis body A and tangent to point of contact, deg
λ	ratio of film thickness to composite roughness
μ	maximum available traction coefficient
μ_x	applied traction coefficient in x direction
μ_y	applied traction coefficient in y direction
ξ	Poisson's ratio
ρ	inverse curvature sum, m^{-1}
σ	composite surface roughness, m
σ_A,σ_B	surface roughness of body, m
σ_0	maximum surface contact pressure, Pa
$\bar{\sigma}$	mean surface contact pressure, Pa
τ_o	maximum reversing orthogonal shear stress, Pa
φ	hysteresis loss factor of material
ω	angular rotation velocity, rad/sec
ω_s	angular velocity difference (spin) between contacting bodies normal to contact area, rad/sec

Subscripts:

A,B	elastic bodies
allow	allowable
c	cone
i	system element
in	inlet
max	maximum
pl	planet roller
out	outlet
s	system
sun	sun roller
x,y	reference planes

1.0 Introduction

Traction or friction drives are perhaps the simplest of all rotary mechanisms, yet relatively little is known of their early history and even less has been written about them (ref. 1). In its simplest form a traction drive is just two smooth, unequal-size wheels in driving contact. Their simplicity suggests that traction drives predate the

gear drive. As speed regulators oil-lubricated traction drives have been in industrial service for more than 50 years, yet the concept of transmitting power via traction remains unfamiliar and even alien to many. Indeed, traction power transfer is commonplace in our daily existence. Our car tires engaged against the road surface or a locomotive's driving wheels against the rail are but two common examples. Traction drives are also found in equipment where simple and economical solutions to speed regulation are required, such as phonograph drives, self-propelled lawnmowers, or even the amusement park ride driven by a rubber tire. Of course, in these examples simple dry contact is involved. This same principle, however, can be harnessed in the construction of an oil-lubricated, all-steel-component transmission transmitting hundreds of kilowatts.

Traction drives can be constructed to give either a single, fixed speed ratio like a gearbox or, unlike a gearbox, a speed ratio that can be continuously varied. This latter arrangement is of extreme interest to drive train designers since it provides them with an essentially "infinite" number of shift points with which to optimize the performance of the drive system.

Because power transfer occurs between smooth rolling bodies, generally across a thin, tenacious lubricant film, traction drives have certain performance characteristics not found in other power transmissions. Traction drives can be designed to smoothly and continuously vary the speed ratio with efficiencies approaching those of the best gear drives. Unlike transmissions with gear teeth, which, even when perfectly machined, generate torsional oscillations as the load transfers between teeth, power transfer through traction is inherently smooth and quiet without any "backlash." A lubricant film trapped between the rollers tends to protect against wear and to dampen torsional vibrations. The operating speed of some traction drives is limited only by the burst strength of the roller material and the available traction in the contact. In many cases traction drives can be designed to be as small as or smaller than their non-traction-drive counterparts. When the drives are manufactured in sufficient quantity, costs can also be quite competitive because of the similarities in manufacturing traction drive components and ordinary mass-produced ball and roller bearings.

Although traction drives have been available for some time (refs. 2 to 8), it is only perhaps since the mid-1960's that they have been considered serious competitors to conventional mechanical power transmissions. The earlier drives, particularly those targeted for automotive applications, had their share of durability problems above nominal power levels. As a consequence relatively few succeeded in the marketplace. The underlying reason for this was that certain critical pieces of technology were generally lacking. Designs were based mostly on trial and error. No uniform failure theories were available to establish service life or reliability ratings. The drive materials and lubricants of the day were crude by today's standards. In short, traction drives were in their technical infancy.

Prompted by the research for more efficient automotive transmissions and bolstered by advances in rolling-element bearing technology, interest in traction drives has been renewed. Today's analytical tools, materials, and traction fluids are far superior to those available before the 1970's. This has led to the reemergence of traction drives and the technology related to their design.

The material contained in this report will assist in the design, selection, application, and evaluation of traction drives. The reader, after reviewing the report, will readily appreciate the level of technical sophistication required in the design of these deceptively simple mechanisms. The material presented herein should be viewed as a starting point for design rather than as an all-inclusive design method.

The fundamentals of traction power transfer are outlined for metal (typically bearing steel) traction drives that operate either with or without a lubricant. Nonlubricated drives are generally constructed with some components of softer materials such as rubber or plastic. Sizing criteria, lubrication considerations, material selection, and methods to estimate service life and power loss are presented. A brief historical review of the evolution of traction drives over the past 100 years is also presented.

2.0 Traction Drive Types and Applications

One of the earliest known examples of a friction drive is that patented by C.W. Hunt in 1877 (fig. 1, ref. 9). (The term "friction drive" is normally used to refer to a drive that is nonlubricated, and "traction drive" to one with oil-wetted components. The terminology may have evolved because nonlubricated drives intentionally use at least one roller that is covered with a high-friction material such as leather, rubber, fiber, or even wood. This notwithstanding, the term "friction" is somewhat of a misnomer since it is the traction force that is responsible for positive motion of the driven element.) The Hunt drive had a single spoked transfer wheel, probably covered with leather, running against a pair of toroidal metal disks. Judging by the pulley flanges attached to the toroidal disks, the drive was intended to regulate the speed of belt-driven machinery such as that commonly found in factories at the turn of the century.

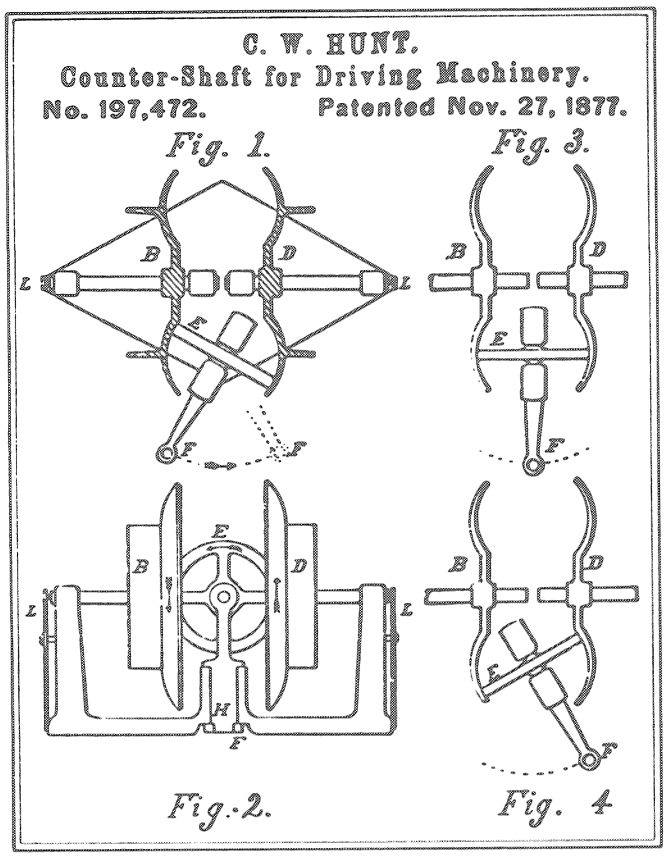

Figure 1.—Hunt's 1877 toroidal friction drive. (From ref. 9.)

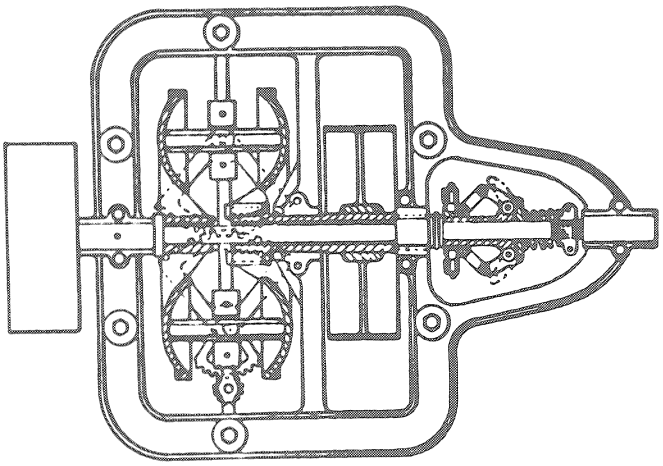

Figure 2.—Hoffman's 1899 toroidal friction drive for belt-driven machinery. (From ref. 10.)

By tilting transfer wheel E, the effective rolling radii of toroids B and D and hence their relative speeds could be altered. A similar drive was devised by W.D. Hoffman as shown in an 1899 British patent application (fig. 2, ref. 10). The toroidal drive arrangement has apparently found great favor with traction drive designers through the years. Work continues on this configuration even today, more than 100 years later (ref. 1).

Friction drives also were used on several types of woodworking machinery made before the 1870's. The 1876 edition of Knight's American Mechanical Dictionary (ref. 2) describes a deal-frame machine for slitting pine timber that employed a friction disk drive for regulating the feed motion. Another source (ref. 3) describes a wood panel-planer whose feed rolls were driven by friction wheels. Appleton's Cyclopedia of Applied Mechanics, published in 1880 (ref. 4), reports of frictional gearing being used on woodworking machinery; one wheel was made of iron and the other, typically the driver, of wood or iron covered with wood. For driving light machinery wooden wheels of basswood, cottonwood, or even white pine reportedly gave good results. For heavy work, where from 30 to 45 kW was transmitted by simple contact, soft maple was preferred. Appleton's Cyclopedia also discusses bevel frictional gearing in which the bevel gear was a smooth-face iron cone driven by a bevel pinion with a wooden rim. The rim was composed of several layers of hardwood followed by soft maple and was bolted onto a flanged hub made of iron.

2.1 Automotive Applications

Not until the introduction of the horseless carriage at the end of the 19th century did the goal of developing a continuously variable transmission (CVT) for a car spark considerable friction drive activity. Mechanical ratchet, hydraulic, and electromechanical drives were all tried, but friction drives, because of their simplicity, were the first automobile transmissions to provide infinite ratio selection. The earliest of these were the rubber V-belt drives that appeared on the 1886 Benz and Daimler cars, the first mass-produced gasoline-engine-powered vehicles. Friction disk drives, similar in construction to the gearless transmission illustrated in a 1906 advertisement (fig. 3, ref. 11) were used as regular equipment on a number of early motor cars. These included the 1906 Carter-car, 1907 Lambert, 1909 Sears Motor Buggy, and 1914 Metz Speedster.

The Carter-car had an extremely simple friction drive: a metal disk driven by the engine crankshaft was in friction contact with a large, fiber-covered spoked wheel mounted on a transverse countershaft. The countershaft, in turn, was connected to the rear axle by an ordinary chain drive. This running gear was generally exposed to the environment beneath the carriage of the motor car. To vary the speed ratio, the driver used a lever to radially position the output follower wheel across the face of the metal disk—in turntable fashion. Neutral was achieved when the follower wheel was centered. Moving the follower wheel past center caused reverse rotation and allowed the vehicle to back up. The smoothness and ease of operation of the Carter-car transmission made it quite popular. It is not well known that W.C. Durant, founder

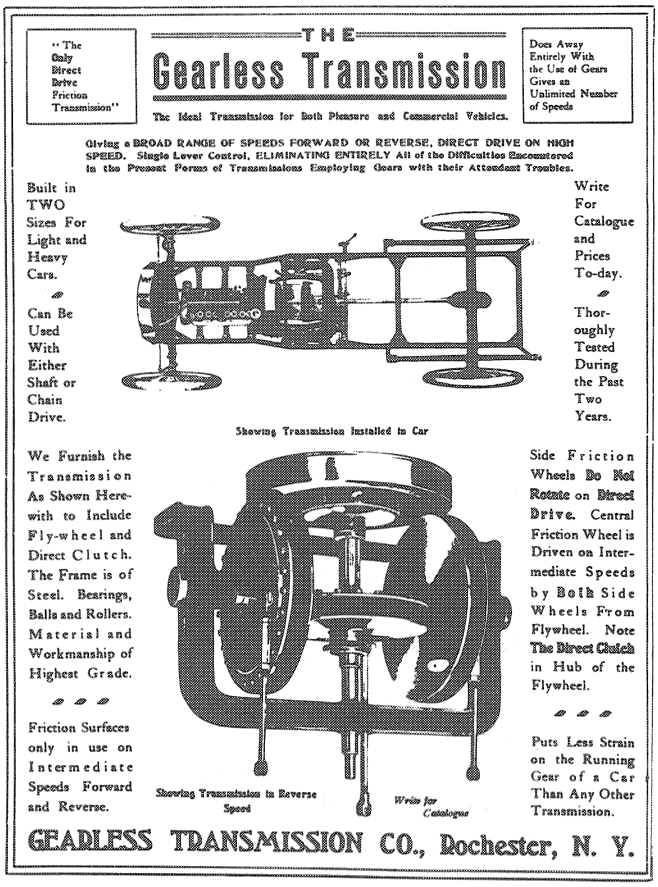

Figure 3.—Early automotive friction drive (ca. 1906). (From ref. 11.)

and first president of General Motors Company, acquired the Carter-car Company in 1908 because of his expectation that friction drives would soon be universally used in automobiles (refs. 12 and 13). In 1910 the Carter-car Company even produced a Model T truck equipped with their friction drive. Despite its catchy slogan, "No clutch to slip—no gears to strip.....a thousand silent speeds and only one control lever, that's a Carter-car," the Carter-car Company's commercial success was shortlived.

From 1909 until 1912 Sears marketed a two-cylinder, 10-kW "Motor Buggy" also equipped with a friction drive (ref. 14). "Absolute simplicity, its positiveness under the most severe conditions and its unequalled flexibility," boasted one of the Sear's ads. However, by about 1915, cars equipped with friction drives had virtually disappeared (ref. 14), presumably, in part, because of the need to frequently renew the friction material.

Despite the limited success of these earlier attempts the goal of designing an automotive transmission that smoothly and automatically shifted was not lost. In the late 1920's the Buick Division of General Motors was given the task of developing a continuously variable, oil-

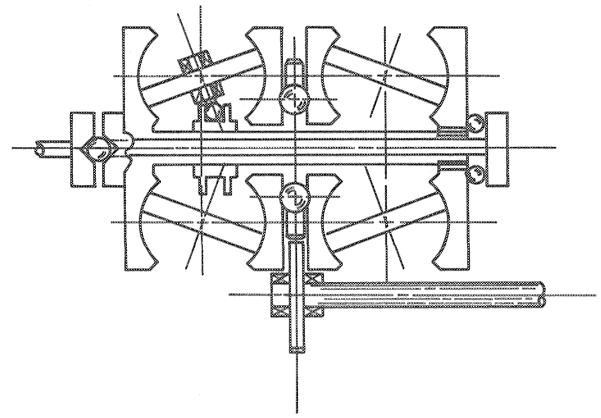

Figure 4.—General Motor's Toric transmission (ca. 1928).

lubricated, steel-on-steel traction drive. This transmission was similar in design to the Hayes double-toroidal traction drive, patented in 1929. The Hayes Self-Selector Transmission (ref. 15), although originally developed in the United States, was later offered as an option on the 1935 British Austin Sixteen (ref. 16).

The General Motors toroidal drive, later called the Toric transmission, is illustrated in figure 4. The geometry of the drive is remarkably similar to that of the 1877 Hunt drive, with the addition of a second toroidal cavity and a ball differential to balance loading between the two cavities. An extensive test program was conducted on this drive. Seventeen road-test vehicles equipped with the Toric drive accumulated over 300 000 miles of road testing (ref. 13). A 20-percent improvement in highway fuel mileage was reported. In 1932 General Motors decided to produce this type of transmission (ref. 12). However, no cars equipped with the Toric drive were ever sold to the public. The reasons for halting production were never made clear. Some say that there were unresolved discrepancies between service life data obtained from road tests and those obtained from laboratory bench tests. Others believe that not enough premium-quality bearing steel, needed in large amounts to make each drive, was available at the time to meet expected production requirements. Whatever the reasons, Alfred P. Sloan, Jr., then president of General Motors, turned the transmission down for production in the belief that it would simply be too expensive to make (ref. 12). The Toric drive was not completely forgotten, however, reappearing in the 1960's on General Motor's experimental gas turbine RTX bus.

General Motor's New Departure Bearing Division produced an industrial counterpart to the Toric drive. By 1935 when production was halted, over 1600 units of the Transitorque traction CVT had been marketed (ref. 15). The drive's design is credited to Richard T. Erban, an early traction drive pioneer, who briefly worked for General Motors during this period (ref. 5).

In England in 1958 after several years of analyzing the Hayes Self-Selector drive, Perbury Engineering, Ltd., retrofitted a modified, scrapped Hayes transmission into a Hillman Minx sedan (ref. 16). The fuel saving was reported to be 20 to 25 percent, but the concept never caught on with any of the several dozen companies that had expressed interest in the drive (ref. 16).

In the United States in 1959 Charles Kraus installed a modified version of a toroidal CVT into an American Motors Nash Rambler (ref. 5). This unit had a semi-toroidal roller geometry similar to that patented in 1932 by Jacob Arter for industrial service. (The Arter drive is still commercially produced in Switzerland.) In 1973 Tracor, Inc., demonstrated a Ford Pinto equipped with an improved version of the Kraus drive lubricated with Monsanto's new traction fluid. Although operational characteristics were established, expected fuel economy improvements were largely negated by the hydraulic losses in the thrust bearings used to clamp the toroids together (ref. 17). More recent toroidal drive designs partially overcome this problem by mounting two toroidal drive cavities back to back along a common shaft, thereby eliminating these troublesome thrust bearings.

2.2 Industrial Applications

Starting with the 1877 Hunt drive adjustable-speed traction drives have been in industrial service for more than 100 years. The bulk of these drives have been performing a speed-matching function for light-duty equipment such as drill presses. Examples of representative adjustable-speed traction drive configurations appear in figure 5. According to Carson (ref. 18) more than 100 U.S. patents on adjustable-speed traction drives are on file. Of these, perhaps a dozen or so basic geometries are in production. Of those commercially available, few are rated at greater than 10-kW power capacity. Reference 19 describes 24 types of variable-speed traction drives that were commercially available in 1963. A recent treatment of the application of traction drives for industrial drive systems appears in reference 20.

The "ball and cone" geometry (fig. 5(c)) was commercially introduced in the 1940's by Jean Kopp in Switzerland. The Kopp Variator is said to be the most widely used traction drive, with more than 250 000 units sold around the world through 1975 (ref. 18). A more recent cone-roller variator developed by Kopp (fig. 5(e)) extends the variator's power rating to 75 kW in a 582-kg package.

The wheel and single-disk drive (fig. 5(k)) typify the Carter-car and Sears Motor Buggy transmissions. Because heavy contact loads must be directly reacted by the support bearings, the torque capacity of this geometry is greatly restricted.

The cone and ring (fig. 5(j)) with reducer drive (not shown), produced by Graham in 1935, is one of the earliest traction drives developed in the United States. Graham drives are available for ratio ranges to 10 and power levels to about 4 kW.

The disk-to-disk drive (fig. 5(l)) also known as the Beier disk drive, was one the earliest (1949) industrial traction drives capable of handling high powers and had current power ratings to 164 kW. The drive components are imported from Japan and assembled and marketed in the United States by Sumitomo Machinery Company.

Applications for modern traction drives are quite diverse:

(1) Marine propulsion drives
(2) Earthmoving equipment
(3) Textile machinery
(4) Farm equipment and agramachinery
(5) Rubber machinery
(6) Propeller drives
(7) Forest products and paper machinery
(8) Crane drives
(9) Construction equipment
(10) Pump drives
(11) Locomotive and railroad machinery
(12) Machine tools
(13) Outdoor tools and recreation vehicles
(14) Oil field drives and offshore rigs
(15) Household appliances
(16) Automobile transmissions
(17) Air-conditioning systems
(18) Steel mill drives
(19) Mining and ore-processing machinery

Specific applications can be found in references 5 to 7 and 18 to 20.

2.3 Fixed-Ratio Traction Drives

Although light-duty, variable-ratio traction drives have been reasonably successful from a commercial standpoint, few fixed-ratio drives have progressed past the prototype stage. This is somewhat surprising in view of the outstanding ability of traction drives to transfer power smoothly and quietly at extremely high or low speeds with good efficiency. They seem particularly well suited for high-speed machine tools, pump drives, and other turbomachinery. In other industrial applications they offer potential cost advantages because traction rollers should not be much more expensive to manufacture in quantity than ordinary rollers in roller bearings.

In terms of earlier work on fixed-ratio traction drives the developmental effort at General Motors Research Laboratories on their planetary traction drive, as described by Hewko (ref. 21), was perhaps the most complete. Several of these drives were built and tested, including a 6-to-1 ratio, 373-kW unit for a torpedo and a

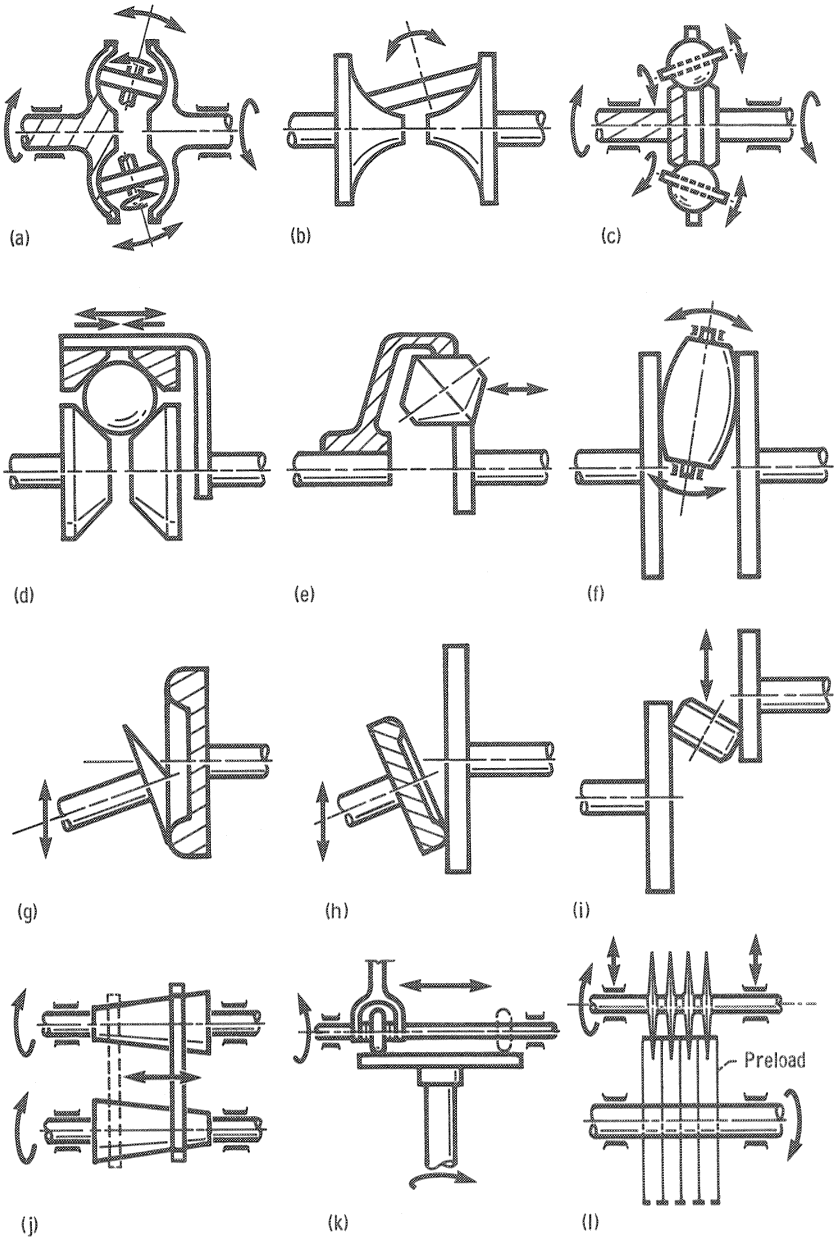

Figure 5.—Typical adjustable-speed traction drive geometries.

3.5-to-1 ratio, 75-kW test drive. The latter drive exhibited better efficiency and lower noise than a comparable planetary gearset.

Interest in fixed-ratio traction drives is also high outside the United States. Tests were conducted in Japan on a planetary traction drive of a construction similar to the General Motors unit for use with a gas-turbine auxiliary propulsion unit (APU) system (ref. 22). Planetary traction drives have also been studied in Finland.

The traction drives described thus far have a simple, single-row planet-roller format (fig. 6). For drives like these the number of load-sharing planets is inversely

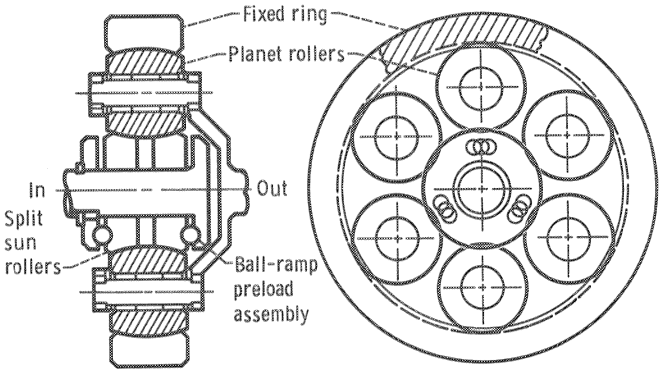

Figure 6.—Single-row planetary traction drive. (From ref. 21.)

related to the speed ratio. For example, a four-planet drive would have a maximum speed ratio of 6.8 before the planets interfered. A five-planet drive would be limited to a ratio of 4.8 and so on.

A remedy to the speed ratio and planet number limitations of simple, single-row planetary systems was devised by Algirdas Nasvytis (ref. 23). His drive system used the sun and ring rollers of the simple planetary traction drive but replaced the single row of equal-diameter planet rollers with two or more rows of "stepped," or dual-diameter, planets. With this new "multiroller" arrangement practical speed ratios of 250 could be attained in a single stage with three planet rows. Furthermore the number of planets carrying the load in parallel could be greatly increased for a given ratio. This significantly reduced individual roller contact loading and correspondingly improved torque capacity and fatigue life. The basic geometry of the Nasvytrac drive (its commercial name) is shown in figure 7.

Nasvytis reported the test results for several early versions of his multiroller drive. The first drive tested was a 373-kW torpedo drive of three-planet-row construction with a reduction ratio of 48.2 and an input speed of 53 000 rpm. To investigate ultra-high-speed operation, Nasvytis tested a 3.7-kW, three-row, 120-to-1 ratio speed increaser that operated at 480 000 rpm for 15 min and ran for 43 consecutive hours at 360 000 rpm without liquid lubrication. Mechanical efficiencies to 97 percent were recorded during parametric tests on improved versions of the Nasvytrac drive (ref. 24). Tests were also conducted with the drive retrofitted to an automotive gas turbine (ref. 24) and installed in a rocket-engine pump drive simulator (ref. 25).

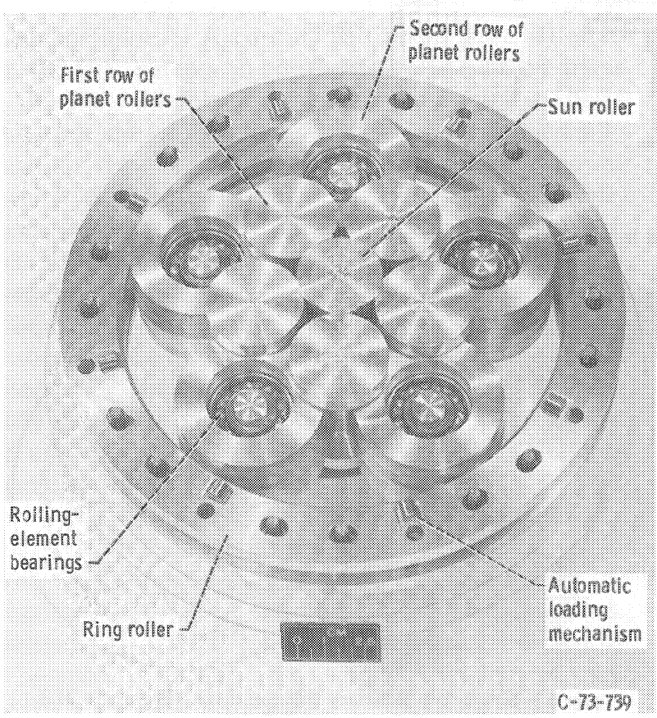

Figure 7.—Geometry of Nasvytis traction (Nasvytrac) drive.

More recent tests of a 370-kW helicopter transmission using a traction roller/gear version of this drive were performed at the Lewis Research Center. This transmission is known as a hybrid traction drive because of the combination of rollers and gears. It carries 58 percent more power in a package that is only 22 percent heavier than the production transmission it simulates (ref. 1). A higher speed version of this transmission has a projected 68-percent increase in system power-to-weight ratio with a 300-percent improvement in fatigue life (ref. 1). Design of a twin-engine, 2240-kW hybrid helicopter transmission has also been completed. This transmission, with an output torque of 94 000 N-m, represents the most powerful traction drive ever devised.

The zero backlash, high torsional stiffness, low torque ripple, and low hysteresis characteristics of traction drives make them particularly well suited for servo-control positioning applications, such as robotic hinge mechanisms and pivot actuators (ref. 26). Furthermore extremely precise positioning can be achieved with proper feedback controls. A good example of this is the linear traction drive feed mechanism on the ultraprecise turning machine reported in reference 27. Positioning resolution of 0.005 μm, equivalent to 0.05 arc-sec, was achieved with this slide drive system (ref. 27).

The theoretical comparisons made in reference 26 indicate that comparably sized and loaded traction drive contacts are two to five times stiffer than gears for the gearsets examined. Because of these favorable servomechanism attributes a hybrid traction drive was incorporated into the design of an advanced propeller pitch-change mechanism for future turboprop aircraft (ref. 28).

3.0 Elastohydrodynamic Film Thickness

A basic understanding of how power is transferred between traction drive rollers is necessary in analyzing the performance of a particular drive. Figure 8 shows a simple lubricated roller pair in traction contact. A sufficiently large normal load N is imposed on the rollers to transmit the tangential traction force T. The amount of normal load required to transmit a given traction force without destructive gross slip is dictated by the available traction coefficient μ, which is the ratio of T to N. Since contact fatigue life is inversely related to the third power of normal load, it is extremely desirable to use lubricants that produce high values of μ. The search for lubricants having high traction capabilities is discussed in section 7.1.

The rollers, as illustrated in the enlarged view of the contact appearing in figure 8, are not in direct contact but are separated by a highly compressed, extremely thin

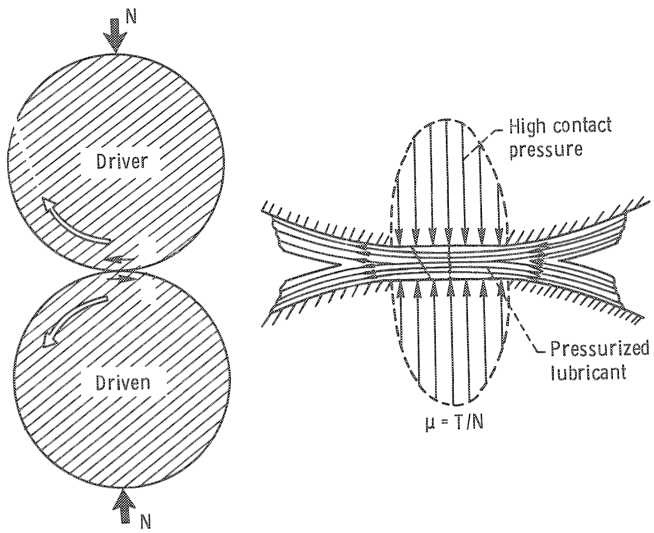

Figure 8.—Power transfer through traction.

lubricant film. Because of the high pressures in the contact zone the lubrication process is accompanied by some elastic deformation of the contact surface. Accordingly this process is referred to as elastohydrodynamic (EHD) lubrication. Grubin (ref. 29) was among the first to identify this phenomenon, which also occurs for other oil-lubricated, rolling machine elements such as bearings and gears. The importance of the EHD film in traction contacts lies in its ability to reduce or eliminate wear while acting as the principal torque-transferring medium.

Hamrock and Dowson (ref. 30) have derived a simplified approach to calculating the EHD film thickness. They provide dimensionless groupings as follows (refer to fig. 9):

Dimensionless minimum film thickness:

$$H_{\min} = \frac{h_{\min}}{R_x} \tag{1}$$

which occurs at the trailing edge of the contact.

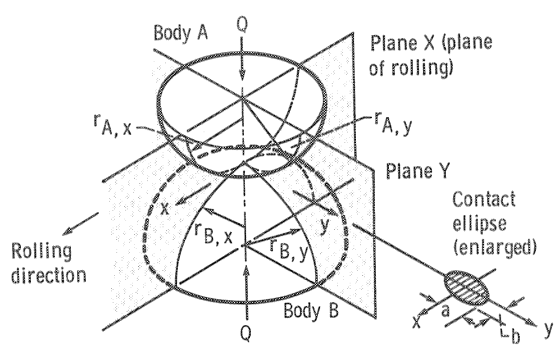

Figure 9.—Geometry of contacting solid elastic bodies.

Dimensionless central film thickness:

$$H_c = \frac{h_c}{R_x} \tag{2}$$

which is the average film thickness across the entire contact. The equivalent radius in the rolling direction R_x is given by

$$\frac{1}{R_x} = \frac{1}{r_{A,x}} + \frac{1}{r_{B,x}} \tag{3}$$

Dimensionless speed parameter:

$$U_D = \frac{\eta_0 U}{E' R_x} \tag{4}$$

where the average surface speed of bodies A and B is

$$U = \frac{u_A + u_B}{2} \tag{5}$$

and where the reduced modulus of elasticity is

$$E' = \frac{2}{\left(\frac{1-\xi_A^2}{E_A} + \frac{1-\xi_B^2}{E_B}\right)} \tag{6}$$

Dimensionless load parameter:

$$W = \frac{Q}{E' R_x} \tag{7}$$

Dimensionless materials parameter:

$$G = \alpha_p E' \tag{8}$$

Contact ellipse ratio:

$$k = \frac{a}{b}$$

where a and b are the radii of the contact ellipse, with radius a oriented perpendicular to the rolling direction x.

The conventional method of calculating the contact ellipse ratio is to find a solution to a transcendental equation that relates the ellipse ratio and the elliptic integrals of the first and second kinds to the geometry of the contacting solids. This is usually accomplished by some iterative numerical procedure. The following simple expression for k, which eliminates the necessity for that procedure, is derived in reference 31:

$$k = \left(\frac{R_y}{R_x}\right)^{2/\pi} \tag{9}$$

for $0.01 \leq R_y/R_x \leq 100$, where the equivalent radius transverse to the rolling direction can be found from

$$\frac{1}{R_y} = \frac{1}{r_{A,y}} + \frac{1}{r_{B,y}} \tag{10}$$

The approximate solution of the ellipse ratio as obtained from equation (9) is within 3 percent of the exact solution for k between 0.056 and 18. For R_y/R_x greater than unity the major diameter of the contact ellipse will be oriented perpendicular to the rolling direction.

In reference 30 the influence of k and the dimensionless speed U_D, load W, and materials G parameters on the minimum and central film thicknesses was investigated theoretically for the viscous-elastic regime. The ellipse ratio was varied from 1 to 8, the dimensionless speed parameter was varied over nearly two orders of magnitude, and the dimensionless load parameter was varied over one order of magnitude. Conditions corresponding to the use of solid materials of bronze, steel, and silicon nitride and lubricants of paraffinic and naphthenic oils were considered in obtaining the exponent on the dimensionless materials parameter. Thirty-four cases were used in obtaining the following dimensionless minimum-film-thickness formula:

$$H_{\min} = 3.63\, U_D^{0.68}\, G^{0.49}\, W^{-0.073} (1 - e^{-0.68k}) \tag{11}$$

For pure cylindrical roller contact (i.e., line contact) $k = \infty$ and the term in the parentheses in equation (11) equals 1.

Prediction of the rolling traction loss associated with rolling-element contacts requires knowledge of the central film thickness as well as the minimum film thickness. The procedure used to obtain the central film thickness is the same as that used to obtain the minimum film thickness and results in the following formula:

$$H_c = 2.69\, U_D^{0.67}\, G^{0.53}\, W^{-0.067} (1 - 0.61 e^{-0.73k}) \tag{12}$$

The measure of the effectiveness of the lubricant film is the "lambda" (λ) ratio (i.e., h_c/σ, the central film thickness divided by the composite surface roughness of the rolling-element surfaces). Usually the root-mean-square (rms) surface finishes of the contacting bodies σ_A and σ_B are used to determine the composite surface roughness as follows:

$$\sigma = (\sigma_A^2 + \sigma_B^2)^{1/2}$$

The λ ratio can be used as an indicator of rolling-element performance. For $\lambda < 1$, surface smearing or deformation, accompanied by wear, will occur on the rolling surface. For $1 < \lambda < 1.5$, surface distress may be accompanied by superficial surface pitting. For $1.5 < \lambda < 3$, some surface glazing can occur with eventual roller failure caused by classical subsurface-originated rolling-element fatigue. At $\lambda \geq 3$, minimal wear can be expected with extremely long life; failure will eventually be by classical subsurface-originated rolling-element fatigue (ref. 32). Although selection of operating parameters to provide a high λ ratio is desirable for good surface protection, it must be balanced against the loss in available traction that accompanies a thick EHD film. The most expedient, although not the least expensive, way of attaining both high λ ratio and high traction is to select a high-quality surface finish at least comparable to that for mass-produced ball and roller bearings. These surface finishes are generally better than 0.25 μm rms.

4.0 Traction Drive Capacity and Durability

Modern industrial traction drives are nearly always constructed from hardened, vacuum-melted bearing steels such as AISI 52100 or case-hardened tapered bearing or gear steels such as AISI 4340, 8620, or 9310. Because these drives are typically lubricated and cooled with mineral or synthetic (high traction) oils, the operating conditions within the contact, that is, the EHD film and cyclic Hertzian stress field, are nearly identical to those of a ball or roller bearing. In fact, except for the presence of a traction force, the volume of material within the contact does not know whether it is in a traction drive or a roller bearing. This same comparison could also be made with respect to a gear contact, which has, in common with traction drives, appreciable traction forces acting near the pitch point of the tooth.

It is therefore not surprising that the materials, heat treatments, surface finishes, tolerances, and other manufacturing processes associated with the mass production of rolling-element bearings and gears also lend themselves to the manufacture of traction drive components. Furthermore it is equally understandable that the life rating methods established for ball and roller bearings are also useful for sizing traction drive rollers. Accordingly rolling-element fatigue life methods will be the main focus of this section.

Other durability considerations, such as a thermal breakdown in the EHD film leading to scuffing failure, are addressed in section 4.5. Sizing criteria based on wear and thermal failure considerations for the design of nonlubricated ("friction") drives, such as those made from rubber-like materials are covered in section 10.0.

In the past, traction drives have been sized for some allowable Hertz (contact) stress in the contact zone on the basis of experience. No concerted effort has been made to size traction drives for a certain fatigue life and reliability level in the way that ball and roller bearings are sized. Hence although most of the drives shown in figure 5 may

function well under some conditions, reliability characteristics are generally not well defined. The drives' expected service lives have not been determined in a manner to allow for comparisons between different types of drives or to predict the effect that widely varying operating conditions might have on fatigue life. The first analytical method to predict the life of a traction drive was developed by Coy, Loewenthal, and Zaretsky (ref. 33). Subsequent analysis was performed (refs. 34 and 35) for a multiroller traction drive. A simplified fatigue life analysis for traction drive contacts was published by Rohn, Loewenthal, and Coy (refs. 36 and 37). This analysis is presented here.

4.1 Contact Stress

Before fatigue life can be estimated, the maximum contact stress for the bodies in question must be determined.

Elliptical contact.—The stress analysis of elastic bodies in contact was developed by H. Hertz (ref. 38). Hertz assumed homogeneous solid elastic bodies made of isotropic material that are characterized by Young's modulus E and Poisson's ratio ξ. Bodies A and B in contact are assumed to have quadratic surfaces near the contact point. The theory of Hertz is summarized by Harris (ref. 39).

For two bodies in contact (fig. 9) planes x and y are the planes of maximum and minimum relative curvature for the bodies. These planes are mutually perpendicular. They are also perpendicular to the plane tangent to the surfaces of the contacting bodies at the point of contact. For consistency in later calculations planes x and y should be chosen so that the relative curvature in plane x is oriented in the rolling direction. The radii of curvature may be positive or negative depending on whether the surfaces are convex or concave, respectively. For example, if body B in figure 9 was a conformal ring roller, body B's radii of curvature would be $-r_{B,x}$ and $-r_{B,y}$.

When the bodies are pressed together, the point of contact is assumed to flatten into a small area of contact bounded by an ellipse with diameters $2a$ and $2b$ as shown in figure 9. The values of a/b (the ellipse ratio k) range from 0 to ∞ for various curvature combinations of contacting surfaces. For spheres in contact $k=1$. For rollers approaching cylinders in contact k tends toward ∞. For true cylinders the flattened area of contact is a rectangular strip, sometimes referred to as line contact. When $k<1$, the long side of the contact is oriented in the x direction.

When performing contact analysis, one must be aware of the geometrical orientation of the rolling radii, crown radii, and principal planes. In some traction drive contacts the principal radii $r_{A,x}$ and $r_{B,x}$ (fig. 9) are equal to the rolling radii of the contacting element and radii $r_{A,y}$ and $r_{B,y}$ are equal to the transverse or crown radii. However, the principal radii for drive contacts using tapered rollers or those in toroidal drives are generally not equal to the rolling radii or their orthogonal components since these radii are not normal to the surface at the point of contact. The principal radii for use in this analysis *must always lie in planes that are perpendicular to the contact plane.*

A typical pair of traction rollers in contact is shown in figure 10. Bodies A and B are generalized traction rollers that rotate, in this case, about coplanar axes. The perpendicular distance from the axis of rotation of a body to the point of contact is the rolling radius (R_A or R_B) of the body. This is the radius that determines rotational surface velocities and speed ratios. The plane of contact is the plane tangent to both bodies at the point of contact. The principal radii $r_{A,x}$ and $r_{B,x}$ lie in the principal plane, which is perpendicular to the plane of contact, and in the rolling direction. Thus the value of $r_{A,x}$ or $r_{B,x}$ is defined by a line segment normal to the contact plane between the point of the contact and some point on the axis of rotation (fig. 10). A trigonometric relation exists between the principal radii ($r_{A,x}$ and $r_{B,x}$) and the rolling radii (R_A and R_B) as a function of the angle between the rotational axes and the contact plane. As shown in the figure the principal transverse radii ($r_{A,y}$ and $r_{B,y}$) lie in the plane of the cross section, which is also perpendicular to the contact plane.

In figure 10 the axes of rotation are in the same plane. This is the case for nearly all traction drives. If the rollers rotate about axes that are significantly noncoplanar (i.e., if extreme misalignment exists), the principal radii must be redetermined on the basis of three mutually perpendicular planes that satisfy the conditions of figure 9. For small misalignments, of the order of 10° or less, the difference in the radii will be very small and can be safely neglected.

The maximum surface (Hertzian) contact pressure or stress at the center of the elliptical pressure distribution is

$$\sigma_0 = \frac{3Q}{2\pi ab} \tag{13}$$

where the contact ellipse radii are

$$a = a^* g; \quad b = b^* g \tag{14}$$

and where

$$\frac{a}{b} = \frac{a^*}{b^*} \tag{15}$$

The auxiliary contact size parameter can be found from

$$g = \sqrt[3]{\frac{3Q}{2\rho}\left(\frac{1-\xi_A^2}{E_A} + \frac{1-\xi_B^2}{E_B}\right)} \tag{16}$$

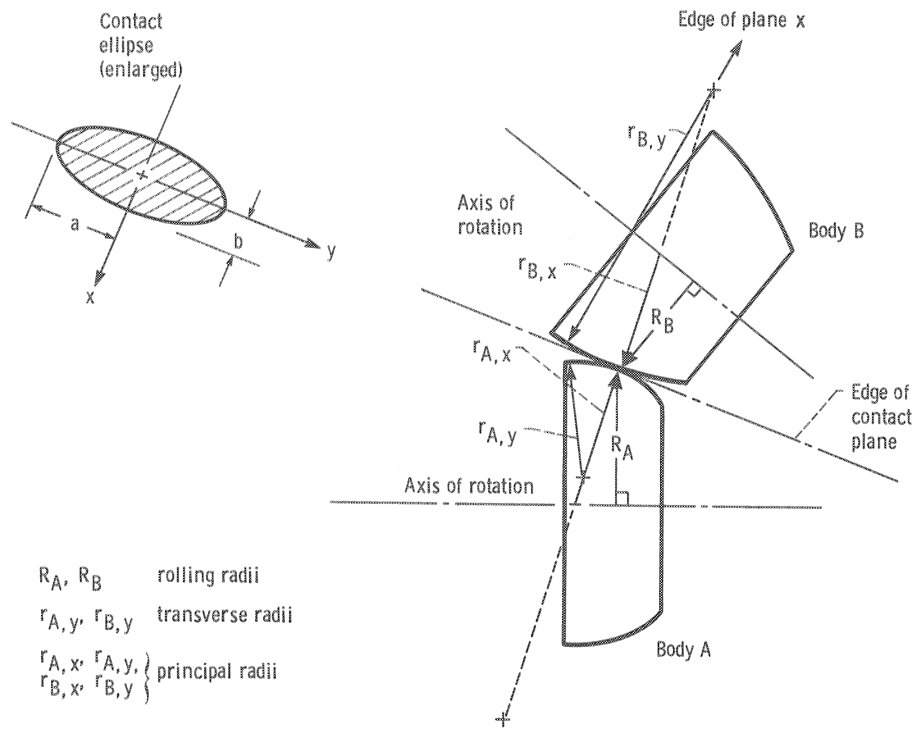

Figure 10.—Geometry of typical traction rollers.

and the inverse curvature sum is

$$\rho = \frac{1}{R_x} + \frac{1}{R_y} = \frac{1}{r_{A,x}} + \frac{1}{r_{B,x}} + \frac{1}{r_{A,y}} + \frac{1}{r_{B,y}} \tag{17}$$

For steel contacting bodies with $E_A = E_B = 207$ GPa and $\xi_A = \xi_B = 0.3$, the auxiliary contact size parameter can be simplified to

$$\begin{aligned} g &= 2.36 \times 10^{-4} \sqrt[3]{\frac{Q}{\rho}} \quad \text{(newton and meter units)} \\ &= 4.50 \times 10^{-3} \sqrt[3]{\frac{Q}{\rho}} \quad \text{(pound force and inch units)} \end{aligned} \tag{18}$$

The values of a^* and b^*, the dimensionless contact ellipse factors, depend strictly on contact shape. They can be determined from the elliptical integrals used in Hertzian theory (ref. 38). Figure 11 shows a^* and b^* plotted as a function of the ellipse ratio k found from the approximation given in equation (9).

Line contact.—For two cylindrical bodies of finite length l the surface contact pressure is distributed uniformly along the length of the cylinders. The maximum value of the contact pressure is along the transverse centerline of the pressure rectangle and is given by

$$\sigma_0 = \frac{2}{\pi} \frac{Q}{lb} \tag{19}$$

where the semiwidth of the pressure rectangle is

$$b = \left[\frac{4}{\pi} \frac{Q}{l} \left(\frac{1-\xi_A^2}{E_A} + \frac{1-\xi_B^2}{E_B} \right) \quad \frac{1}{\left(\frac{1}{r_{A,x}} + \frac{1}{r_{B,x}} \right)} \right]^{1/2} \tag{20}$$

For steel contacting bodies

$$\begin{aligned} b &= 3.35 \times 10^{-6} \left[\frac{Q}{l} \left(\frac{r_{A,x} r_{B,x}}{r_{A,x} + r_{B,x}} \right) \right]^{1/2} \\ &\qquad \text{(newton and meter units)} \\ &= 2.78 \times 10^{-4} \left[\frac{Q}{l} \left(\frac{r_{A,x} r_{B,x}}{r_{A,x} + r_{B,x}} \right) \right]^{1/2} \\ &\qquad \text{(pound force and inch units)} \end{aligned} \tag{21}$$

4.2 Fatigue Life Model

Although several failure modes ranging from scuffing (thermal failure) to corrosion pitting may be encountered, a properly designed and lubricated traction drive will eventually fail from fatigue. Many investigations have been conducted on the fatigue of rolling-element bearings. Because of the similarity in the expected failure mode, namely, rolling-element fatigue, the life analysis methods used to establish rolling-element bearing

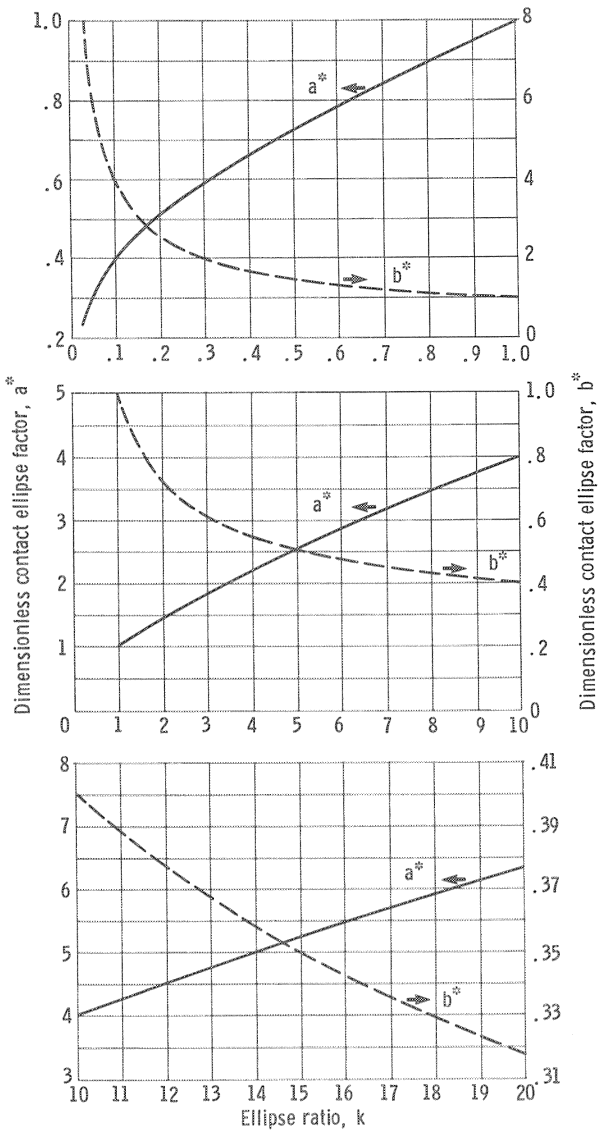

Figure 11.—Dimensionless contact ellipse factors as function of ellipse ratio.

capacity ratings are applicable to determining the service life and capacity of traction drive contacts.

Lundberg and Palmgren published a statistical theory for the failure distribution of ball and roller bearings in 1947 with later modifications in 1952 (refs. 40 and 41). The mode of failure was assumed to be subsurface-originated (SSO) fatigue pitting. Lundberg and Palmgren theorized that SSO fatigue pitting was due to high stresses in the neighborhood of a stress-raising defect in the bearing material. This theory is used by bearing manufacturers to establish rolling-element bearing fatigue life ratings. In references 42 and 43 the theory is applied to predicting the fatigue life of spur and helical gears. The predicted life of a steel gearset was confirmed with life data from full-scale spur gear tests (ref. 43). The theory has also been adapted to analyzing the fatigue lives of traction drives (ref. 33).

For a steel rolling element the number of millions of stress cycles endured before failure occurs is given by the following equation (ref. 33):

$$L=\left(\frac{K_1 z_o^h}{\tau_o^c V_s}\right)^{1/e} \tag{22}$$

This equation is a modified form of the Lundberg-Palmgren theory for contact-fatigue life prediction and is applicable to gears, bearings, and other rolling-contact elements. The critical shear stress τ_o is considered by Lundberg and Palmgren to be the maximum orthogonal reversing shear stress that occurs just below the surface of the contacting elements. Although this stress is not the largest of the subsurface stresses, it has the largest fluctuating component, which is critical to the fatigue process. The stressed volume term V_s is important since Lundberg-Palmgren theory is based on the probability of encountering a fatigue-initiating flaw in the volume of the material that is being stressed. The depth to the critical stress z_o is a relative measure of the distance the fatigue crack must travel in order to emerge at the surface and thus cause failure. For rolling-element bearings (and rollers in traction drives) made of AISI 52100 steel with a Rockwell-C 62 hardness and a 90-percent probability of survival, the following values are appropriate for use in equation (22) to determine life in millions of stress cycles:

$$K_1=1.430\times10^{95} \quad \text{(newton and meter units)}$$
$$=3.583\times10^{56} \quad \text{(pound force and inch units)}$$

For traction drives made of steel of lower quality or with lower hardness, this life factor must be reduced. On the basis of life tests of ball and roller bearings, the accepted exponent values are $h=7/3$, $c=31/3$, and $e=10/9$ for elliptical point contacts or $e=9/8$ for line contacts (refs. 40 and 41).

The magnitude of the critical stress (i.e., the subsurface maximum orthogonal reversing shear stress τ_o and its depth z_o in eq. (22)) is a function of k. These parameters can be found in reference 39 in terms of $2\tau_o/\sigma_0$ and z_o/b plotted against b/a. Also needed for equation (22) is the stressed volume V_s, which for a rolling-element contact is given by

$$V_s=az_o 2\pi|R| \tag{23}$$

where R is each body's rolling radius (fig. 10). Thus the term $2\pi R$ is equal to the length of the rolling track traversed during one revolution.

Elliptical contacts.—Estimation of the theoretical fatigue life of a rolling-element contact based on equations (22) and (23) and figures appearing in reference 39 is fairly straightforward. However, for a traction drive with

many contacts the calculations can become tedious and the relations between life and contact size, shape, and load are unclear. In references 36 and 37 a simpler method is developed, which expresses the life of each body in an equation in terms of material constants, applied load, and contacting body geometry. This method assumes that both contacting bodies are of the same material (i.e., $E_A = E_B$ and $\xi_A = \xi_B$) and uses the exponents and material factors already given. Fatigue life can then be calculated by

$$L = K_3(K_2)^{9/10}[Q^{-10/3}(E'\rho)^{-7}|R|^{-1}]^{9/10} \tag{24}$$

where L is the 90-percent survival life of a single contacting element in millions of stress cycles and

$$K_3 = 8.18 \times 10^{90} \quad \text{(newton and meter units)}$$
$$= 1.49 \times 10^{56} \quad \text{(pound force and inch units)}$$

$$K_2 = \left(\frac{z_0}{b}\right)^{4/3}\left(\frac{\tau_0}{\sigma_0}\right)^{-31/3}(a^*)^{28/3}(b^*)^{35/3} \tag{25}$$

$$E' = \frac{E}{1-\xi^2} \tag{26}$$

Since the contacting bodies are assumed to be steel, with $E = 207$ GPa and $\xi = 0.3$, equation (24) becomes

$$L = K_4(K_2)^{0.9}Q^{-3}\rho^{-6.3}|R|^{-0.9} \tag{27}$$

where

$$K_4 = 2.32 \times 10^{19} \quad \text{(newton and meter units)}$$
$$= 6.43 \times 10^{8} \quad \text{(pound force and inch units)}$$

The geometry variable K_2 in equation (25) contains four factors, each of which depends only on the ellipse ratio k. The term K_2 is plotted against k in figure 12(a) for $k<1$ and in figure 12(b) for $k>1$. From reference 37 K_2 can also be directly calculated from the relative curvature difference F by the following approximation:

$$K_2 = 4.80 \times 10^6(1-F)^{-1.37}(1+F)^{-5.63} \tag{28}$$

for $1<k<20$, where $F=(1/R_x - 1/R_y)/\rho$. As shown in figure 12(b) there is reasonable agreement with the full solution, particularly for higher values of k.

Thus equation (27) can be used to calculate each contacting body's life by inserting the material constant K_4 shown above for steel and selecting the geometry parameter K_2 from figure 12 based on k. In the special case where the rolling radii are also equal to the principal radii (i.e., $R_A = r_{A,x}$ and $R_B = r_{B,x}$) and body A is the external roller,

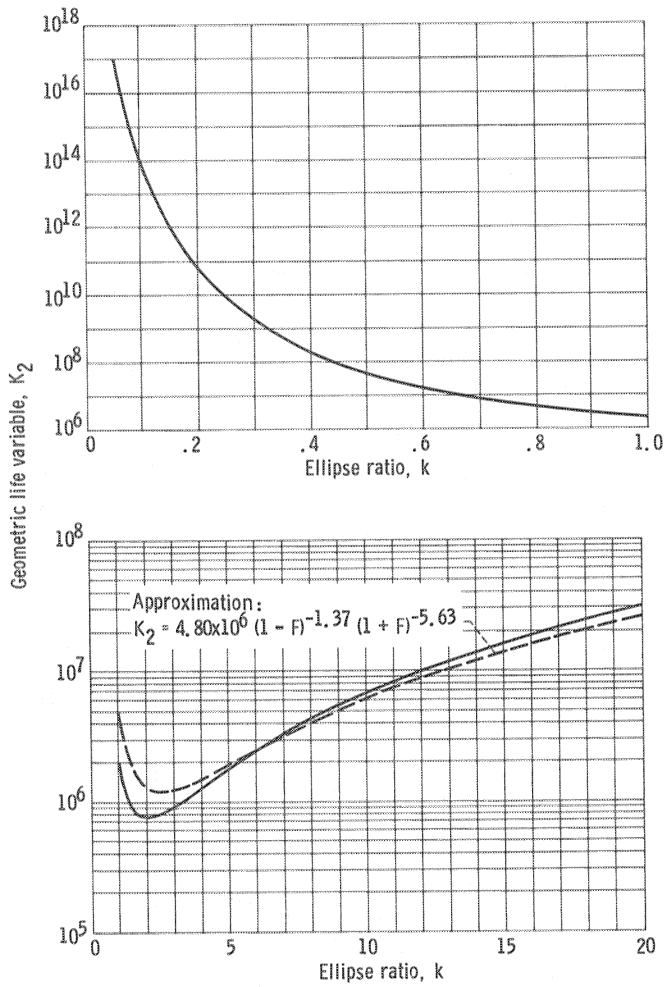

Figure 12.—Geometric life variable as function of ellipse ratio.

$$\rho = \frac{2}{R_A}\left(\frac{1+\dfrac{R_A}{R_B}}{1+F}\right) \tag{29}$$

and from equation (27)

$$L_A = K_5(K_2)^{0.9}Q^{-3}R_A^{5.4}\left(\frac{1+\dfrac{R_A}{R_B}}{1+F}\right)^{-6.3} \tag{30}$$

where

$$K_5 = 2.95 \times 10^{17} \quad \text{(newton and meter units)}$$
$$= 8.16 \times 10^{6} \quad \text{(pound force and inch units)}$$

and where R_A is the rolling radius of the body whose 90-percent survival life in millions of stress cycles is L_A and R_B is the rolling radius of the mating body. It then follows that $L_B = L_A\ (|R_A/R_B|)^{0.9}$.

An expression for the maximum surface contact pressure can also be developed for steel bodies from equations (13), (14), and (16), where

$$\sigma_0 = \frac{8.55\times10^6}{a^*b^*} Q^{1/3}\rho^{2/3} \qquad \text{(newton and meter units)}$$

$$= \frac{2.36\times10^4}{a^*b^*} Q^{1/3}\rho^{2/3} \qquad \text{(pound force and inch units)} \tag{31}$$

Line contacts—The analysis presented thus far has been confined to point contacts. For a pure line (rectangular) contact it can be shown that, if $e=9/8$,

$$L_A = K_6 Q^{-4} R_A^{4.30} l^{3.11}\left(1+\frac{R_A}{R_B}\right)^{-5.19} \tag{32}$$

where

$$K_6 = 2.15\times10^{34} \qquad \text{(newton and meter units)}$$

$$= 8.42\times10^{19} \qquad \text{(pound force and inch units)}$$

and R_A and R_B are as defined for equation (30).

It is of historical interest to note that Lundberg and Palmgren took, in their original 1947 work (ref. 40), Weibull slope $e=3/2$ for the line contact case. This resulted in $L\propto Q^{-3}$ and it follows that $L\propto\sigma_0^{-6}$. However, this sixth-power relation between life and stress is contrary to the approximate ninth-power relation exhibited by most rolling-contact fatigue data. In recognition of this, in their 1952 study (ref. 41) they conducted numerous fatigue tests on tapered, cylindrical, and spherical roller bearings. From these data they concluded that $e=9/8$, yielding a load exponent of -4 and a stress exponent of -8, would better represent the data.

From a practical standpoint pure line or rectangular contact is rarely encountered in practice. Rollers in roller bearings are customarily crowned over at least part of their length and invariably have some end-relief treatment. This is done to mitigate the concentrated edge stresses that result from the contact between a finite-length roller and a raceway. These edge stresses are aggravated by misaligned loads. Without such surface modifications even slight asymmetric loads would lead to rapid edge failure. Therefore some amount of end relief of traction rollers is strongly recommended. If the potential for large misalignment exists, a slight crown across the entire roller length would be the safest approach. However, blended crown radii that straddle some roller flat length are also acceptable, provided that the blending is done smoothly. The extent of crown length would be a function of the expected misalignment. For example, crown lengths that are one-third of the total are not uncommon for roller bearings. Fatigue life calculations for rollers with partial crowns can only be treated approximately with equations (30) and (32). Under light loads the contact will be primarily rectangular, being confined to the flat length. With increasing loads the contact region will spread to the roller ends, taking a more elliptical distribution.

System life.—Heretofore the equations expressed rolling-element fatigue life for a single rolling element in terms of millions of stress cycles. However, for a traction drive it is system life in time units that is important. All bodies in a system accumulate stress cycles at different rates because their speeds of rotation and number of stress cycles per revolution may not all be the same. To compare lives of the various bodies, clock time should be used. Assume that the speed in revolutions per minute of the ith body is n_i and that there are v_i stress cycles per revolution; then the life of body i in hours is given by

$$H_i = \frac{L_i}{v_i n_i}\frac{10^6}{60}$$

The life of the system is then found by applying Weibull's rule (ref. 33). If the system consists of j rolling bodies and the life of each is designated $H_i (i=1 \text{ to } j)$, the system life in hours is given by

$$H_s = \left[\frac{1}{H_1^e}+\frac{1}{H_2^e}+\ldots+\frac{1}{H_j^e}\right]^{-1/e} \tag{33}$$

Thus for the simplest arrangement, a single pair of rollers, the contact life in hours for an elliptical contact would be

$$H_s = \left[\frac{1}{(H_1)^{10/9}}+\frac{1}{(H_2)^{10/9}}\right]^{-9/10}$$

where $e=10/9$ and H_1 and H_2 are equal to the individual lives of each roller.

Reliability.—The material constant K_1 required in equation (22) was deduced from fatigue test data at a 90-percent probability of survival. Such a fatigue life is the life which 90 percent of a large number of identical traction drive systems will equal or exceed under a given operative condition. Rolling-element bearing capacities, given in manufacturers' catalogs, are generally defined at this 90-percent life. However, the service lives of many gearboxes and other mechanical components are based on some mean or average time before failure. The effect of different reliability levels on rolling-element and traction contact-fatigue life for $e=10/9$ is shown in figure 13. Note that the life at the median life level (50 percent of components will survive) is over five times the life at 90-percent survival. Because of the statistical distribution of rolling-element fatigue life, the median fatigue life is not equal to the mean or average life. For

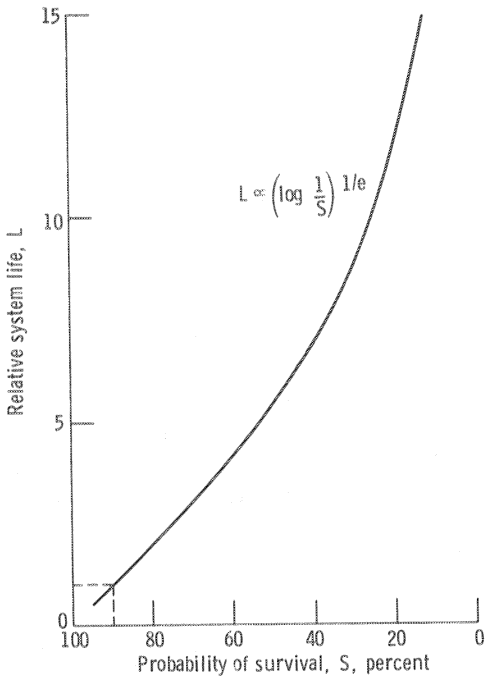

Figure 13.—Relative system life as a function of probability of survival.

the value in equation (22) of $e = 10/9$ for point contacts, the mean life corresponds to the life at which 61.7 percent of all components will fail. One should thus be aware of the difference between designing for 90-percent reliability and designing on the basis of mean life as is the case for many machine elements.

Life adjustment factors.—Advances in rolling-element bearing technology since the publication of the Lundberg-Palmgren theory have generally extended bearing fatigue lives. These advances were the use of improved materials and manufacturing techniques along with a better understanding of the variables affecting fatigue life. In recognition of these advances factors have been developed for adjusting Lundberg-Palmgren fatigue life ratings for ball and roller bearings (ref. 44). Several of these factors are considered to be equally applicable to traction drive elements in view of the similarities in contact geometry, operating conditions, failure modes, materials, and lubrication (ref. 33). The appropriate factors are the material, processing, and lubrication factors. An additional factor, not considered for rolling-element bearings in reference 44 but important to traction drive contacts, is the potentially deleterious effect that traction may have on fatigue life. The addition of a tangential force component to the contact may alter the subsurface stress field, and this may in turn change the fatigue life. Some investigators (ref. 45) have found a shortening in life from rolling-element fatigue tests when relative sliding and traction are introduced; others (ref. 46) have observed no change or even an improvement in fatigue life on the driven roller surface. Since insufficient data currently exist to properly quantify the effects of traction on rolling-element fatigue life, a degree of conservatism is in order when sizing a drive for a given service life.

In the present analysis these life adjustment factors are not considered. Comparisons are made on the basis of the unmodified theoretical predictions. Application of the analysis developed herein to an actual traction drive should include the life adjustment factors published in reference 44.

4.3 Effects of Size, Traction Coefficient, and Contact Shape

The relative effects of roller size and speed on drive system life and torque capacity are of great interest to the designer of traction drive systems. Generally for a given power level and life the size of the power-transmitting element, such as a gear or a traction drive roller, can be reduced as speed is increased since torque decreases. This effect and several others can easily be studied for general and specific cases through the use of equation (27).

Size effects.—It is evident from equation (27) that for a given rolling contact, increasing the load will decrease life by a power of 3. In other words, for a constant available traction coefficient and body size, life is related to torque according to $L \propto T_0^{-3}$. In addition, a direct relation exists between life and element size (radius and contact width). For constant torque, traction coefficient, and ellipse ratio, $L \propto (\text{Size})^{8.4}$. Similarly, since load is directly related to torque and inversely related to radius, we may write $Q \propto (\text{Torque/Size})$. Substituting this in equation (27) and holding life constant produces $\text{Torque} \propto (\text{Size})^{2.8}$.

It should be emphasized that although these general relations are very useful for preliminary sizing, they hold only for a constant available traction coefficient. In detailed drive design the effect of changes in operating conditions on the lubricant's traction coefficient must also be considered.

Traction coefficient effects.—Traction data (refs. 47 to 49) for various lubricants show that the maximum available traction coefficient μ decreases with increasing surface velocity and decreasing contact pressure. Typical traction data from a twin-disk machine are given in reference 49. To provide a safe margin against gross slippage, 75 percent of the maximum coefficient is often used as the operating coefficient in a traction drive.

An arbitrary roller pair of constant speed ratio and $k = 5$ operating at a given power level was analyzed for fatigue life. The contacting rollers were assumed to operate first under a fixed applied traction coefficient μ_x and second with 75 percent of the highest possible traction coefficient based on the data of reference 49. The appropriate value of μ to use in this comparison was found from an iterative process since μ depends on the contact pressure and speed and vice versa.

Figure 14 shows the effect of size on contact fatigue life. Figure 15 includes the effects of both size and speed on life. In figure 14 an increase in size extends life as would be expected. Raising the relative rotational speed in figure 15 accumulates more stress cycles per hour, but since the speed and torque are inversely related for constant power, the decrease in torque and thus in normal load is more significant. This results in longer life at higher speeds. Additionally, figure 15 shows that for a constant-life condition, the rolling traction element can be smaller at higher rotational speeds.

The reason for longer life in either the constant-μ or variable-μ case is that increasing a traction roller's size or rotational speed for constant power reduces the tangential force and thus the normal load and contact pressure. However, reducing the contact pressure or increasing the surface speed produces a loss of available traction coefficient and thus requires a higher normal load to transmit the torque. This loss in μ causes a flattening of the life trend with increasing size (fig. 14). In fact, for the range shown, the life curve reaches a maximum and then diminishes, indicating an optimum size for best life. Similarly the life trends in figure 15(b) also flatten because of a loss in μ. The curves of the 1.5 and 2 size rollers show an optimum speed.

The importance of the available traction coefficient to the performance of a traction drive can be related to various design parameters. The drive's overall size (i.e., element diameters), system life, torque capacity, weight, and power-to-weight ratio are quite sensitive to the lubricant's traction coefficient. By substituting $Q=T/\mu$ (where T is the tractive force) into equation (27), the direct effect of the traction coefficient on these

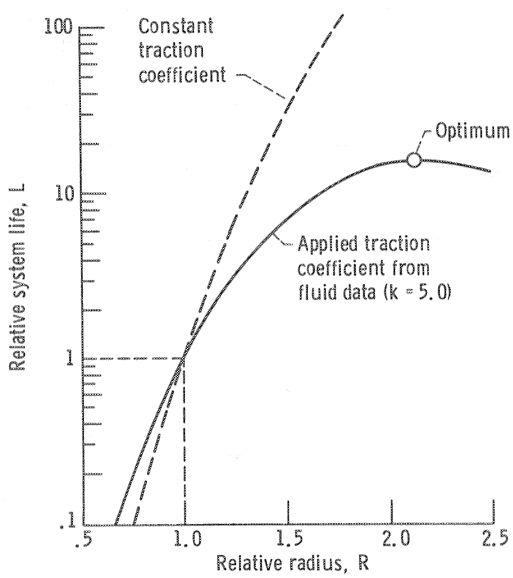

Figure 14.—Relative system life as a function of relative radius for roller pair in simple traction contact. Power, speed, and ellipse ratio are constant.

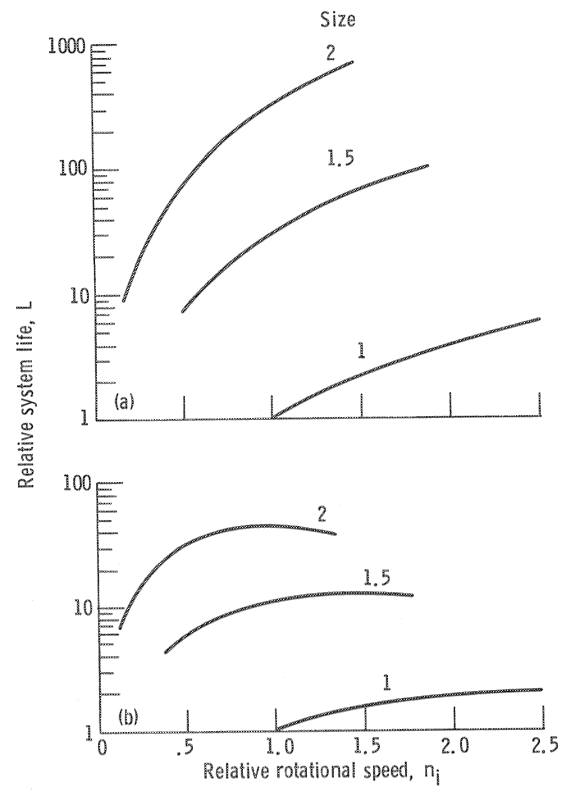

(a) Constant applied traction coefficient.
(b) Applied traction coefficient from fluid data ($k=5$).

Figure 15.—Relative system life as a function of relative rotational speed for various size roller pairs in simple traction contact. Power, speed ratio, and ellipse ratio are constant.

parameters can be determined, as shown in figure 16, where the ellipse ratio is held constant. The curves are arbitrarily normalized relative to $\mu_x=0.05$. The trend and proportionality between μ_x and each of the three parameters is valid where the other two parameters are held constant. Life shows the highest sensitivity to μ_x, but all three performance factors improve at higher values of the traction coefficient.

Effect of contact shape.—Traction contact life is also influenced by the relative curvatures of the bodies. For a typical pair of traction rollers for constant normal load, speed, and rolling radii, varying the transverse radii can have a large effect on the estimated fatigue life. It is evident from figure 17 that an increase in k will enlarge the area of contact and correspondingly reduce contact pressure with an attendant improvement in life. However, this effect is somewhat diminished when the loss in the available traction coefficient due to the decrease in contact pressure is taken into account. Furthermore contacts with large k tend to have significantly lower traction coefficients under spin and also higher power losses. Figure 18 shows the adverse effects of spin on power loss, which are discussed in section 6.5.

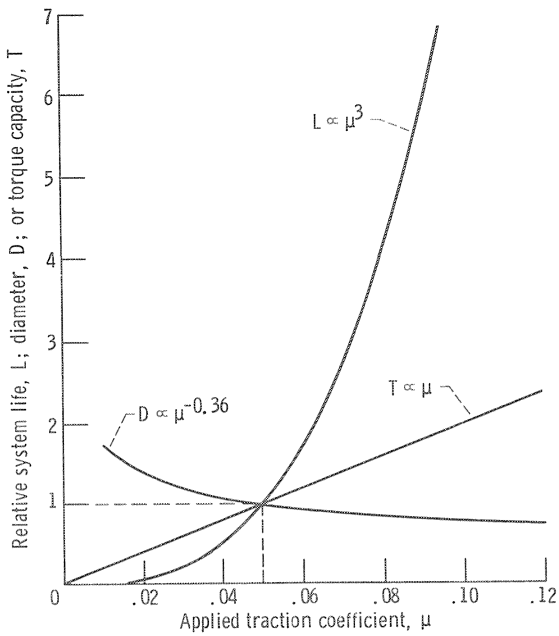

Figure 16.—Relative system life, diameter, and torque capacity as functions of applied traction coefficient for constant ellipse ratio.

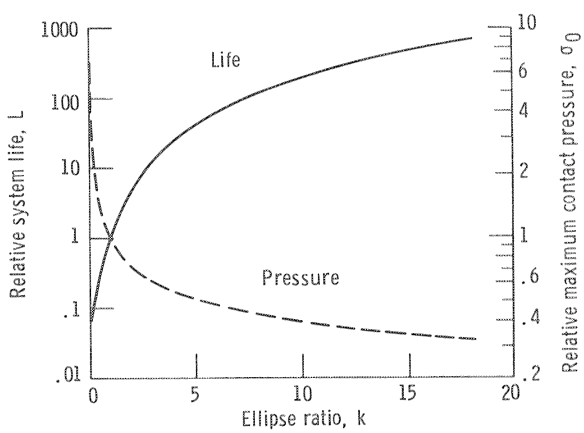

Figure 17.—Relative system life and maximum Hertz pressure as functions of ellipse ratio. Load, rolling radii, and traction coefficient are constant.

4.4 Effects of Multiple Contacts

Traction drives with minimum weight and size generally require multiple load-sharing contacts. The extent to which multiple parallel contacts reduce unit loading and improve life and power capacity can easily be explored with the analysis presented herein. The configurations used to demonstrate this are (1) a set of multiple identical planet rollers in external contact with a central sun roller and (2) a set of multiple identical planet rollers in internal contact with a ring roller. These arrangements typify the multiple contacts found in many types of traction drives.

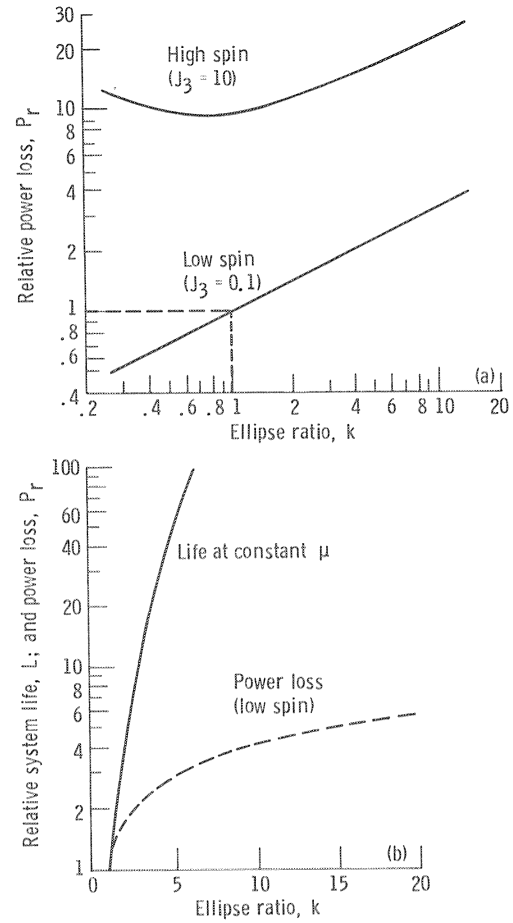

Figure 18.—Relative system life and power loss as functions of ellipse ratio.

By beginning with a simple two-roller contact transmitting a certain power, a multiple-roller cluster is formed by adding additional rollers without changing speed, roller size, and sun or ring torque. The life increase and contact pressure decrease for multiple-roller contacts are shown in figure 19. Because of the parallel paths each element is loaded in proportion to the inverse of the number of planets in the cluster. However, life is not proportional to the cube of the number of planets as equation (27) alone would indicate. The system life decreases with an increase in the number of components according to equation (33), and the sun or ring experiences more stress cycles per revolution with more planets. Figure 19 is valid for both external and internal contact configurations of any size, speed ratio, and allowable number of rollers for constant torque, traction coefficient, ellipse ratio, and element size. An expression for life as a function of the number of planets can be derived from equation (27):

$$L \propto \left[\frac{1}{N^{-2e} + N^{-3e+1}} \right]^{1/e}$$

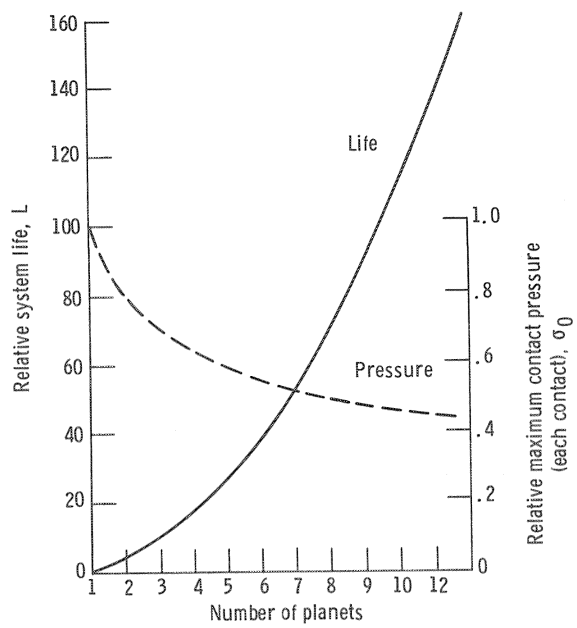

Figure 19.—Relative system life and maximum Hertz pressure as functions of number of planets for external or internal contact. Torque, rolling radii, ellipse ratio, and traction coefficient are constant.

Sample life calculations for a three-planet, external-contact configuration made of AISI 52100 steel are shown in table I.

Another advantage of the multiple-contact geometry is the relative compactness of such a traction drive assembly. Figure 20 shows the relative cluster diameter and contact pressure versus the number of planet rollers. This figure is valid for both external and internal configurations of any ratio operating under constant sun or ring torque conditions at equal system fatigue lives and ellipse ratios. The effect of planet number on the relative sun or ring torque capacity is illustrated in figure 21 for constant size, ellipse ratio, traction coefficient, and fatigue life in both external and internal contact

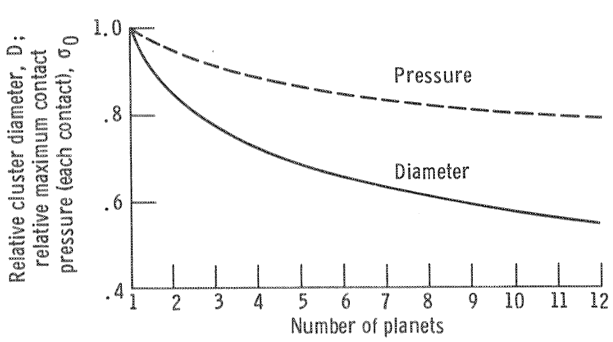

Figure 20.—Relative cluster diameter and relative maximum Hertz pressure as functions of number of planets for external or internal contact. System life, ellipse ratio, traction coefficient, and torque are constant.

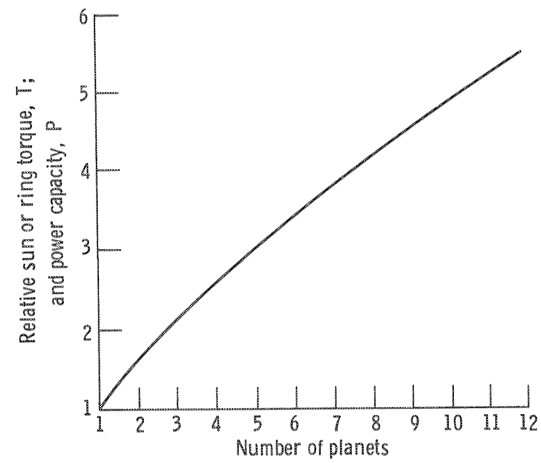

Figure 21.—Relative torque and power capacity as functions of number of planets for external or internal contact. System life, rolling radii, ellipse ratio, and traction coefficient are constant.

arrangements. Figures 19 to 21 show that, for a given application, using the maximum number of load-sharing rollers possible within geometrical ratio limits is advantageous to fatigue life, drive size, and torque capacity.

4.5 Other Durability Considerations

Traction drives, like rolling-element bearings, should be sized on the basis of rolling-element fatigue life. For most applications, other than those that are particularly short lived, the stress levels required for acceptable fatigue life are generally well below those for static yield failure. For example, maximum bending stress in the Nasvytrac drive (ref. 24) at a peak sun-roller torque of 42 N-m is less than 350 MPa and maximum contact stresses are less than 2.2 GPa. For the case-hardened steel rollers the expected yield stress in bending would be approximately 1400 MPa and the Brinell stress limit would be of the order of 4 GPa.

Because of these relatively low maximum operating stress levels, occasional momentary overloads of several times the maximum design value can generally be tolerated. Furthermore, if these transient overloads are brief and do not occur too frequently, only a relatively small penalty to the drive's total fatigue life will result.

A traction drive's sensitivity to shock loads also depends on the ability of the contact surface to avoid skidding or heating damage. If the drive is equipped with a fast-acting loading mechanism, and if the overload is sufficiently brief to avoid overheating the contact, no surface damage should occur (in principle).

Scuffing failure.—The normally expected failure mode of a properly designed, oil-lubricated traction drive is rolling-element fatigue. A certain degree of surface polishing or a small amount of wear may be noticed at certain drive ratios and operating conditions. In general,

TABLE I.—SAMPLE LIFE CALCULATIONS

Arrangement ..... External, three load-sharing rollers
Sun diameter, mm 25
Planet diameter, mm 50
Load, each contact, N..... 1000
Sun speed, rpm..... 10 000
Transverse radii (sun), mm 500
Transverse radii (planets), mm 100

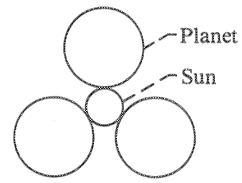

Parameter	Symbol	Formula	Result
Normal load, each contact, N	Q	----------	1000
Orthogonal prinicipal radii, m	$r_{A,x}$	----------	0.0125
	$r_{A,y}$	----------	0.5
	$r_{B,x}$	----------	0.025
	$r_{B,y}$	----------	0.1
Inverse curvature sum, m^{-1}	ρ	$\frac{1}{r_{A,x}} + \frac{1}{r_{A,y}} + \frac{1}{r_{B,x}} + \frac{1}{r_{B,y}}$	132
Relative curvature difference	F	$\frac{\frac{1}{r_{A,x}} + \frac{1}{r_{B,x}} - \frac{1}{r_{A,y}} + \frac{1}{r_{B,y}}}{\rho}$	0.818
Geometric life variable	K_2	$4.80 \times 10^6 (1-F)^{-1.37} (1+F)^{-5.63}$	1.71×10^6
Sun rolling radius, m	R_{sun}	----------	0.0125
Sun life, millions of cycles	L_{sun}	$K_4 (K_2)^{0.9} Q^{-3} \rho^{-6.3} R_{sun}^{-0.9}$	2.14×10^4
Sun stress, cycles/rev	u_{sun}	----------	3
Sun speed, rpm	n_{sun}	----------	10 000
Sun life, hr	H_{sun}	$\left(\frac{L}{un}\right)_{sun} \left(\frac{10^6}{60}\right)$	11 900
Planet rolling radius, m	R_{pl}	----------	0.025
Planet life, millions of cycles	L_{pl}	$L_{sun} \left(\frac{R_{sun}}{R_{pl}}\right)^{0.9}$	1.15×10^4
Planet stress, cycles/rev	u_{pl}	----------	1
Planet speed, rpm	n_{pl}	----------	5000
Plant life, hr	H_{pl}	$\left(\frac{L}{un}\right)_{pl} \left(\frac{10^6}{60}\right)$	38 300
System life, (without adjustment factors), hr	H_s	$\left[\left(\frac{1}{H_{sun}}\right)^{10/9} + 3\left(\frac{1}{H_{pl}}\right)^{10/9}\right]^{-9/1}$	6900

wear of this type is normally encountered during run-in of most machine elements and is not harmful. Although wear covers a wide spectrum of severity, the removal of the original grinding marks from the surface of contacting elements is indicative of a more serious condition. When significant wear occurs, the surfaces are usually operating under boundary lubrication conditions, where the presence of lubricant contaminants may also be a contributing factor. Enhancing the EHD film thickness through lowering lubricant temperatures or changing to higher viscosity oil can often help alleviate this condition, as can improving the surface finish.

Under more extreme operating conditions when unusually high contact loads or temperatures are present and when substantial levels of sliding or spin exist, the boundary lubricating film can break down, leading to scuffing damage. Scuffing or scoring damage is not commonly encountered in service for most concentrated contact machine elements, such as gears and bearings. In those cases where scuffing may occur, the use of extreme-pressure (EP) additives in the oil to form a chemically reactive surface film has proven to be successful in inhibiting the onset of scuffing. The effect of an EP additive film on traction has not been studied in detail, but presumably it reduces the available traction coefficient under boundary lubrication conditions while having a lesser effect with thicker lubricant films.

Because the nature of boundary lubrication is not well defined, the mechanism of scuffing is also not well understood. Although certain empirical criteria have been advanced by various investigators to predict the onset of scuffing, no one criterion has been found to hold under all conditions. An excellent review on this subject was prepared by Dyson (ref. 50). One of the leading criteria is that advanced by Blok (ref. 51) in 1939. Blok postulated that there is a single critical scuffing temperature that is constant for a given material-oil combination, regardless of the surface or operating condition. This is nominally about 230 °C (ref. 52) for hardened steel surfaces with mineral oils. Scuffing could be expected if the total contact temperature (the sum of the steady-state surface temperature and the instantaneous temperature rise of the surface as passed through the contact) exceeded this critical scuffing temperature. The steady-state surface temperature can be taken as approximately equal to the lubricant outlet temperature. The instantaneous surface temperature rise $\Delta\tilde{T}$, or so called flash temperature, is given by Blok for line contact to be

$$\Delta\tilde{T}=\frac{1.11fQ|\sqrt{u_A}-\sqrt{u_B}|}{\beta_t l\sqrt{2b}}$$

where

$\Delta\tilde{T}$	flash temperature, °C
f	coefficient of friction
Q	normal load, N
u_A, u_B	surface velocities of the bodies, m/sec
β_t	Blok's thermal coefficient, N/°C m sec$^{1/2}$
l	length of line contact, m
b	semiwidth of contact pressure rectangle, m

Blok's thermal coefficient β_t is a property of the roller material, typically 13 200 N/°C m sec$^{1/2}$ for steel (ref. 52). The Blok equation was originally developed for rectangular contacts. For elliptical contacts it is customary (ref. 52) to approximate the ellipse with a rectangle having the same minor contact width $2b$ and the same maximum contact pressure. This pressure equivalence can be accomplished by setting $l=(4/3)\ a$. The error associated with this approximation diminishes as the contact's ellipse ratio increases.

Although a number of investigators have obtained rather good correlation between the occurrence of scuffing and the critical contact temperature, a greater number of researchers have had results that were inconsistent with Blok's hypothesis (ref. 50). Thus at this time Blok's hypothesis should be viewed more as a relative measure of the susceptibility of scuffing than in absolute terms.

Another scuffing criterion of long standing is known as the frictional power intensity factor P_f of the form

$$P_f=f\bar{\sigma}\Delta U$$

where

P_f	frictional power intensity, W/mm^2
f	coefficient of friction
$\bar{\sigma}$	mean Hertzian pressure, N/mm^2
ΔU	velocity difference between the two bodies, m/sec

and where

$$\bar{\sigma}=\frac{2}{3}\sigma_0 \qquad \text{(elliptical contact)}$$

$$=\frac{\pi}{4}\sigma_0 \qquad \text{(line contact)}$$

The frictional power intensity P_f is a measure of the heat load dissipated per unit area of the contact.

Dyson (ref. 50) compiled experimental values of P_f from many sources at conditions where scuffing failure occurred. All referred to hardened steel surfaces lubricated with mineral oils. Although some data were as low as 40 and as high as 700 W/mm^2, the bulk of the frictional power intensity data ranged from 100 to 200 W/mm^2. In a traction drive contact, if the power loss per unit area of contact is greater than about 120 W/mm^2, the possibility of scuffing should be considered.

Bearing life.—Although concern centers around the system fatigue life of the individual traction-carrying elements in the drive, many drive designers tend to overlook the service lives of the supporting ball and roller bearings when making life estimates. If the normal or clamping force on the traction elements is transmitted through rolling-element bearings, these bearings can become the shortest-lived components in the drive system. According to the Weibull rule, the drive life will always be less than that of its shortest-lived component. Hence the bearings can be the weakest component in the drive system if not properly sized. Furthermore particular attention has to be paid to systems containing many bearings since the system bearing life will often be much shorter than the life of any one individual bearing according to equation (33).

5.0 Traction Phenomena

5.1 Traction Curve

The tribological properties of the lubricant in the contact, particularly its traction characteristics, are fundamental to the design of traction drives. Figure 22 shows a typical traction-versus-slip curve for a traction fluid. This type of curve is typically generated with a twin-disk traction tester (refs. 47 to 49 and 53). Imposing a traction force across a lubricated disk contact and rotating at an average surface velocity U gives rise to a differential surface velocity ΔU. Three distinct regions can generally be identified on a traction curve. In the linear region the traction coefficient increases linearly with slip. In the non-Newtonian region it increases in a nonlinear fashion, reaches a maximum, and then begins to decrease. Finally the curve shows a gradual decay with slip in the thermal region because of internal heating

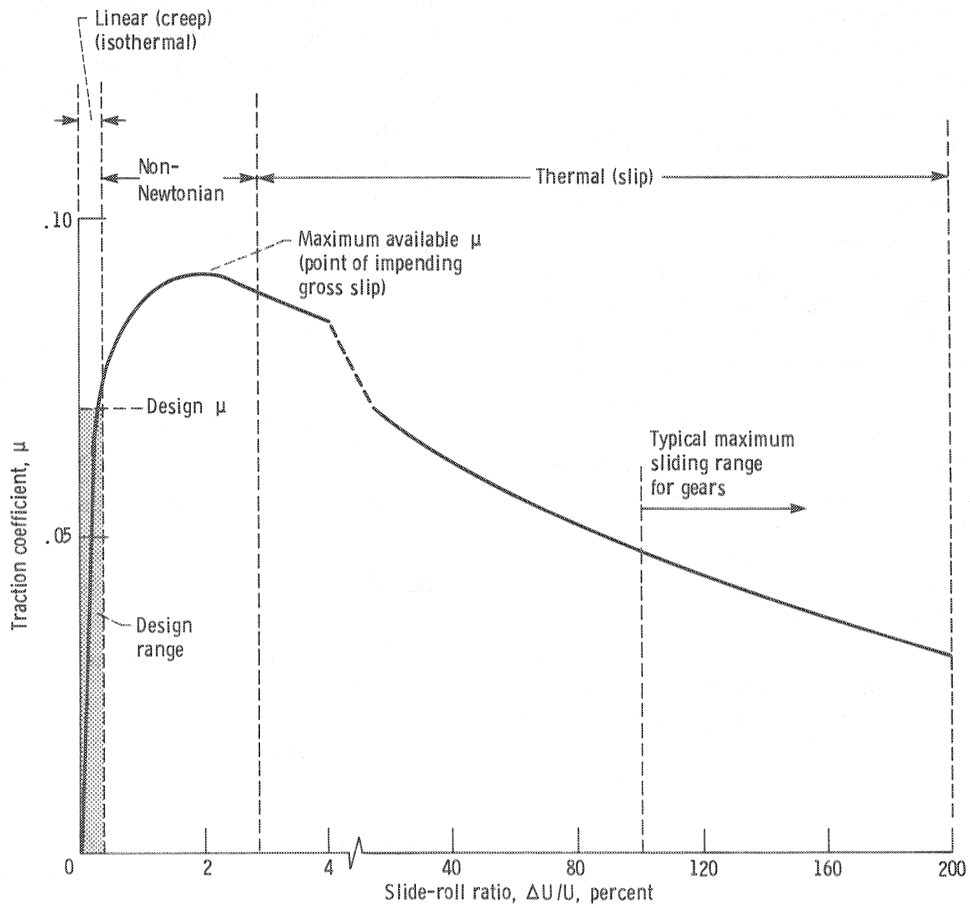

Figure 22.—Typical traction curve showing design range for traction drives.

within the oil film. It is the ascending (linear plus start of nonlinear) region of the traction curve that is of the greatest interest to traction drive designers. The design traction coefficient, which dictates how much normal load is needed to transmit a given traction force, is always chosen to be less than (by generally 20 to 30 percent) the peak available traction coefficient to provide a safety margin against slip. Traction drives are generally equipped with a torque-sensitive loading mechanism that adjusts the normal contact load in proportion to the transmitted torque. Such mechanisms ensure that the contact will always have sufficient load to prevent slip without needlessly overloading the contact under light loads. Their design is discussed in more detail in section 9.0.

5.2 Creep

In the linear region of the traction curve the transfer of torque will cause a small difference in velocity to be developed between the surfaces of the driver and driven rollers. This small velocity difference, generally less than 1 percent of the rolling velocity for low-spin contacts, is often referred to as creep rather than slip. This is because during creep only part of the contact is experiencing sliding, so-called microslip, while during slip there is total sliding motion.

Creep is always present to some extent between rolling bodies that are transmitting torque, whether lubricated or not. In a dry contact creep can be thought of as the tangential stretching of material as it enters the contact. Carter in 1926 was one of the first to identify the creep occurring between a locomotive's driving wheel and the rail (ref. 54). Typically a region of microslip occurs between the surfaces in the trailing region of the contact while the surfaces in the leading region are locked together without relative motion (ref. 55). As the tangential traction force is increased, the microslip region encompasses more and more of the contact until at some point the whole contact is in total slip. This is the point of impending gross slip. It occurs when the ratio of traction force to normal load is equal to the maximum available traction coefficient. When a mechanism to increase the normal load with increasing traction is present, the point of impending gross slip is not reached.

Creep in a lubricated contact is typically the result of the elastic shear or stretching of the lubricant film and the roller material. Under the high pressures in most traction drive contacts the viscosity of the lubricant film increases by several orders of magnitude. The film tends to behave like a plastic material, having elastic/plastic yield characteristics. Since the lubricant film gets stiffer with increasing pressure and is so thin, usually less than a micrometer, it has relatively high "stiffness" (small tangential deformation) under torque transfer. In fact, as pointed out by Tevaarwerk (ref. 56), for many traction drives that regularly operate at contact pressures above 1.2 GPa, most of the creep takes place in the steel rollers and not in the thin EHD film. Johnson, Nayak, and Moore (ref. 57) have developed relatively simple methods to determine how much of the elastic effect is due to the roller material and how much is due to the film.

The amount of creep in a lubricated traction drive contact can vary from as little as 0.1 percent of the rolling velocity at high pressures and low speeds to 3 or 4 percent, or more, when pressures are low, speeds are high, and side slip (misalignment) or spin (circumferential contact slip) is appreciable. These creep values are quite small relative to those for gears, where sliding velocities can be 100 percent, or higher, of the pitch line velocity at the tooth engagement and disengagement points. Nevertheless it is important to minimize traction contact creep through the proper selection of operating conditions, geometry, and lubricant. Every percentage point of loss in creep represents a percentage point of loss in speed and a corresponding percentage point of loss in mechanical efficiency. Also thermal effects that accompany high creep rates tend to reduce the available traction coefficient. This often means that higher loads have to be applied to transmit the required torque, shortening the drive system's service life.

5.3 Traction Coefficient

Perhaps the single most important factor affecting the torque capacity, life, and size of a traction drive is the maximum value of the available traction coefficient. It is this parameter that determines the necessary contact load. Since the fatigue life of a contact is inversely proportional to the cube of contact load for point contacts, a 50-percent improvement in the traction coefficient would, for example, mean a 240-percent increase in life for a given drive under a given set of operating conditions (fig. 16).

In a typical traction drive contact severe transient operating conditions are imposed on the lubricant. The lubricant is swept into the contact, exposed to contact pressures of 10 000 times atmospheric or greater, and then returned to ambient conditions, all in a few milliseconds. Clark, Woods, and White (ref. 58) in 1951 were the first to observe experimentally that under these high pressures and shear rates the lubricant exhibits shearing properties of a plastic solid and will yield at some critical shear stress. Although it had been known from static high-pressure viscometry experiments that an oil would become dramatically more viscous with increasing pressure and eventually solidify under high enough pressure, this was the first time that this effect was observed under the highly transient conditions of a traction contact. This solidification phenomenon was later observed by Smith (ref. 59) and Plint (ref. 60), among others. Thus in most traction drive contacts it is

the "yield strength" of this plastic-like lubricant film that sets the maximum available traction coefficient. This criterion is analogous to that for dry sliding contact, where the yield strength of the surface asperities is the principal indicator of peak friction levels.

6.0 Performance Predictions

The distribution of local traction forces in the contact of a traction drive can be rather complicated, as illustrated in figure 23. The figure shows the distribution of local traction vectors in the contact when longitudinal traction, misalignment, and spin are present. These traction forces will align themselves with the local slip velocities. In traction drive contacts some combination of traction, misalignment, and spin is nearly always present. To determine the performance of a traction drive contact, the elemental traction forces must be integrated over the contact area.

Because of the parabolic pressure distribution the elemental traction forces are largest near the center of the contact and diminish in magnitude near the contact perimeter. As expected, when traction is in the rolling direction, the forces align themselves in the rolling direction. Adding misalignment introduces a side-slip velocity and causes the vectors to align with the resultant side-slip angle. Using conical rollers generally results in a circumferential slip pattern referred to as "spin." This rotary motion is due to the contact being in pure rolling only at its center. At the right edge of the contact the upper roller is sliding over the lower roller because of the mismatch in contact radii. At the left edge the situation is reversed and so is the slip direction. Because of solid-body rotation a complete pattern of spin exists over all of the contact. Methods to calculate spin and its effects on traction contact performance can be found in section 6.3 and also in reference 61.

The power through the contact is determined from a summation of the traction force components aligned in the rolling direction times their respective rolling velocities. With misalignment clearly only a portion of the traction force is generating useful traction; the remainder is generating useless side force. For pure spin no useful traction is developed since the elemental traction forces cancel one another. Since the contact power loss is proportional to the product of the elemental traction forces and slip velocities, the presence of spin and misalignment can significantly decrease the efficiency of the contact. Even small misalignment angles can be important. For example, a misalignment as small as 0.25° can double the losses in a traction contact. Furthermore both spin and misalignment lower the available traction coefficient and reduce the amount of torque that can be transmitted safely. Side-slip velocities produced in drives that axially slide one roller over another in order to change the ratio will have a similar adverse effect on the traction coefficient. Designs that minimize spin and side slip can be quite efficient. Contact efficiencies of 99 percent or higher are possible.

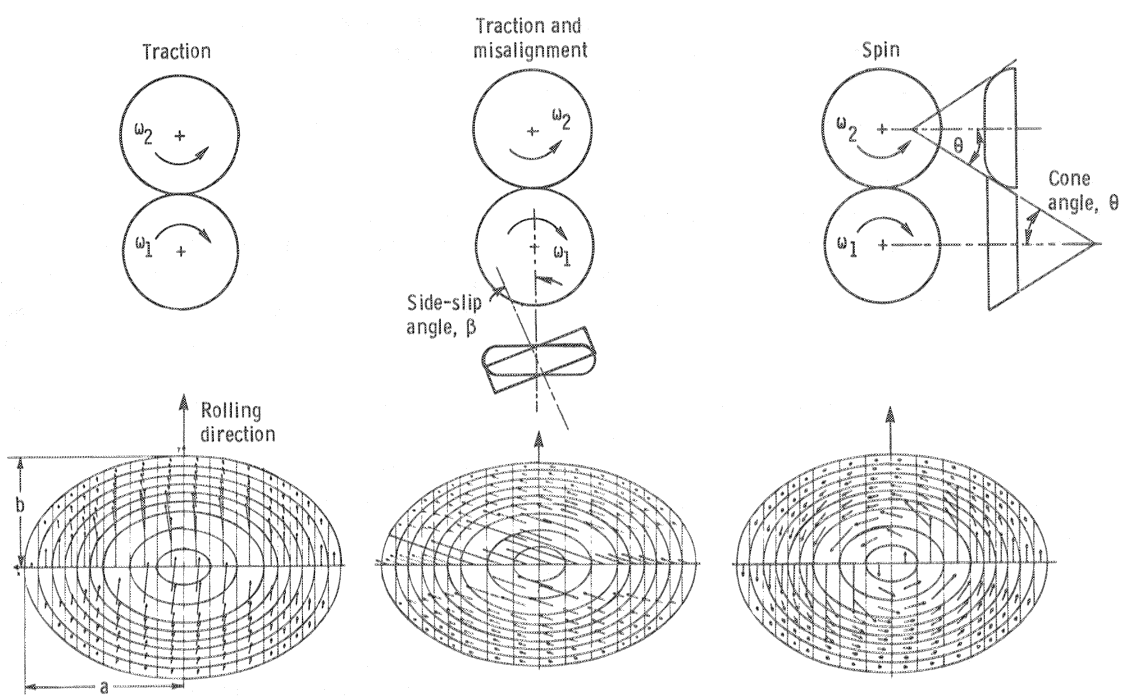

Figure 23.—Effect of misalignment and spin on contact traction vectors.

6.1 Traction Experiments

Although there had been previous attempts to analyze the losses associated with ball bearings (ref. 62), the first systematic attempt to research the losses of traction drive contacts occurred at the "Institut fur Machinenelemente und Forder Technik" located at the Technical University of Braunschweig in Germany between 1955 and 1960 (refs. 63 to 66). These investigations, which are summarized in an excellent manner by Wernitz (ref. 67), include analysis and test work on both simple traction contact test machines and a commercially available Kopp Variator. Tables and plots were developed that permit the calculation of friction losses due to creep (microslip) and spin (circumferential slip). This analysis treats the EHD film in the contact as behaving as perfectly plastic; that is, the material yields at some critical shear stress, exhibiting no elastic behavior. This model gives satisfactory results for contacts experiencing relatively high local strain rates such as those drives with moderately high spin. In reference 68 Magi takes a similar but more general approach. He gives examples with experimental justification.

6.2 Theory

In the 1960's and early 1970's numerous papers were presented on the prediction of traction in EHD contacts. Some of these include Cheng and Sternlicht (ref. 69), Dyson (ref. 70), and Trachman and Cheng (ref. 71).

About this time Poon (ref. 72) and Lingard (ref. 73) developed grid methods to predict the available traction forces of a contact experiencing spin. Poon's method uses the basic traction data from a twin-disk machine together with contact kinematics to predict the available traction. Lingard used a theoretical approach in which the EHD film exhibits a Newtonian viscous behavior at low shear rates until a critical limiting shear stress is reached. At this point the film yields plastically with increasing shear rate. This model shows good correlation with experimental traction data from a toroidal, variable-ratio drive of the Perbury type. This same model was also used successfully by Gaggermeier (ref. 53) in an unusually comprehensive investigation of the losses and characteristics of traction drive contacts. In addition to copious amounts of twin-disk traction data for numerous lubricants under various combinations of slip, side slip, and spin, Gaggermeier (ref. 53) also investigated the sources of power losses for an Arter type of toroidal drive. His findings were that, of the total power losses, the load-dependent bearing losses and the drive idling (no load) losses are greater than the losses due to traction power transfer. This underscores the need to pay close attention to these tare losses in order to end up with a highly efficient traction drive.

A later, comprehensive traction contact model is that proposed by Johnson and Tevaarwerk (ref. 48). Their model covers the full range of viscous, elastic, and plastic behavior of the EHD film. This type of behavior depends on the Deborah number (a relative measure of elastic to inelastic response) and the strain rate. At low pressures and speeds (low Deborah number) the film exhibits linear viscous behavior at low strain rates. It becomes increasingly nonlinear with increasing strain rate. At the higher pressures and speeds more typical of traction drive contacts, the response is linear and elastic at low strain rates. At sufficiently high strain rates the shear stress reaches some limiting value and the film shears plastically as in some of the earlier traction analytical models.

In references 56 and 74 Tevaarwerk presents graphical solutions developed from the Johnson and Tevaarwerk elastic-plastic traction model. These solutions are of practical value in the design and optimization of traction drive contacts. Knowing the initial slope (related to shear modulus) and the maximum traction coefficient (related to limiting shear stress) from a zero-spin, zero-side-slip traction curve, one can find the traction, creep, spin torque, and contact power loss over a wide range of spin values and contact geometries (ref. 49).

The solutions appearing in references 56 and 74 are general and provide a good basis for estimating the performance of a traction contact with a known geometry. These solutions will be repeated here in part without theoretical justification. Those interested in the theoretical basis of the Johnson and Tevaarwerk analysis should consult references 48, 56, and 74.

6.3 Traction Contact Kinematics

Before detailed traction contact performance calculations can be made, the magnitude of the local slip velocities within the contact must be determined. It is these slip velocities that are responsible for the traction force patterns appearing in figure 23. The differential velocities generated within the contact consist of longitudinal creep or slip ΔU, side slip ΔV, and spin. Creep is the differential velocity ΔU in the rolling direction arising from the shear forces generated between the rollers across the lubricant film. The side-slip velocity ΔV is transverse to the rolling direction and is usually due to a misalignment between the rollers' axes of rotation. It is related to the average rolling velocity U by the expression

$$\frac{\Delta V}{U} = \tan \beta \tag{34}$$

where β is the misalignment angle.

Spin is the result of a mismatch in roller radii at contact points on either side of the point of pure rolling. It usually occurs in traction drives with conical rollers or rollers with nonparallel rotation axes. Spin is present in all variable-ratio drives at one or more positions of

operation. As previously discussed, the spin velocity causes a loss in power and also reduces the available traction coefficient. Furthermore contact spin can generate appreciable side forces similar to those that cause a spinning ball to roll along a curved path. Unlike side slip ΔV, the magnitude and direction of spin change across the contact, with steadily increasing spin velocities moving away from the center of the contact. However, the angular spin velocity ω_s remains constant about a line normal to the contact and joining the geometric centers of the driving and driven roller pairs. This line is not coincident with the "center of the contact area" because of the forward displacement of the pressure distribution with the formation of an elastohydrodynamic oil film (ref. 74).

Consider the general contact geometry of a pair of traction rollers as shown in figure 24 (from ref. 61). The ratio of spinning to rolling angular velocities is given by

$$\frac{\omega_s}{\omega_A} = \sin\theta - \frac{R_A}{R_B}\sin(\gamma-\theta) \tag{35}$$

where

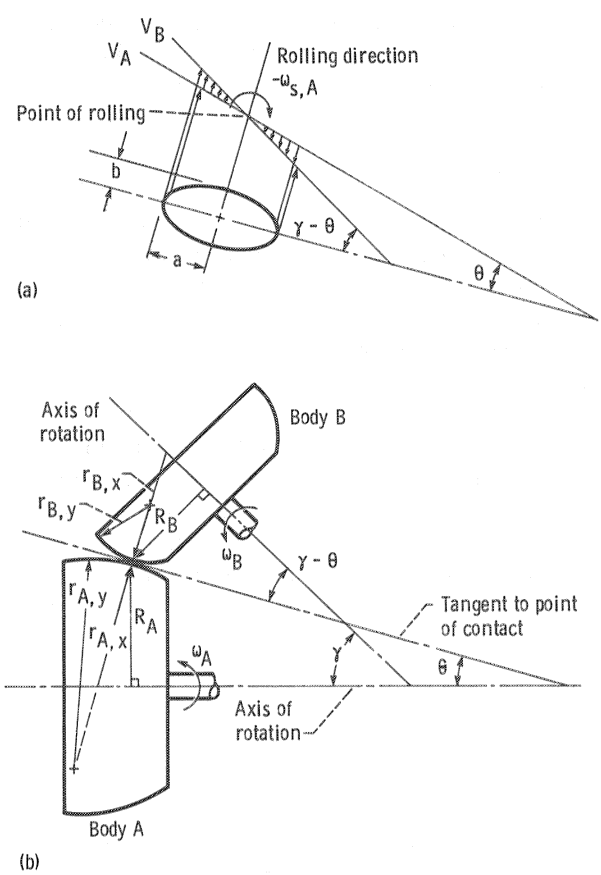

(a) Spin contact pattern on roller A.
(b) Contact geometry for spin calculations.

Figure 24.—Spin pattern and general contact geometry for spin calculations. (From ref. 60.)

ω_s angular spin velocity
ω_A angular rolling velocity of body A
γ included angle between rotation axes
θ included angle between rotation axis of body A and tangent to point of contact

and where R_A and R_B are the rolling radii of bodies A and B, respectively. The principal rolling radii $r_{A,x}$ and $r_{B,x}$, which are normal to the plane of contact, and the principal transverse radii $r_{A,y}$ and $r_{B,y}$ shown in figure 24 are used to calculate the contact area, stress, and fatigue life as discussed in section 4.0.

For traction contact performance calculations the ratio of angular spin to rolling velocity ω_s/U is useful to know. Noting that $U=\omega_A R_A$, this ratio can be deduced from equation (35) as follows:

$$\frac{\omega_s}{U} = \frac{\sin\theta}{R_A} - \frac{\sin(\gamma-\theta)}{R_B} \tag{36}$$

For a variable-ratio traction drive the rolling radii of one or both bodies or the spin angle will change with a change in speed ratio. Equation (36) can be used to compute the amount of spin at each position. Setting equation (36) to zero shows that two conditions result in zero spin:

$$\gamma=\theta=0$$

and

$$\frac{R_A}{R_B} = \frac{\sin\theta}{\sin(\gamma-\theta)}$$

The first condition is the trivial solution for two parallel, crowned cylinders. The second condition corresponds to the case where the tangent to the point of contact intersects the point where the rotation axes of bodies A and B cross (i.e., a tapered bearing or bevel gear). Although variable-speed drives can be constructed to achieve zero spin at one or more points, there will always be intermediate positions of operation where one of these conditions will not be satisfied. A wide variety of spin-producing geometries can be devised, as illustrated in figure 25. The greatest spin is for $\theta=\pm 90°$ and $\gamma=0°$, which corresponds to two disks with parallel, offset rotation axes making face contact.

6.4 Dimensionless Traction Parameters

In the Johnson and Tevaarwerk model (refs. 56 and 74) several dimensionless parameters are identified that best generalize the results of their analysis. These parameters can be written in terms of the fundamental shear modulus and limiting shear stress properties of the lubricant or in terms of the measured initial slope m and peak traction coefficient μ from a simple experimental traction curve

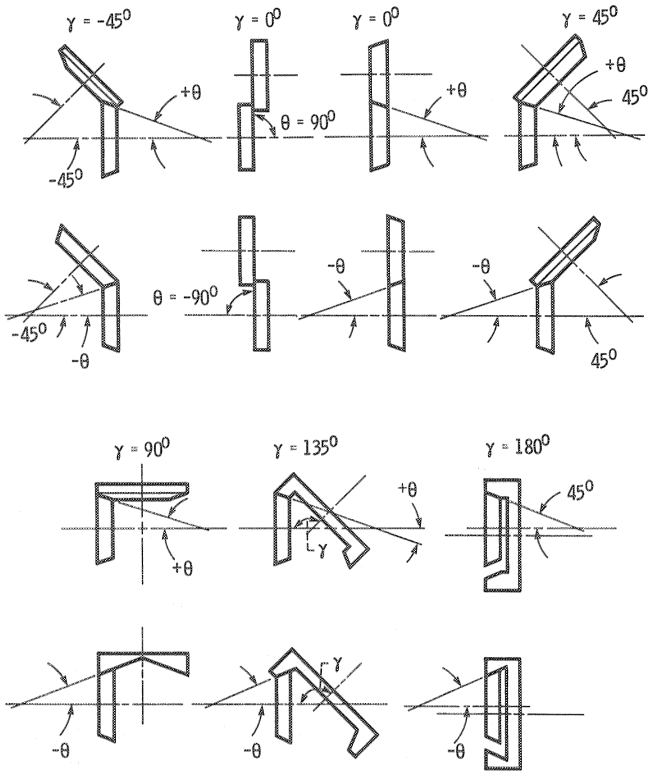

Figure 25.—Representative spin-producing geometries.

(fig. 26). At this time it is more reliable to work with actual traction data than with fundamental fluid property data. Fluid property data are usually generated under experimental conditions that are much different than those in a traction contact. For the Johnson and Tevaarwerk dimensionless groupings slope and traction coefficient data must be obtained from a zero-side-slip, zero-spin traction curve for the lubricant in question. These reference data must also be obtained at the same contact pressure, temperature, and surface velocity and for the same contact ellipse ratio, area, and disk material as the contact to be analyzed. Approximate compliance corrections to the slope can be made, however, if the ellipse ratio and contact area of the reference data are

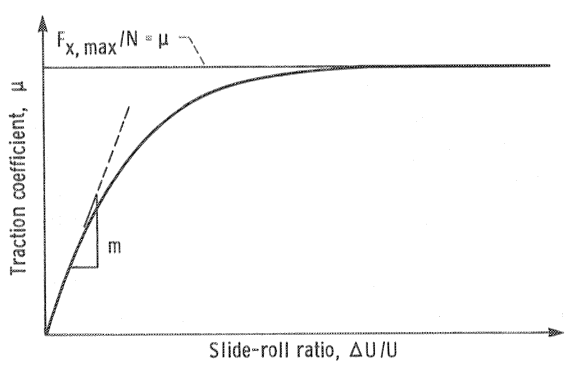

Figure 26.—Typical isothermal traction curve showing maximum traction coefficient and traction slope.

different from those of the contact to be evaluated. Traction data of two common traction fluids over a wide range of operating conditions appear in section 7.2.

With the Johnson and Tevaarwerk analysis, knowing just m and μ from a simple traction test leads to the prediction of the entire traction-versus-creep curve under any combination of side slip and spin provided that thermal heat effects are not large ($J_3 \lesssim 30$). Otherwise thermal corrections should be applied (refs. 75 and 76). The traction force perpendicular to the rolling direction and contact power losses can also be readily determined.

The solutions to this analysis are given in terms of the following dimensionless parameters:

Slip

$$J_1 = C\frac{\Delta U}{U} \tag{37}$$

Side slip

$$J_2 = C\frac{\Delta V}{U} \tag{38}$$

Spin

$$J_3 = C\frac{\omega_s\sqrt{ab}}{U} \tag{39}$$

Traction

$$J_4 = \frac{\mu_x}{\mu} \tag{40}$$

Side traction

$$J_5 = \frac{\mu_y}{\mu} \tag{41}$$

Torque normal to the contact

$$J_6 = \frac{T_0}{\mu Q\sqrt{ab}} \tag{42}$$

Total power loss

$$J_7 = J_4J_1 + J_5J_2 + J_6J_3$$

$$= \frac{C}{\mu QU}(F_x\Delta U + F_y\Delta V + T_0\omega_s) \tag{43}$$

where C is the lubricant contact parameter

$$C = \frac{3\pi}{8}\frac{m}{\mu}\sqrt{k} \tag{44}$$

The power loss term J_7 can be put in a more convenient form in terms of a loss factor LF, where

$$\mathrm{LF}=\frac{J_7}{J_4}=C\left(\frac{\text{Power loss}}{\text{Power input}}\right) \tag{45}$$

The ratio of power loss to power input can thus be determined by inverting equation (45) after finding the lubricant contact parameter C and the loss factor LF for the contact being analyzed.

6.5 Effect of Slip, Side Slip, and Spin on Traction

The graphical solutions appearing in references 56 and 74 can be used to predict the influence of slip, side slip, and spin on the traction available in the x (rolling) direction. Figure 27 shows the theoretical effects of slip and spin at various contact ellipse ratios. Figure 28 shows the effect of slip and side slip at $k=1$. Both figures are, in effect, theoretical traction curves. It is apparent from figure 27 that spin tends to increase slip except at low spin values ($J_3 \lesssim 0.3$). At low spin most of the contact is being strained elastically (energy is recoverable), so there is little adverse effect. If no spin is present and there is no side slip, a simple relation exists between traction J_4 and slip J_1 of the form

$$J_4=\frac{2}{\pi}\left(\tan^{-1}S+\frac{S}{1+S^2}\right) \tag{46}$$

where

$$S=\frac{2}{3}\frac{J_1}{\sqrt{k}}$$

It can be observed from equation (46) that contacts with small values of k, and hence larger values of S, will have better traction. The traction in the contact is directly related to the total lubricant strain. Since low-ellipse-ratio contacts have longer contact lengths in the direction of rolling, they permit a higher buildup strain and hence more traction.

Figure 28 shows that side-slip velocities J_2 tend to reduce traction in the rolling direction. The side-slip velocity (misalignment) reorients the traction force vector away from the rolling direction. This traction force vector J^* is resolved into a traction component in the rolling direction J_4 and a side traction component J_5. These components can be calculated by the following expressions:

$$J_4=\frac{J_1}{\left(J_1^2+J_2^2\right)^{1/2}}J^* \tag{47}$$

$$J_5=\frac{J_2}{\left(J_1^2+J_2^2\right)^{1/2}}J^* \tag{48}$$

where

$$J^*=\frac{2}{\pi}\left(\tan^{-1}S+\frac{S}{1+S^2}\right)$$

and where

$$S=\frac{2}{3}\left(\frac{J_1^2+J_2^2}{k}\right)^{1/2}$$

Under the condition of pure spin (i.e., no slip) the total strain on the fluid film in a contact perpendicular to the rolling direction steadily increases in the inlet region, reaches a maximum, and then steadily decays to zero at the outlet of the contact. This accumulated axial strain gives rise to side traction J_5, which can be a significant fraction of the maximum traction coefficient, particularly for contacts with low ellipse ratios. The maximum value of J_5 under pure spin conditions is shown in figure 29. At a given k the magnitude of J_5 will increase with spin, reach a maximum, and then decrease for increasing spin as elastic effects diminish. This can be seen from figure 30 for $k=1$. Increasing slip in the rolling direction has a relatively minor effect on J_5 until the slip reaches some value where elastic effects are negligible. At this point there is a precipitous drop in the side traction.

It is clear from equations (40) and (41) that multiplying the computed values of J_4 and J_5 by the maximum available traction coefficient will give the appropriate values of μ_x and μ_y at any slip, side-slip, or spin condition. If significant spin is present ($J_3 \gtrsim 30$), it is likely that thermal heating will cause some reduction in the value of μ. Using the value of μ under the spin condition present, if such data are known, to correct J_4 and J_5 will yield the most accurate results. Data of this type are given for two traction fluids in section 7.2. Analytical methods to account for thermal effects in the film can be found in references 75 and 76.

6.6 Traction Contact Power Loss

Ignoring the rolling traction loss for the moment, the losses in a traction contact have three components: longitudinal slip, side slip, and spin as given by equation (43). By ratioing the dimensionless contact loss term J_7 to the longitudinal traction term J_4, we can establish a loss factor LF as given by equation (45).

Figure 31 shows the effects that traction J_4 and spin J_3 have on LF at k of 1, 4, and 8 for no misalignment ($J_2=0$). Small amounts of spin tend to have a relatively minor effect on power loss because the lubricant film is

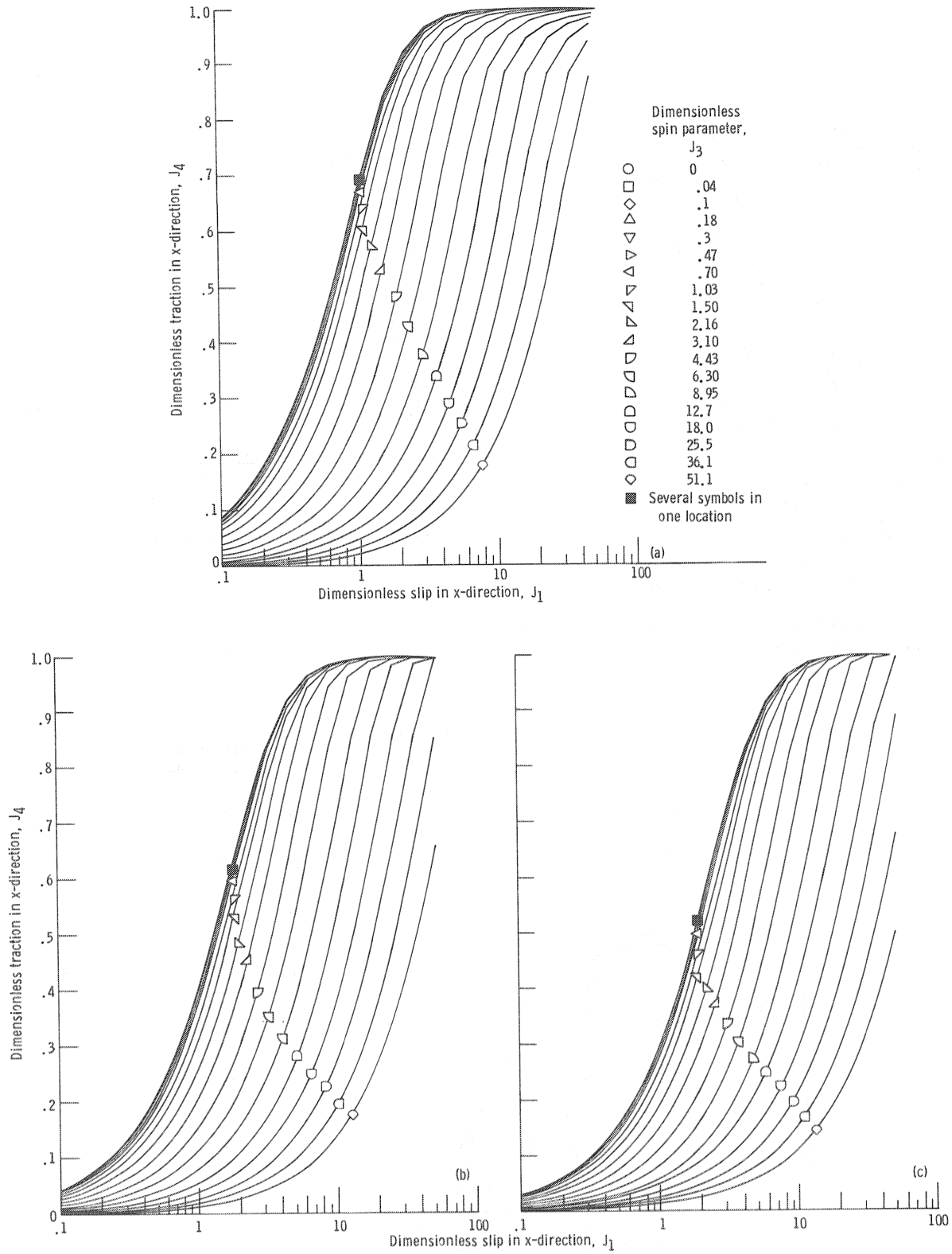

(a) $k = 1$.
(b) $k = 4$.
(c) $k = 8$.

Figure 27.—Traction as function of slip for various values of spin and ellipse ratio k.

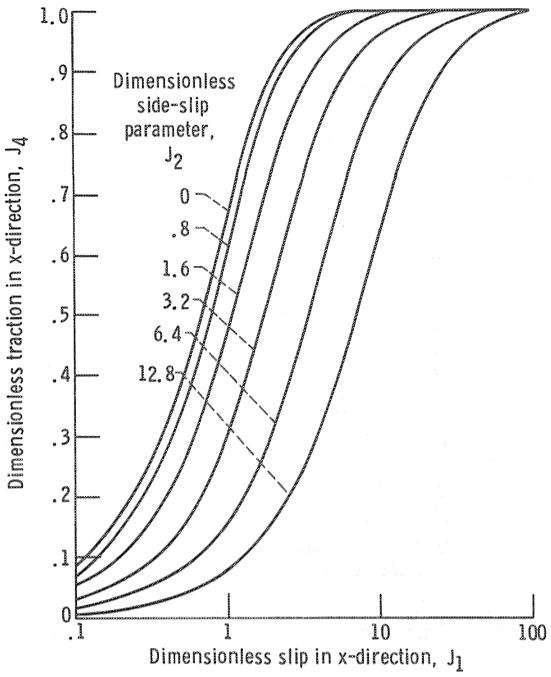

Figure 28.—Dimensionless traction curves for combined slip and side slip as function of slip for an ellipse ratio of 1.

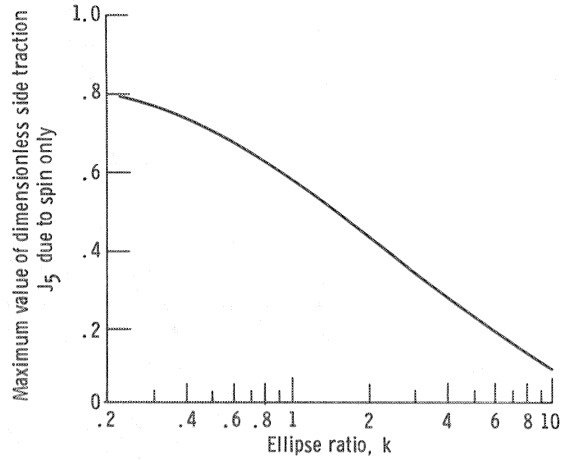

Figure 29.—Maximum side force as function of ellipse ratio for contacts under spin only.

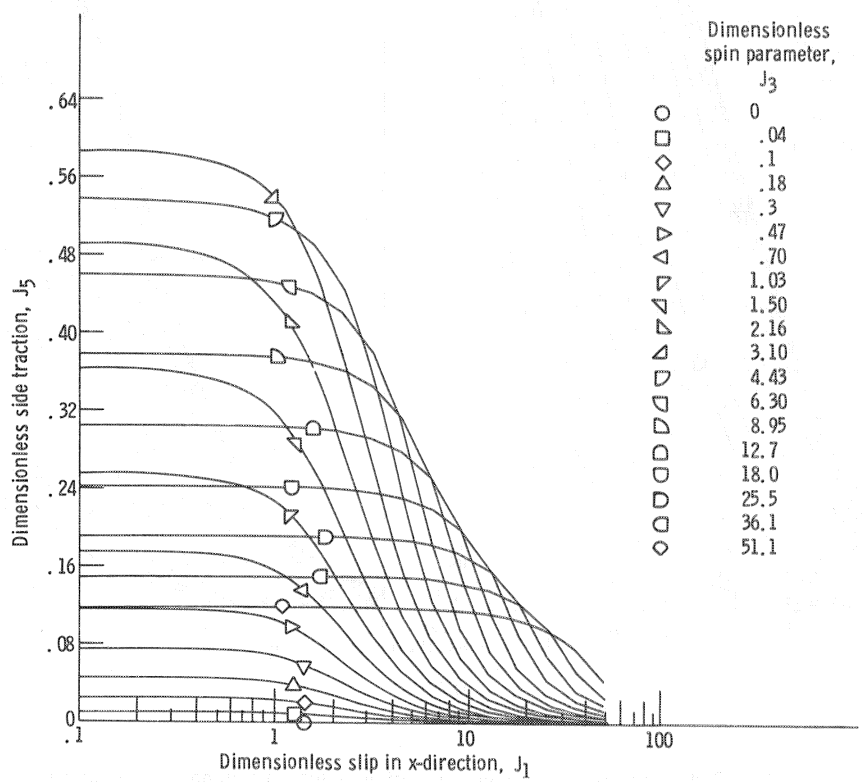

Figure 30.—Traction as function of slip for various values of spin and an ellipse ratio of 1.

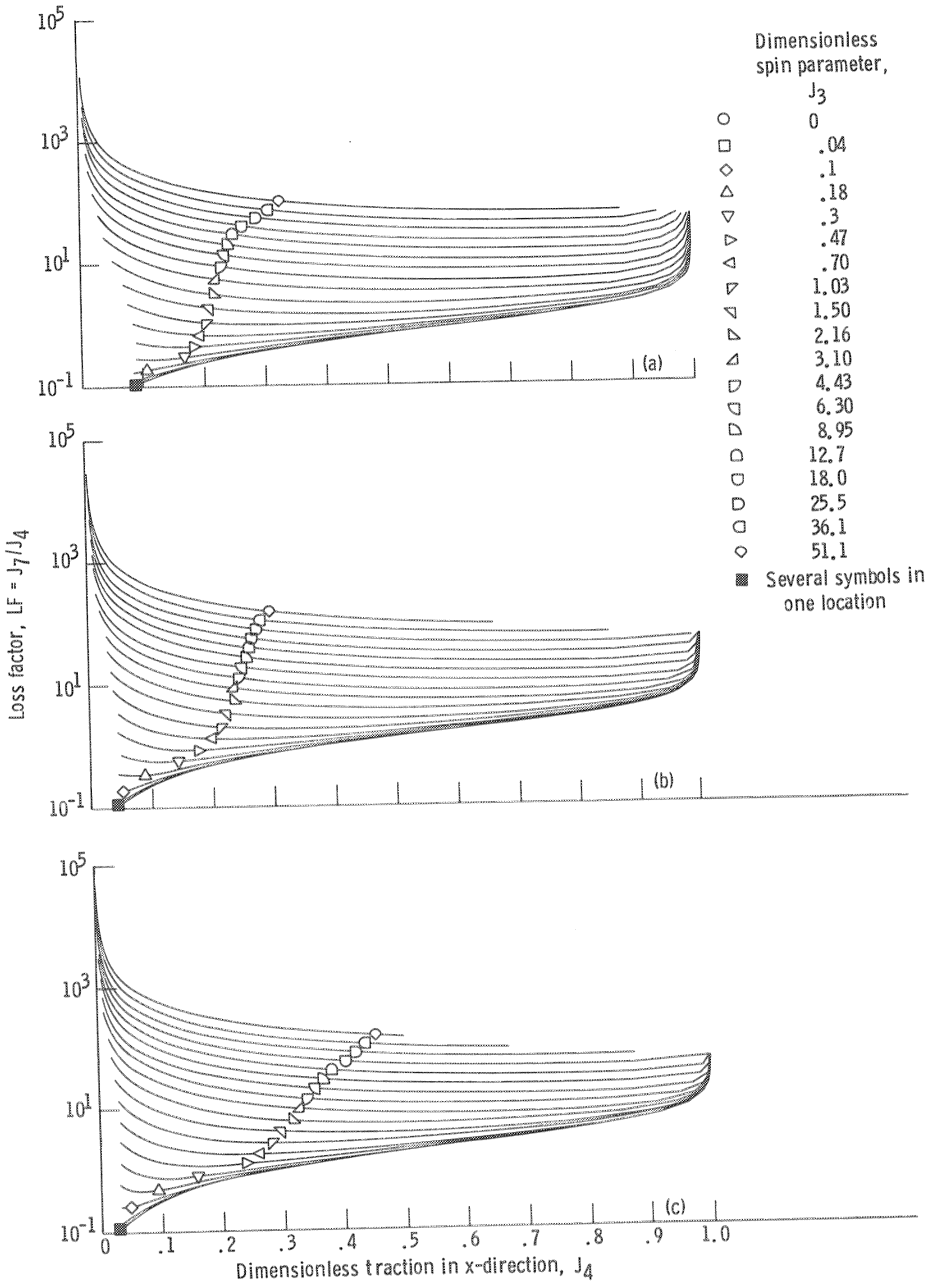

(a) $k = 1$.
(b) $k = 4$.
(c) $k = 8$.

Figure 31.—Loss factor as function of traction at various values of spin and ellipse ratio k.

being sheared elastically. Beyond a certain threshold value of spin inelastic behavior dominates and increasing spin causes higher contact losses.

In most traction drives a mechanism is used to automatically adjust the normal load in direct proportion to the transmitted force. The result is that the traction coefficient in the contact μ_x is forced to be a constant. The geometry of the loading mechanism, as discussed in section 9.0, is selected to be some fraction, typically 70 to 80 percent, of the maximum traction coefficient available under the most unfavorable operating conditions. This provides some safety margin from slipping. Under operating conditions where the available traction is high, such as at low speeds and temperatures, the ratio of the applied traction coefficient μ_x to the maximum available traction coefficient μ, or in other words J_4, is relatively low. Under less favorable operating conditions the available traction decreases and J_4 becomes larger. The effect of J_4 on contact performance is shown in figure 31. At low spin lower J_4 values result in higher contact efficiency (i.e., lower loss factor LF); at higher spin there is either no change or a small decrease in efficiency.

At a constant J_4 of 0.75 imposed spin has little or no influence on the loss factor LF at low spin, as can be seen from figure 32. The losses in the contact at low spin are basically those due to creep. From a design point of view spin J_3 up to approximately 1 can be allowed without ill effects. At higher spin LF increases directly with spin as the lubricant film in the contact yields plastically. Contacts with high ellipse ratios tend to have higher creep losses and hence a higher loss factor at low spin. At high spin, however, LF is a minimum for $k=1$ and increases with k values that are either higher or lower (fig. 18).

6.7 Other Contact and Drive Losses

The Johnson and Tevaarwerk method that was just outlined will provide a reasonable estimate of the losses in a traction contact transmitting power. However, these losses, while obviously significant, are not the only losses to be considered when assessing the performance of a traction drive. Some traction drive designs require large support bearings through which some or all of the clamping loads between roller components must pass. The power losses associated with these bearings can be as great or greater than the contact losses. As previously mentioned, in Gaggermeier's experimental investigation (ref. 53) with the Arter type of toroidal drive, the load-dependent bearing losses were comparable to the contact losses due to power transfer. The drive idling (no load) losses were as large or larger than both of these losses combined. These idling losses include oil splashing losses,

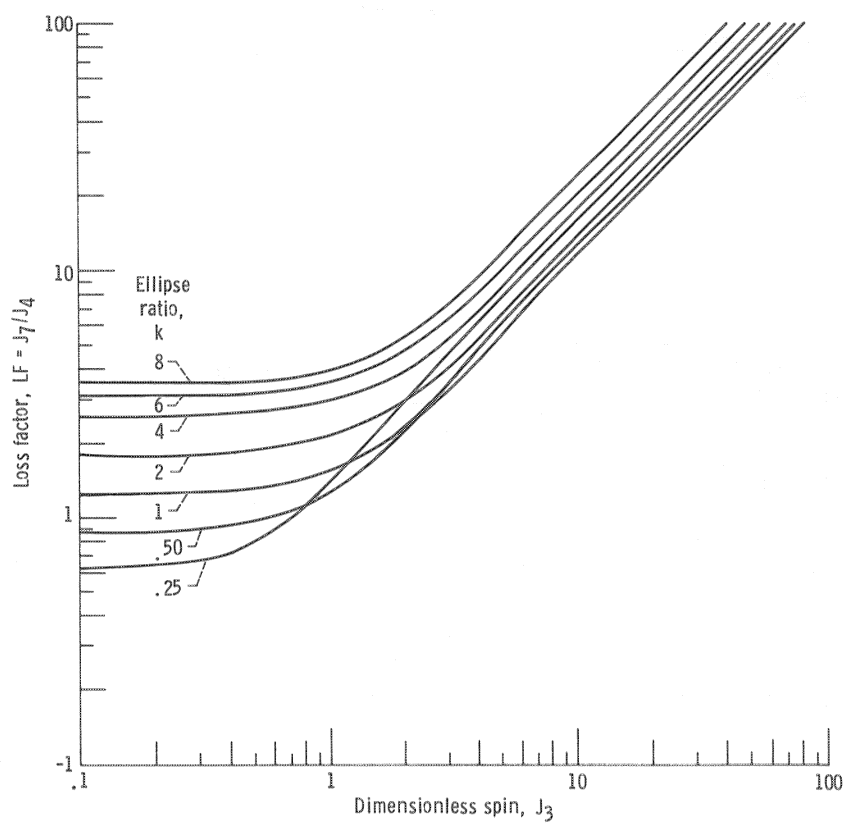

Figure 32.—Loss factor as function of spin and ellipse ratio. Dimensionless traction parameter in x direction, $J_4 = 0.75$.

air windage, seal drag, and those losses in the traction rollers and bearings that are independent of transmitted load. Although empirical or semiempirical methods have been developed for predicting rolling-element and fluid-film bearing losses (e.g., refs. 39 and 77 to 79) the prediction of these other losses is not as clearly defined. Their determination is best left for actual testing of the drive unit under no load with the exception of the rolling loss of the traction rollers themselves. This loss is primarily due to the resistance encountered in the formation of an EHD film and the attendant buildup of hydrodynamic pressure. The experimental work of Crook (ref. 80) helped establish that the rolling traction F_r for a contact of length l is given by

$$F_r = 9 \times 10^7 h_c l \tag{49}$$

where

F_r rolling traction force, N
h_c central film thickness (from eq. (12)), m
l length of line contact, m

In terms of power loss equation (49) can be written

$$P_r = 9 \times 10^7 h_c l U \tag{50}$$

where

P_r rolling traction power loss, W
U average surface velocity, m/sec

The rolling traction losses normally become significant at relatively high speeds (>50 m/sec). But even at lower speeds they can be an appreciable percentage of the drive idling losses.

In addition to the rolling traction loss there is a normally small hysteresis loss. The hysteresis loss is the difference between the energy needed to compress the roller material in the Hertzian contact and that returned to the system as the surface returns to its undeflected state. The hysteresis resistance is defined by Greenwood and Tabor (ref. 81) by the expression

$$\frac{F_h}{Q} = \frac{3}{16} \frac{b}{R_x} \varphi \tag{51}$$

where φ is the hysteresis loss factor of the material, normally about 1 percent for hard steel, and b is the contact ellipse radius in the rolling direction. For steel and many other highly elastic materials the hysteresis component of power loss is relatively insignificant and can normally be neglected.

7.0 Fluid Traction Properties

7.1 Traction Fluids

Because of the importance of the traction coefficient to the life, size, and performance of a traction drive, considerable attention has been given to identifying fluids with high traction properties, starting in the late 1950's with Lane's experiments (ref. 82). Hewko (ref. 47) obtained traction performance data that indicated that the lubricant composition and surface topography had the greatest overall effects on traction and that naphthenic mineral oils gave better performance than paraffinic oils.

Some of these early investigations led to the development of commercial traction fluids. Reference 83 describes the development of a formulated traction fluid, designated as Sunoco Traction Drive Fluid 86. This fluid evolved into Sun Oil's TDF-88, a commercial traction fluid currently available on a limited basis. Hamman, et al. (ref. 84) in examining some 26 test fluids identified several synthetic fluids that had up to 50 percent higher traction coefficients, depending on test conditions, than those reported for the best naphthenic oils. This research laid the groundwork for the development of Monsanto's family of commercial traction fluids (Santotrac-30, 40, 50, and 70). These fluids are the most widely used traction oils today. Accelerated five-ball fatigue tests (ref. 85) indicate that these synthetic cycloaliphatic traction fluids have good fatigue life performance, comparable to that of the reference tetraester oil used in this experiment. A recent addition to the commercial traction fluid market has been produced by the Mitsubishi Oil Co., Ltd. Their Diamond Traction Fluid, marketed in three viscosity grades, is said to offer high traction coefficients, good wear, and antioxidation properties.

It should be kept in mind that, although the use of traction fluids is preferable, it is not mandatory. This is best illustrated by the experiments of Gaggermeier (ref. 53) in which traction coefficients for 17 lubricants were measured on a twin-disk traction tester at both high and low contact pressures and surface speeds. The traction fluids in his tests showed substantially higher traction coefficients than any of the commercial naphthenic mineral oils tested. The greatest differences occurred at relatively low pressures and high surface speeds (fig. 33). At relatively high pressures and low speeds the traction fluids showed less of an advantage. Under such conditions a good-quality naphthenic mineral oil would serve almost as well. For most traction drive applications, however, there is considerable incentive to using a

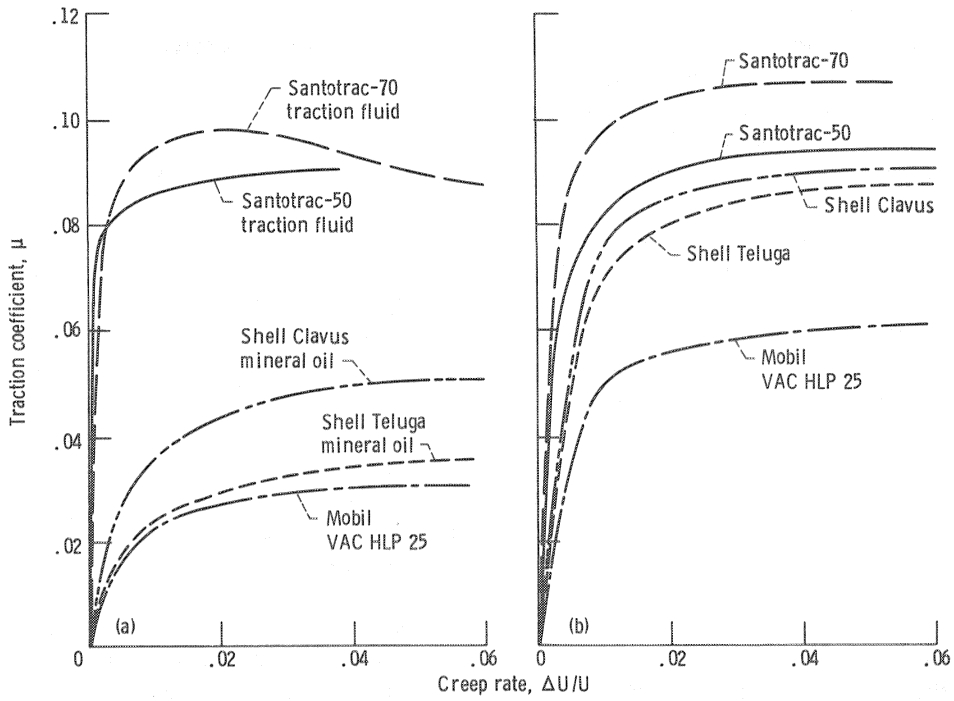

(a) Low pressure and high speed. Maximum Hertz pressure, 1.09 GPa; surface velocity, 8.3 m/sec.
(b) High pressure and low speed. Maximum Hertz pressure, 1.86 GPa; surface velocity, 0.83 m/sec.

Figure 33.—Traction characteristics of traction fluids and oils. Oil inlet temperature, 50 °C. (From ref. 45.)

traction fluid, with expected traction improvements falling somewhere between the two examples of figure 33.

7.2 Traction Fluid Data

To apply the Johnson and Tevaarwerk analysis to the design of a traction contact, the initial slope m and the maximum traction coefficient μ must be determined under the appropriate operating conditions. Experimental traction data of this type were analyzed in reference 49 for Santotrac-50 and TDF-88 traction fluids over the range of operating conditions that might be encountered in a traction drive. The properties of these lubricants are given in table II. A regression analysis applied to the data (refs. 49 and 86) resulted in the following correlation equation, which can be used to predict the initial slope (at zero spin only) and the maximum traction coefficient μ. The correlation is of the form

$$\mu = C_1 + C_2\sigma_0 + C_3\sigma_0^2 + C_4U + C_5U^2 + C_6\tilde{T} + C_7k + C_8\frac{\omega_s\sqrt{ab}}{U}$$

$$m = C_1 + C_2\sigma_0 + C_3 \ln \sigma_0 + C_4U + C_5U^2 + C_6\tilde{T} + C_7k \tag{52}$$

where

TABLE II.—TRACTION LUBRICANT PROPERTIES

Property	Santotrac-50	TDF-88
	Lubricant description	
Kinematic viscosity, cm²/sec at–		
37.8 °C	0.34	0.42
100 °C	0.056	0.054
Flashpoint, °C	163	209
Fire point, °C	174	220
Autoignition temperature, °C	316	----------
Pour point, °C	−37	−37
Specific heat at 37.8 °C, J/kg K	2130	1895
Thermal conductivity at 37.8 °C, J/m sec °C	0.10	0.11
Specific gravity at 37.8 °C	0.889	0.888

σ_0 maximum contact stress, GPa
U average rolling velocity, m/sec
$\tilde{T}$ lubricant inlet temperature, °C

and the correlation coefficients are given in table III. These correlation coefficients are based on 73 and 101 initial slope data points and 187 and 147 traction coefficient data points for the Santotrac-50 and TDF-88 fluids, respectively. The correlation's regression coefficient, a measure of the accuracy of the regression and the scatter of the test data, is greater than 0.82 for

TABLE III.—CORRELATION COEFFICIENTS FOR SANTOTRAC-50 AND TDF-88

Coefficient	Santotrac-50	TDF-88	Santotrac-50	TDF-88
	Initial slope, m		Maximum traction coefficient, μ	
C_1	101.4	51.3	0.0726	0.0733
C_2	−45.49	−6.53	.0477	.0443
C_3	69.44	17.20	−.0102	−.0116
C_4	−.289	−.646	-6.92×10^{-4}	-7.36×10^{-4}
C_5	1.30×10^{-3}	4.99×10^{-3}	2.47×10^{-6}	2.38×10^{-6}
C_6	6.63×10^{-2}	.236	-2.13×10^{-4}	-9.08×10^{-5}
C_7	−2.99	−1.24	-3.41×10^{-4}	-1.88×10^{-3}
C_8	----------	---------	−1.22	−.443

slope and greater than 0.88 for traction coefficient for either fluid. (A correlation coefficient of 0 indicates no correlation; a value of 1.0 indicates a perfect correlation.)

The likely usable range of the correlation is

σ_0, GPa ..... 1.0 to 2.5
U, m/sec ..... 1.0 to 100
$\tilde{T}$, °C ..... 30 to 100
k ..... 0.5 to 8
$\omega_s\sqrt{ab}/U$ ..... 0 to 0.04

Slope correction.—The initial slope m of an experimental traction curve is a measure of the tangential stiffness of the lubricant film and metal surface combination. The initial slope is related to the apparent elastic shear modulus of the contact system $\bar{G}$ by the expression

$$m=\frac{4}{\pi}\frac{\bar{G}}{\sigma_0}\frac{b}{h_c}$$

Therefore two systems with the same apparent shear modulus operating at the same pressure, temperature, velocity, and ellipse ratio will have different initial slopes m if their contact semiwidths b in the rolling direction or their EHD film thicknesses h_c are different.

Reference 85 shows that at constant operating conditions $h_c\propto(R_x)^{0.33}$ and $b\propto R_x$, where R_x, the equivalent rolling radius of the bodies, is proportional to the size of the bodies (eq. (3)). Thus, to use slope data generated experimentally with traction rollers of one size (parameters without asterisks) to predict the performance of a second set of rollers running under the identical operating conditions but of a different size (parameters with asterisks), a slope correction factor m^*/m must be applied to the slope calculated in equation (52). The slope correction factor is the ratio of the two initial slopes and for steel rollers can be found from the expression

$$\frac{m^*}{m}=\left\{\left(\frac{R_x}{R_x^*}\right)^{0.67}+7.66\times10^{-3}m\sigma_0e^{-0.21/k}\times\left[1-A\left(\frac{R_x}{R_x^*}\right)^{0.67}\right]^{-1}\right\} \tag{53}$$

where $A=1.43-0.383/k+0.0995/k^2$.

The slope data correlation presented in the previous section were generated with disks having an equivalent radius R_x of 22.57 mm for the Santotrac-50 data and 12.50 mm for the TDF-88 data. Figure 34 gives m^*/m factors to apply to m calculated from equation (55) for each of these fluids as a function of the ellipse ratio k and the contact factor $m\sigma_0e^{-0.21/k}$, where σ_0 is the maximum contact pressure in gigapascals.

7.3 Effect of Operating Conditions

From a large body of traction data generated on a twin-disk tester (refs. 47, 49, 53, 87, and 88), it was found that an increase in contact pressure is beneficial to the available traction coefficient but that increases in surface velocity, temperature, ellipse ratio, misalignment, or spin (circumferential slip) have a negative effect. Figures 35 and 36 show the typical effects that pressure and speed have on the maximum traction coefficient and initial slope, respectively, on the basis of the correlation given in equation (52) for Santotrac-50. It is clear that low speed and high pressure benefit both parameters. However, if contact pressures are too high, fatigue life suffers. Similarly, low surface velocities will produce thin EHD films that can result in wear and also shorten fatigue life.

8.0 Performance Calculation Example

To illustrate the application of the performance methods outlined in this report, an example performance calculation will be performed. The traction contact to be

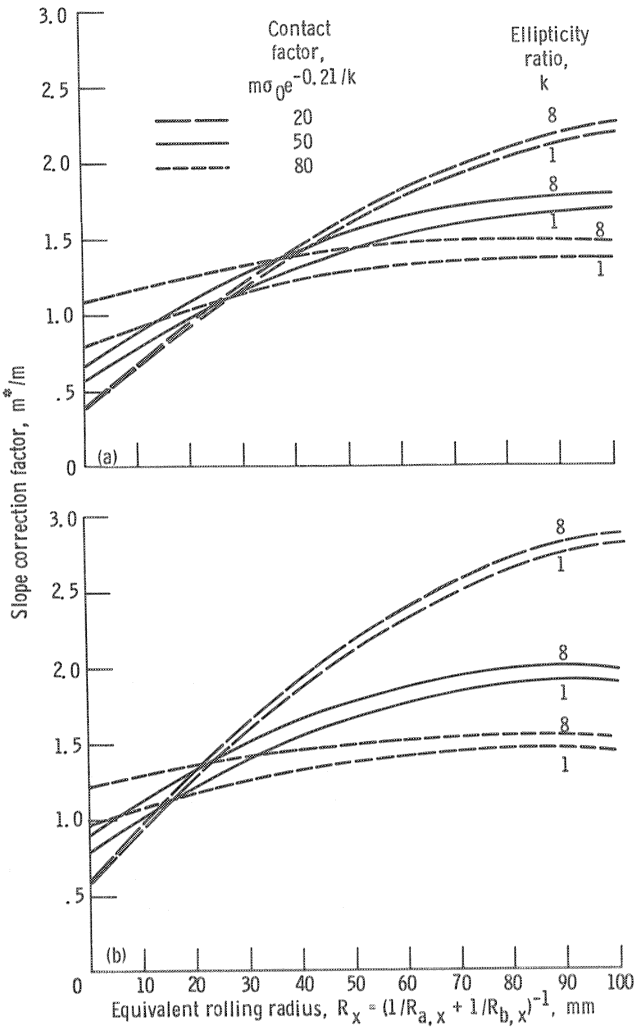

(a) Santotrac-50 traction fluid.
(b) TDF-88 traction fluid.

Figure 34.—Correlation of size effects using slope correction factor.

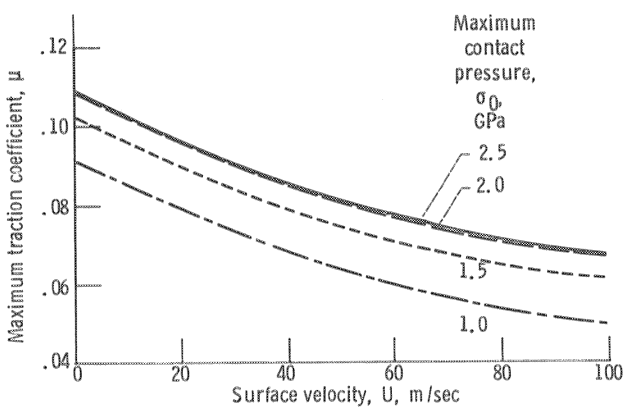

Figure 35.—Maximum traction coefficient as function of surface velocity, predicted from Santotrac-50 correlation. Oil inlet temperature, 80 °C; ellipse ratio, 5; spin, zero.

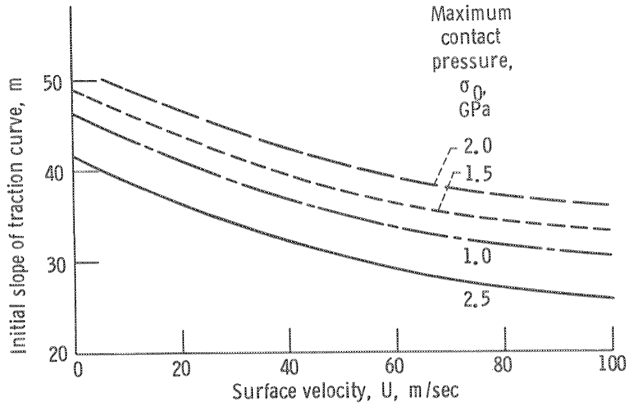

Figure 36.—Initial slope as function of surface velocity, predicted from Santotrac-50 correlation. Oil inlet temperature, 80 °C; ellipse ratio, 5; spin, zero.

analyzed will be modeled after the test disks of Gaggermeier (ref. 53) in order that the predicted results can be compared with independently generated test data. In one set of tests traction-versus-slip curves were generated under three levels of spin for Santotrac-50 at a constant normal load Q of 1900 N, a constant disk temperature of 50 °C, and a constant surface velocity U of 8.4 m/sec. Three sets of test disks with the geometry shown in figure 37 but differing cone angles of 0°, 20°, and 30° were used to vary the contact spin. It will be instructive to determine the effect that spin has on the traction-versus-slip characteristics and the performance of this traction contact. Thus $R_x = 0.02$ m and $R_y = 0.04$ m from equations (3) and (10), respectively.

8.1 Contact Stress, Shape, and Size

For the bodies shown in figure 37, $r_{A,x} = r_{B,x} = r_{B,y} = 0.04$ m and $r_{A,y} = \infty$. From equation (17) it follows that $\rho = 75$ m^{-1} and from equation (16) that $g = 6.93 \times 10^{-4}$ m for steel bodies with $Q = 1900$ N. Using the ellipse ratio approximation $k = a/b = 1.6$ from equation (9) in figure 11 gives the dimensionless contact semiaxes $a^* = 1.3$ and $b^* = 0.8$. Multiplying a^* and b^* by

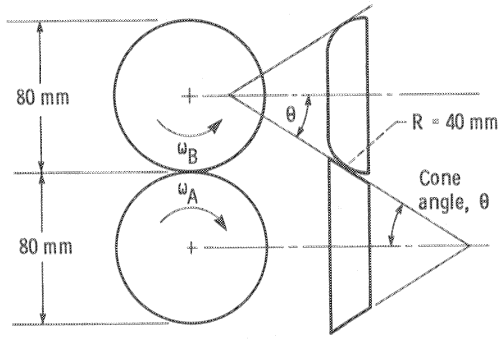

Figure 37.—Steel test disks for Gaggermeier's traction experiments for ellipse ratio of 1.6. (From ref. 53.)

g according to equation (14) yields $a=9.0\times10^{-4}$ m and $b=5.5\times10^{-4}$ m. Thus $k=a/b=1.6$. The maximum Hertz stress can now be found from equation (13) to be $\sigma_0=1.8$ GPa.

8.2 Traction-Versus-Slip Characteristics

Traction in x direction.—To determine the dimensionless spin parameter J_3 for the 0°, 20°, and 30° disks, the magnitude of the ω_s/U parameter must first be calculated from equation (36) for $\gamma=0°$ and $\theta=0°$, 20°, and 30°. Doing this yields $\omega_s/U=0$, 17.1, and 25.0 m^{-1}, respectively. Multiplying by $\sqrt{ab}$ gives $\omega_s\sqrt{ab}/U=0$, 0.0120, and 0.0176, respectively.

Next the traction contact parameter C is calculated from equation (44) by computing μ and m from the Santotrac-50 correlation shown in equation (52) for $k=1.6$, $\sigma_0=1.8$ GPa, $\tilde{T}=50$ °C, $U=8.4$ m/sec, and $\omega_s\sqrt{ab}/U=0$. This gives $\mu=0.109$ and $m=56.5$. Correcting slope m for size from either figure 34 or equation (53) gives the slope correction factor $m^*/m=1.17$. Thus the corrected slope $m^*=1.17\times56.5=66.1$, and from equation (44)

$$C=\frac{3\pi}{8}\left(\frac{66.1}{0.109}\right)\sqrt{k}=904$$

Therefore from equation (39) for $\theta=0°$, 20°, and 30° $J_3=0$, 10.8, and 15.9, respectively.

The curves in figure 27 can be used to develop μ_x-versus-$\Delta U/U$ curves by taking small increments of $\Delta U/U$, computing the corresponding incremental slip values J_1 from equation (37), and looking up the appropriate incremental traction values J_4 at the spin level J_3 of interest. This is done for $k=1.6$ by interpolating between J_4 at $k=1$ (fig. 27(a)) and J_4 at $k=4$ (fig. 27(b)). To find the incremental μ_x values from equation (40), the J_4 values found are then multiplied by the appropriate maximum traction coefficient μ at the spin level of interest. For this example, for the Santotrac-50 correlation of equation (52), $\mu=0.109$, 0.094, and 0.088 at the spin levels corresponding to 0°, 20°, and 30°, respectively.

Plotting the computed incremental μ_x values versus the chosen incremental $\Delta U/U$ values results in the traction-versus-creep-rate curves shown in figure 38. Included for comparison are the actual test data points from Gaggermeier's experiments (ref. 53). The calculated traction is about 10 percent higher than that measured at the no-spin condition but shows good agreement at the other two levels of spin. The available traction coefficient is significantly reduced with spin, and more slip occurs.

Traction in y direction.—The calculation just performed considers only the traction occurring in the x, or rolling, direction. Spin generates a side traction force

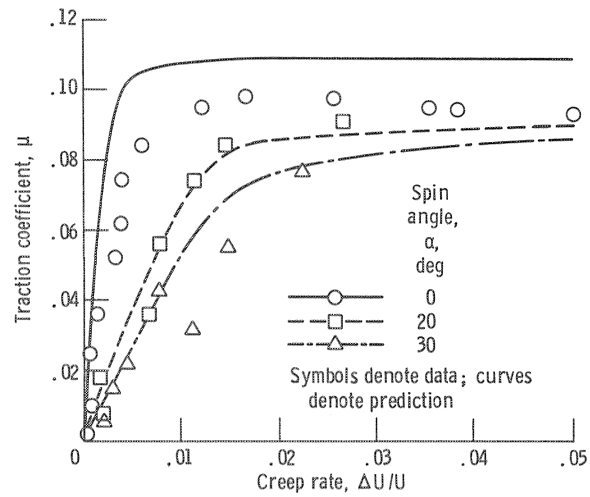

Figure 38.—Comparison of calculated traction-versus-creep-rate curves with Gaggermeier's test data (ref. 53). Traction fluid, Santotrac-50; maximum Hertz pressure, 1.8 GPa; surface velocity, 8.4 m/sec ; oil inlet temperature, 50 °C; ellipse ratio, 1.6.

J_5. The maximum magnitude of this traction can be found from figure 30 at the given three levels of spin, $J_3=0$, 10.8, and 15.9. The peak J_5 values for $k=1$ are, respectively, $J_5=\mu_y/\mu=0$, 0.34, and 0.26. The J_5 values for $k=1.6$ would be slightly higher. The maximum side force F_y due to spin is approximately 34 and 26 percent of the maximum tangential traction force F_x at the given operating condition.

8.3 Power Loss

Contact loss.—The expected traction power loss of the contact can be estimated at the three selected levels of spin. For the purposes of calculation, assume that an automatic loading mechanism is installed that applies a constant traction coefficient μ_x of 0.07 under all operating conditions.

The loss factor LF is found for $k=1.6$ from an interpolation between figures 31(a) and (b) at the appropriate J_4 slip value and J_3 spin value. Equation (45) is then solved to find the ratio of power loss to power input. The results, presented in table IV, show that traction contact losses increase rapidly with spin. The losses at zero spin are quite small, being entirely due to the small predicted slip. The test data in figure 38 suggest that the measured slip and hence power loss at $\mu_x=0.07$ would be somewhat larger than predicted.

It is instructive to determine the effects of a small amount of misalignment, say $\beta=0.25°$, on the computed results. For the zero spin case $C=904$, so $J_2=3.94$ from equations (34) and (38). Equation (47) can be used to iteratively determine J_1, which provides the required $J_4=0.64$. Having found J_1, then J_5 can be calculated from equation (48) and J_7 from equation (43). Performing these calculations results in a loss factor LF

TABLE IV.—POWER LOSS

[Applied traction coefficient in x direction, μ_x, 0.07.]

Included angle, θ, deg	Dimensionless spin parameter, J_3	Maximum available traction coefficient, μ	Dimensionless traction parameter in x direction, J_4	Loss factor, LF	Ratio of power loss to power input
0	0	0.109	0.64	1.20	0.0013
20	10.8	.094	.74	12.9	.014
30	15.9	.088	.80	19.4	.021

of 7.97 from equation (45). Thus the power loss with just 0.25° of misalignment is about 6½ times that with the rollers perfectly aligned. Nevertheless the contact efficiency is still better than 99 percent.

The detrimental effects of misalignment will not always be as severe as this. If the local slip velocities in the contact are already appreciable, the additional side slip due to misalignment will have a lesser effect. This would be the case for lubricant contacts that are relatively soft (i.e., low slope m) and for those having significant spin. For example, adding a misalignment angle of 0.25° to the spin case where $\theta = 20°$ increases the power loss by only 10 percent. The conclusion to be drawn is that extremely efficient or low-slip contacts are particularly sensitive to the adverse effects of misalignment.

In addition to the contact traction loss losses due to support bearings, rolling traction, windage, and churning should also be considered. As discussed in section 6.7 these other losses are often as great as or greater than the contact losses.

Rolling traction loss.—By estimating the central EHD film thickness, the power loss due to rolling of the traction contact can be determined. For the operating conditions given, noting that $\alpha_p = 2.6 \times 10^{-8}$ (N/m^2)$^{-1}$ (ref. 89) and $\eta_0 = 1.94 \times 10^{-2}$ N sec/m^2 at 50 °C, the central film thickness is found from equation (12) to be $h_c = 0.90 \times 10^{-6}$ m.

If the minimum λ ratio (h_c/σ) is set to 2 in order to avoid surface distress, the composite surface roughness should be no greater than 0.45×10^{-6} m. In other words, the surface roughness of each roller should be less than approximately 0.32×10^{-6} m.

From equation (50), taking $l = 2a = 1.8 \times 10^{-3}$ m, the rolling traction power loss is

$$P_r = 9 \times 10^7 (0.9 \times 10^{-6})(1.8 \times 10^{-3})(8.4) = 1.22 \text{ W}$$

The hysteresis loss, from equation (51), is

$$P_h = F_h U = \frac{3}{16} \varphi \frac{w}{R_x} QU$$

$$= \frac{3}{16}(0.01)\frac{5.5 \times 10^{-4}}{0.020}(1900)(8.4) = 0.82 \text{ W}$$

The total rolling loss is thus 1.22 + 0.82, or 2.04 W.

Although this rolling loss is quite small, the ratio of power loss to power input at $\theta = 0°$ was found to be only 0.0013. Thus for a normal contact load of $Q = 1900$ N, the transmitted power is

$$\mu_x QU = (0.07)(1900)(8.4) = 1117 \text{ W}$$

and the traction contact loss is (0.0013)(1117) = 1.45 W. The rolling traction loss and the traction contact loss are thus generally comparable at zero spin. At higher spin values or in the presence of misalignment the traction contact loss becomes dominant. (Support bearing losses must also be considered for an accurate assessment of drive losses.)

9.0 Loading Mechanism Design

It is essential that sufficient normal load be imposed between the roller components in a traction drive to prevent slip. The simplest, but not necessarily the most effective, means is to impose between the rolling elements a constant clamping force large enough to prevent slip under the most adverse operating conditions. Because shock and transient overtorque loads can occur in most drive lines, this constant clamping load must be larger than that normally needed under full torque. No information is currently available to determine exactly how much of a contact overload is required for shock loads. It obviously depends on the duration and the intensity of the shock load, the sensitivity of the given traction drive contacts to momentary slip, and the dynamics of the drive line. If the momentary slip is

sufficiently brief to avoid a sudden thermal collapse of the protective EHD film, no surface damage should occur. Loaded gear teeth regularly encounter momentary slide-to-roll ratios $\Delta U/U$ of 100 percent or more at points of entry and exit during the meshing cycle without ill effects. On the other hand, some traction contacts have been observed to scuff under very brief exposure to high slip. Until more definitive data become available, it is prudent to select the clamping load to be high enough to accommodate any of the expected shock loads.

9.1 Constant Loading

The obvious disadvantage of a constant clamping load is that the drive contacts are needlessly overloaded during periods of low power transmission. Contact overloading not only generates extra power losses, contributing to lower part-load efficiency, but more importantly shortens drive system fatigue life. However, if the driven equipment operates essentially at a near-maximum constant torque level with only minor expected shock loads, a constant clamping load might be the best choice because of its simplicity. Preloading with a constant load spring is preferable to a hard clamped load to assure uniformity of loading under possible structural deflections.

9.2 Variable Loading

Often the duty cycle fluctuations are sufficiently large to negate the use of a constant loading mechanism. Mechanisms can be constructed to vary the normal contact load as a function of the transmitted load, a function of the speed ratio, or some combination of both. Because the response time of the loading mechanism should be as short as possible, it is desirable to keep the mass of the moving parts low (inertial effects) and the travel distance short to minimize or eliminate the possibility of sticking.

Figure 39 shows typical examples of variable loading mechanisms. A spring is one of the simplest means of providing variable loading action for variable-ratio drives. Its main disadvantage is that the spring force developed is a function of displacement rather than force, so the contact may be overloaded under low-torque conditions at certain ratios. This is illustrated in figure 39(a), where the spring loader is installed on a variable-ratio planetary drive. This drive downshifts as the outside rings, grounded to the case, move closer together, causing the radially free planets to move inward and thus spreading the input shaft rollers further apart. The compression of the springs increases the spring reaction forces and, in turn, the contact normal forces. Thus the contact normal force increases with drive reduction ratio. This is desirable since the torque multiplication also increases with drive reduction ratio and there is usually a need for higher normal loads to

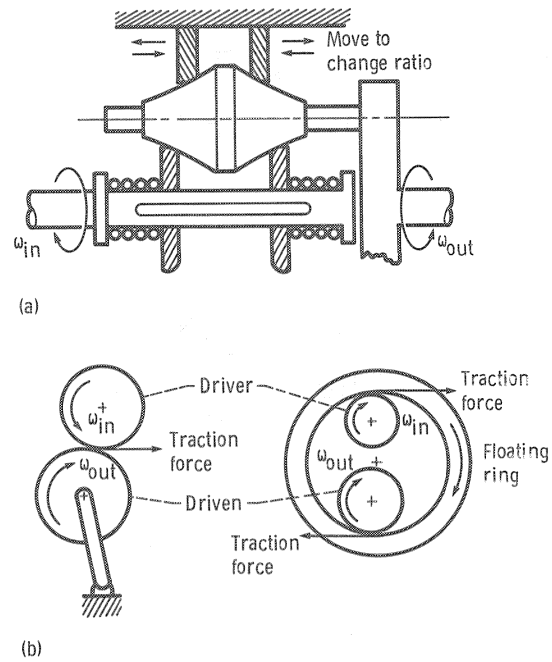

(a) Ratio-dependent, spring loading mechanism.
(b) External and internal traction force loading mechanisms.

Figure 39.—Loading mechanism arrangements.

accommodate the higher torque levels. However, if torque demand should drop at this spring position, there would be no way to lessen the contact normal load.

The traction force can be used in a direct way to provide torque-dependent contact normal loads. Figure 39(b) shows two simple examples of loading mechanisms that operate on this principle. The "wedging action" produced by the traction force depends on both the offset between the drive elements and the elastic deflections of the roller and the structural elements in the system. Although the proper geometry to achieve the desired loading can be complicated to predict analytically, this means of loading is generally reliable and responds quickly.

Perhaps the most common means to achieve variable loading action is with a cam mechanism, as illustrated in figure 40. Usually a torque-induced traction force is used to roll ball or roller elements along a ramp cut into the faces of opposing drive elements. Because of the ramp angle β' the tangential force exerted on the ball or roller induces the generation of an axial force F_a. This axial force provides the clamping load between drive elements. The advantages of this approach are that the ramp angle can be easily tailored to suit the expected traction characteristics of the system and that the mechanism has low friction and is quick acting. Furthermore a simple relation can be established between the ramp angle β' and the applied traction coefficient μ_x that is independent of structural deflections. At the ball-ramp contact the

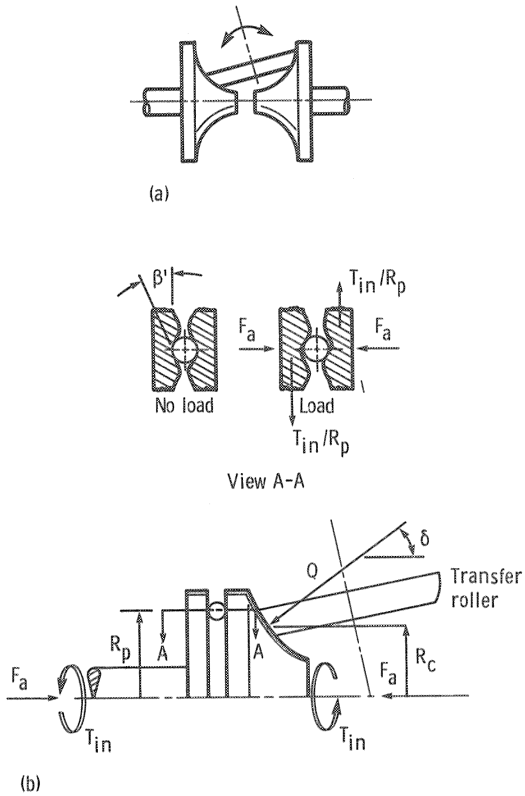

(a) Simplified view of Arter type of toroidal drive.
(b) Input contact showing preload mechanism.

Figure 40.—Preload mechanism using rolling cams.

relation between the torque input T_{in} and the induced axial force F_a is given by

$$T_{in} = (F_a \tan \beta')R_p \tag{54}$$

where R_p is the pitch radius of the ball-cam contact. At the traction roller contact the relation between T_{in} and the applied traction coefficient is

$$T_{in} = \mu_x Q R_c$$

where

Q normal contact load, N

R_c cone rolling radius, m

since $Q = F_a/\cos \delta$, it follows that

$$T_{in} = \mu_x \frac{F_a}{\cos \delta} R_c \tag{55}$$

By equating equations (54) and (55), μ_x can be found from

$$\mu_x = (\tan \beta')(\cos \delta)\frac{R_p}{R_c} \tag{56}$$

Since the normal load angle δ and the rolling radius R_c change with the tilt of the transfer roller, the applied traction coefficient μ_x varies with the speed ratio of the drive. The illustration shown in figure 40(b) shows only the input contact of an Arter type of toroidal drive. The output contact (fig. 40(a)) is loaded by the same axial force as the input contact, but because the transfer roller may be contacting the output toroid at a different angle, the applied traction coefficient may be different. Therefore the ramp angle must be chosen so that the applied traction coefficient at either the input or output contact is less than the maximum available traction coefficient under the least favorable operating conditions. At all other conditions the contact will be overloaded by some amount; that is, the actual normal force applied will be larger than the normal force required to transmit the torque safely. Normally a single ramp mechanism is used on either the input or output side of the drive. However, for some traction drives a loading mechanism on both input and output contacts may be used to minimize contact overloading. A variable ramp angle or curved cam may also be used to better match the increase in the lubricant's traction coefficient with an increase in contact pressure.

10.0 Friction Wheels and Rings

W. Wernitz in reference 90 presented information for the design of nonlubricated friction contacts such as a rubber or high-strength plastic wheel against a metal drum or ring (fig. 41). The development of rubberlike materials with good thermal, wear, and kneading (hysteresis) characteristics has contributed greatly to the development of these friction drives. If properly designed, they offer a smooth, simple, inexpensive means of speed change with little or no maintenance. Although operating stress levels for dry friction drives must be substantially smaller than those for oil-lubricated steel ones, appreciable power can still be transmitted because of the high friction coefficient levels. A maximum power

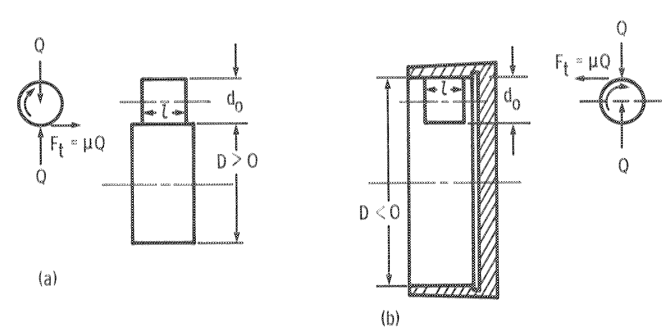

(a) External drive
(b) Internal drive.

Figure 41.—Friction wheels.

of approximately 75 kW can be transmitted by large (up to 75 cm diameter) friction drives. Peripheral velocities should be limited to 30 m/sec or less. An automotive pneumatic tire is one familiar example. Although the high friction coefficient levels of a friction contact help to reduce support bearing loads, rugged bearings are still required. The presentation herein is essentially that of Wernitz (ref. 90).

Referring to figure 41, the torque transmitted is

$$T_0 = \frac{F_t d_o}{2} = \frac{fQd_o}{2}$$

where the coefficient of friction

$$f \leq f_{\text{allow}} = \frac{f_{\max}}{S_r}$$

and where

S_r factor to ensure against slip

Q normal load

F_t tangential force

A useful empirical stress parameter K is defined as follows:

$$K = \frac{Q}{ld_m}$$

where

$$\frac{1}{d_m} = \frac{1}{d_o} \pm \frac{1}{D}$$

and l is contact width. The negative sign applies to concave curvature. Thus it follows that

$$T_0 = \frac{fKld_m d_o}{2} \tag{57}$$

For laminated wood, reinforced fabrics, and plastics running dry against cast iron at approximately 3.8 m/sec, f_{allow} equals 0.3 to 0.4 ($S_r = 1.5$) and K_{allow} equals 0.5 to 1.0 N/mm^2. For reinforced plastics running against cast iron the maximum K_{allow} is 1.0 N/mm^2 with $fK_{\text{allow}} = 0.3$ N/mm^2. For rubber running against cast iron the maximum K_{allow} is 0.35 N/mm^2 with $fK_{\text{allow}} = 0.15$ N/mm^2. Because the effects of peripheral velocity and generated heat have not been taken into account, the fK_{allow} product should be used as a general guide for soft materials. For constant contact pressure (without an automatic loading mechanism), only 75 percent of these values should be used and S_r should be somewhat greater than 1.5.

Dry metal pairs, not unlike a locomotive wheel against a rail, can also be used as friction drives. The allowable stress parameter K_{allow} (in N/mm^2) is 2 to 4 for cast iron/steel, 3.5 to 7.0 for AISI 1045/1065, and 2 to 4 for AISI 1075/1065. These values are all based on $f = 0.15$.

10.1 Rubber Friction Wheels Against Steel or Cast Iron

The proportions given here are for special types of rubber (80 to 90 Shore hardness) particularly resistant to abrasion, kneading, heat, and aging that are *vulcanized* on cast-iron hubs with $d_o = 4$ to 16 cm. Referring to figure 42 for geometric proportions, $d_i = 0.625\ d_o$. The diameter of vulcanization l_i equals $d_o/4$, which for a taper angle of 12° results in a friction face width of $l = 0.7(l_i) = d_o/5.7$. An experimentally determined expression for the allowable rolling pressure follows for $U = 1$ to 30 m/sec:

$$K_{o,\text{allow}} = \frac{Q_{\text{allow}}}{ld_o} = \frac{K^*}{\sqrt[3]{1 + d_o/D}} \left(\frac{1}{U}\right)^{3/4}$$

(newton and meter units)

$$= \frac{Q_{\text{allow}}}{ld_o} = \frac{K^*}{\sqrt[3]{1 + d_o/D}} \left(\frac{40}{U}\right)^{3/4} \tag{58}$$

(pound force and inch units)

where $K^* = 0.41$ to 0.55 N/mm^2; the correction for diameter D, d_o/D, applies only to convex (external) curvature; and the term $\sqrt[3]{1 + d_o/D}$ is set equal to unity for concave curvature (internal drive).

The preceding expression for $K_{o,\text{allow}}$ takes into account the effect of generated heat and also the increased hysteresis losses attributable to indentation. For $U \leq 1$ m/sec

$$K_{o,\text{allow}} = \frac{K^*}{\sqrt[3]{1 + d_o/D}} \tag{59}$$

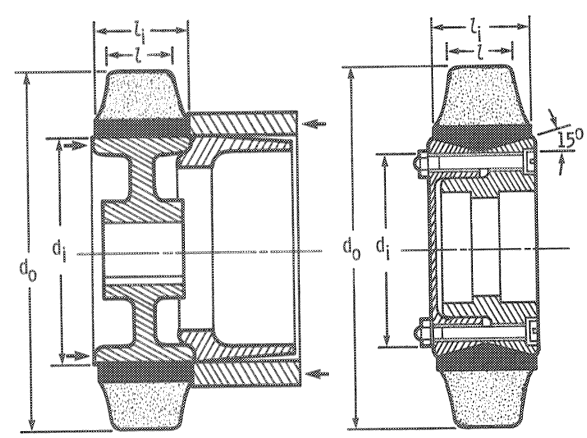

Figure 42.—Rubber friction rings (with steel-wire stiffeners).

For dry, continuous operation, f_{allow} is 0.7; for dry intermittent operation f_{allow} is 0.5; and for operation under humid conditions, f_{allow} is 0.1 to 0.3.

Slip should generally not exceed 2 to 3 percent under conditions of continuous operation. Brief slip of 4 percent or higher for higher friction coefficients has been experienced in smooth intermittent service without detrimental effects.

It is recommended that moderate rolling speeds, $U=2.5$ to 10 m/sec, be considered in order to reduce slip and improve performance and durability. For small rubber friction wheels ranging from 4 to 16 cm in diameter, the practical maximum power that can be transmitted under dry, continuous operation ranges from 0.1 to 2 kW. Several friction wheels may be arranged in parallel to transmit proportionately greater power.

The temperature rise at the friction surface of wheels made of soft materials should not exceed 28 °C. The heat generated is attributable primarily to hysteresis losses. In the absence of tangential loading the maximum temperature occurs at the center of the rubber. The hysteresis loss is primarily a function of velocity, indentation depth, and material properties. The temperature is further influenced by frictional work, which manifests itself primarily as a surface temperature rise.

10.2 Rubber Friction Rings Against Steel or Cast Iron

Friction rings made of special rubber reinforced with steel wire stiffeners operating against steel or cast iron are similar to those previously described except that they are *pressed* onto a cylindrical metal hub (fig. 42(a)) or *screw fastened* onto a tapered section with an angle of 15° (fig. 42(b)). The important dimensions of such rings are $d_o=18$ to 76 cm; $d_i=0.5\ d_o$ to $0.85\ d_o$; $l_i=0.10\ d_o$ to $0.33\ d_o$; $2l_i/(d_o-d_i)=1.3$ to 1.875; and $l=l_i-(d_o-d_i)\times\sin 15°$. The allowable rolling pressure probably cannot be precisely described because of the variable ratios of friction surface width to rubber thickness. There is a somewhat greater velocity dependence than for vulcanized rubber.

For low surface velocities, $U\leq 0.2$ m/sec, the following relation may be used for constant contact pressures:

$$K_o=\frac{Q}{l_i d_o}=\frac{1}{\sqrt[3]{1+d_o/D}}(K-m_f d_o) \tag{60}$$

where $D>0$ for convex contact. For concave curvature ($D<0$), set $\sqrt[3]{1+d_o/D}$ equal to unity. The limits of K and m_f are, respectively, 0.41 to 0.55 N/mm² and 0.02 to 0.03 N/mm. Representative values are $K_o=0.48$ N/mm² and $m_f=0.03$ N/mm.

Maximum horsepower transmission is obtained at higher surface velocities. A constant power transmission can be expected between approximately 3 and 15 m/sec. Moderate peripheral velocities of 3 to 10 m/sec are recommended for low slip. The maximum allowable peripheral velocities may be assumed to be 15 m/sec for small friction rings and 30 m/sec for large rings ($d_o>35$ cm). For this type of friction ring the maximum transmitted horsepower can be estimated from the following relation, which applies for $3\leq U\leq 15$ m/sec:

$$\text{Power}=fl_i\epsilon\log\left(\frac{d_o}{d_c}\right) \tag{61}$$

where representative values of ϵ and d_c are 3.1 kW/cm and 11.7 cm, respectively, for 18 cm $\leq d_o\leq$ 76 cm. The same values of maximum allowable coefficient of friction, slip, and temperature rise are valid as for the vulcanized friction wheels discussed previously.

10.3 Arrangements

In machines operating continuously at constant load the rolling drive may be safely pressed against the driven wheel with a calculated contact force. During a rest period an indentation occurs that causes rough running at startup. This usually disappears after several revolutions. Most machines operate, however, under conditions of variable and shock loading. It is desirable under such operating conditions to control contact pressure in order to increase life and efficiency and to prevent detrimental overloads.

Figure 43 shows several designs that maintain a well-controlled contact pressure by means of spring-loaded pivoted drives. A control angle α' of 35° to 38° is used in external drives; 38° to 40° in internal drives. For the arrangement shown in figure 43(a) under no rotation,

$$Q_0=\frac{S_0 b'-G'W}{e} \tag{62}$$

where Q_0 is the preload of the contact due to spring load. For dry running ($f_{allow}=0.7$), $Q_0\approx 0.1\ Q_{allow}$. For frequent starting and shock loading ($f_{allow}=0.5$), $Q_0\approx 0.33\ Q_{allow}$. For humid operating conditions ($f_{allow}=0.3$), $Q_0\approx 0.6\ Q_{allow}$. When the tangential force $F_t=fQ$ is applied during rotation, the coefficient of friction may be expressed as

$$f=\frac{1-Q_0}{Q}\tan\alpha' \qquad \text{where } f\leq\tan\alpha'$$

To avoid excessive contact forces caused by temporary line-of-contact overloads, $f=0.7$ may generally be used and values of α' selected accordingly.

The spring load S_0 for no rotation from equation (62) is

$$S_0=\frac{G'W+Q_0 e}{b'}$$

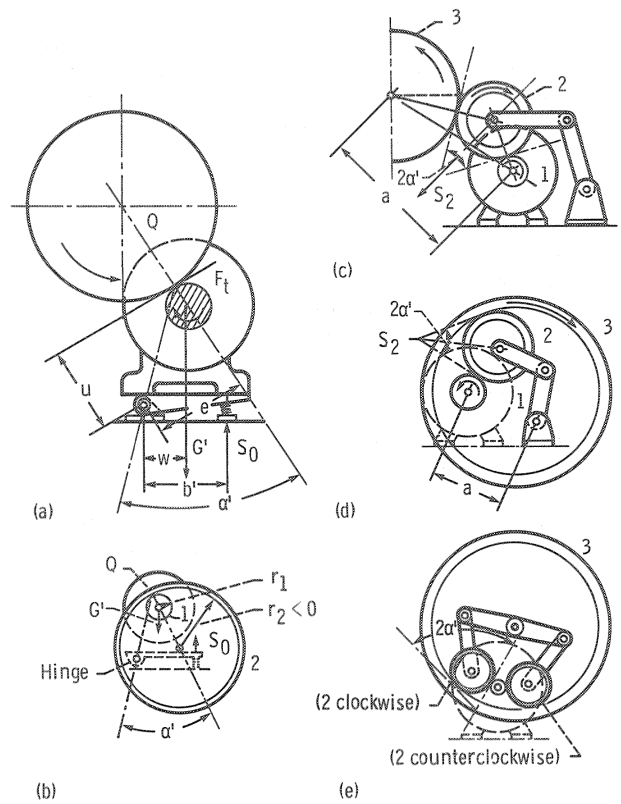

(a) Device for automatically controlling contact force (external drive).
(b) Device for automatically controlling contact force (internal drive).
(c) External drive.
(d) Internal drive.
(e) Reversible internal drive.

Figure 43.—Friction drives.

The recommended spring rate is

$$K_s = \frac{S_0}{\Delta} = \frac{25F_{t,max}}{d_o} = \frac{25fQ_{\text{allow}}}{d_o}$$

from which the spring deflection Δ can be found as

$$\Delta = \left(\frac{G'W + Q_0 e}{Q_{\text{allow}} b}\right)\left(\frac{d_o}{25f}\right) \tag{63}$$

Either the small or large wheel may be rubber clad. Experience has shown, however, that it is best to use the small wheel as the rubber wheel for ratios up to 8 and the large wheel for ratios up to approximately 18. The mating wheel should be constructed of steel or cast iron. Figure 43(b) is an internal drive arrangement similar in concept to figure 43(a). Friction wheels may also be used as idlers for spanning large center distances, as shown in figures 43(c) to (e). By properly selecting the control angle α' the wedging action of the traction force will cause self-preloading.

Lewis Research Center
National Aeronautics and Space Administration
Cleveland, Ohio, July 23, 1985

References

1. Loewenthal, S.H.; Rohn, D.A.; and Anderson, N.E.: Advances in Traction Drive Technology. SAE Paper 831304, 1983.
2. Knight, Edward H.: Knight's American Mechanical Dictionary. Vol. I. Hurd and Houghton, 1876, p. 680.
3. Trobridge: Census Office Report on Power and Machinery Used by Manufacturer–Washington, 1888, p. 220.
4. Appleton's Cyclopedia of Applied Mechanics. Vol. II. D. Appleton and Co., 1880, pp. 36–37.
5. Yeaple, F.: Metal-to-Metal Traction Drives Now Have a New Lease on Life. Prod. Eng. (NY), vol. 42, no. 15, Oct. 1971, pp. 33–37.
6. Carson, R.W.: New and Better Traction Drives Are Here. Mach. Des., vol. 46, no. 10, Apr. 18, 1974, pp. 148–155.
7. McCormick, D.: Traction Drives Move to Higher Powers. Des. Eng., Dec. 1980, pp. 35–39.
8. Hewko, L.O.: Traction Drives and Their Potential Role in Energy Conservation. Presented at the Joint ASLE Energy-Sources Technology Conference, New Orleans, LA, Feb. 1980.
9. Carson, R.W.: 100 Years in Review: Industrial Traction Drives. Power Transmission Design, vol. 19, no. 10, Oct. 1977, pp. 99–100.
10. Fellows, T.G.; et al.: Perbury Continuously Variable Ratio Transmission. Advances in Automobile Engineering, Pt. II, Pergamon Press (Oxford), 1964, pp. 123–142.
11. Clymer, F., Historical Motor Scrapbook. Vols. 1 and 2. Clymer Motor Publications, 1944.
12. Sloan, Alfred P.: My Years with General Motors. Doubleday and Co., Inc., New York, 1963.
13. Caris, D.F.; and Richardson, R.A.: Engine-Transmission Relationship for Higher Efficiency. SAE Trans., vol. 61, 1953, pp. 81–96.
14. Improved Technology Is Giving an Old Principle a New Drive. Monsanto Magazine, Summer 1974, pp. 14–16.
15. Carson, R.W.: Focus on Traction Drives: 100 Years of Traction Drives. Power Transmission Design, vol. 17, no. 5, May 1975, pp. 84, 88.
16. Perry, F.G.: The Perbury Transmission. ASME Paper 80-GT-22, Mar. 1980.
17. Carson, R.W.: Focus on Traction Drives. Power Transmission Design, vol. 17, no. 3, Mar. 1975, pp. 48–49.
18. Carson, R.W.: Today's Traction Drives. Power Transmission Design, vol. 17, no. 11, Nov. 1975, pp. 41–49.
19. Dvorak, D.Z.: Your Guide to Variable-Speed Mechanical Drives. Prod. Eng. (NY), vol. 34, Dec. 1963, pp. 63–74.

20. Heilich, F.W.; and Shube, E.E.: Traction Drives. Marcel Dekker, Inc., New York, 1983.
21. Hewko, L.O.: Roller Traction Drive Unit for Extremely Quiet Power Transmission, J. Hydronautics, vol. 2, no. 3, July 1968, pp. 160–167.
22. Nakamura, L.; et al.: A Development of the Traction Roller System for a Gas Turbine Driven APU. SAE Paper 790106, Feb. 1979.
23. Nasvytis, A.L.: Multiroller Planetary Friction Drives. SAE Paper 660763, 1966.
24. Loewenthal, S.H.; Anderson, N.E.; and Rohn, D.A.: Evaluation of a High Performance Fixed-Ratio Traction Drive. J. Mech. Des., vol. 103, no. 2, Apr. 1981, pp. 410–422.
25. Meyer, S.; and Connelly, R.E.: Traction Drive for Cryogenic Boost Pump. NASA TM-81704, 1981.
26. Rohn, D.A.; and Loewenthal, S.H.: An Analysis of Traction Drive Torsional Stiffness. ASME Paper 84-DET-100, 1984.
27. Bryan, J.B.: Design and Construction of an Ultraprecision 84 Inch Diamond Turning Machine. Precision Engineering, vol. 1, no. 1, 1979, pp. 13–17.
28. Steinetz, B.M.; et al: An Advanced Pitch Change Mechanism Incorporating a Hybrid Traction Drive. AIAA Paper AIAA-84-1383, June 1984.
29. Grubin, A.N.: Fundamentals of the Hydrodynamic Theory of Lubrication of Heavily Loaded Cylindrical Surfaces. Investigation of the Contact of Machine Components, Kh.F. Ketova, Ed., Translation of Russian Book No. 30, Central Scientific Institute for Technology and Mechanical Engineering, Moscow, 1949, Chapter 2. (Available from Department of Scientific and Industrial Research, Great Britain, Transl. CTS-235 and Special Libraries Association, Transl. R-3554.)
30. Hamrock, B.J.; and Dowson, D.: Isothermal Elastohydrodynamic Lubrication of Point Contacts, Part III-Fully Flooded Results. J. Lubr. Technol., vol. 99, no. 2, Apr. 1977, pp. 264–276.
31. Brewe, D.; and Hamrock, B.J.: Simplified Solution for Stresses and Deformations. J. Lubr. Technol., vol. 105, no. 2, Apr. 1983, pp. 171–177.
32. Zaretsky, E.V.; and Anderson, W.J.: EHD Lubrication. Mach. Des. vol. 40, no. 26, Nov. 1968, pp. 167–173.
33. Coy, J.J.; Loewenthal, S.H.; and Zaretsky, E.V.: Fatigue Life Analysis for Traction Drives with Application to a Toroidal Type Geometry. NASA TN D-8362, 1976.
34. Coy, J.J.; Rohn, D.A.; and Loewenthal, S.H.: Life Analysis of Multiroller Planetary Traction Drive. NASA TP-1710, 1981.
35. Coy, J.J.; Rohn, D.A.; and Loewenthal, S.H.: Constrained Fatigue Life Optimization of a Nasvytis Multiroller Traction Drive. J. Mech. Des., vol. 103, no. 2, Apr. 1981, pp. 423–429.
36. Rohn, D.A.; Loewenthal, S.H.; and Coy, J.J.: Simplified Fatigue Life Analysis for Traction Drive Contacts. J. Mech. Des., vol. 103, no. 2, Apr. 1981, pp. 430–439.
37. Rohn, D.A.; Loewenthal, S.H.; and Coy, J.J.: Sizing Criteria for Traction Drives. Advanced Power Transmission Technology, NASA CP-2210, G.K. Fischer, ed., 1983, pp. 299–316.
38. Hertz, H.: Miscellaneous Papers, Part V-The Contact of Elastic Solids. The MacMillan Company (London), 1896, pp. 146–162.
39. Harris, T.A.: Rolling Bearing Analysis. Second ed., Wiley, New York, 1984.
40. Lundberg, G; and Palmgren, A.: Dynamic Capacity of Rolling Bearings. Acta Polytech. Mech. Eng. Ser., vol. 1, no. 3, 1947.
41. Lundberg, G.; and Palmgren, A.: Dynamic Capacity of Roller Bearings. Acta Polytech. Mech. Eng. Ser., vol. 2, no. 4, 1952.
42. Coy, J.J.; Townsend, D.P.; and Zaretsky, E.V.: Dynamic Capacity and Surface Fatigue Life for Spur and Helical Gears. J. Lubr. Technol., vol. 98, no. 2, Apr. 1976, pp. 267–276.
43. Townsend, D.P.; Coy, J.J.; and Zaretsky, E.V.: Experimental and Analytical Load-Life Relation for AISI 9310 Steel Spur Gears. J. Mech. Des., vol. 100, no. 1, Jan. 1978, pp. 54–60.
44. Bamberger, E.N.; et al.: Life Adjustment Factors for Ball and Roller Bearings. American Society of Mechanical Engineers, New York, 1971.
45. MacPherson, P.B.: The Pitting Performance of Hardened Steels. ASME Paper 77-DET-39, 1977.
46. Soda, N.; and Yamamoto, T.: Effect of Tangential Traction and Roughness on Crack Initiation/Propagation During Rolling Contact. ASLE Trans., vol. 25, no. 2, Apr. 1982, pp. 198–206.
47. Hewko, L.O.; Rounds, F.G., Jr.; and Scott, R.L.: "Tractive Capacity and Efficiency of Rolling Contacts," Rolling Contact Phenomena, J.B. Bidwell, ed., Elsevier, Amsterdam, 1962, pp. 157–185.
48. Johnson, K.L.; and Tevaarwerk, J.L.: Shear Behavior of Elastohydrodynamic Oil Films. Proc. R. Soc. London A, vol. 356, no. 1685, Aug. 24, 1977, pp. 215–236.
49. Loewenthal, S.H; and Rohn, D.A.: Elastic Model of the Traction Behavior of Two Traction Lubricants. ASLE Trans., vol. 27, no. 2, Apr. 1984, pp. 129–137.
50. Dyson, A.: Scuffing-A Review-Pt. 1, Tribol. Int., vol. 8, no. 2, Apr. 1975, pp. 77–87 and Part II, The Mechanism of Scuffing. vol. 8, no. 3, June 1975, pp. 117–122.
51. Blok, H.: Seizure-Delay Method for Determining Seizure Protection of EP Lubricants. J. Soc. Automot. Eng., vol. 44, no. 5, May 1939, pp. 193–210, 220.
52. Ku, P.M.; Staph, H.E.; and Carper, H.J.: Gear Tooth Scoring Investigation. USAMRDL-TR-75-33, Southwest Research Institute, July 1975.
53. Gaggermeier, Helmut: Investigations of Tractive Force Transmission in Variable Traction Drives in the Area of Elastohydrodynamic Lubrication. Ph. D. Dissertation. Technical University of Munich, July 1977.
54. Carter, F.W.: On the Action of a Locomotive Driving Wheel. Proc. R. Soc. London A, vol. 112, 1926, pp. 151–157.
55. Johnson, K.L.: Tangential Tractions and Microslip in Rolling Contact. Rolling Contact Phenomena, J.B. Bidwell, ed., Elsevier Publishing Co., 1962, pp. 6–28.
56. Tevaarwerk, J.L.: Traction Drive Performance Prediction for the Johnson and Tevaarwerk Traction Model. NASA TP-1530, 1979.
57. Johnson, K.L.; Nayak, L.; and Moore, A.J.: Determination of Elastic Shear Modulus of Lubricants from Disk Machine Tests. Elastohydrodynamics and Related Topics: Proc. 5th Leeds-Lyon Symposium on Tribology, D. Dowson, et al., eds., Mech. Eng. Publ. Ltd., 1979, pp. 204–213.
58. Clark, O.H.; Woods, W.W.; and White, J.R.: Lubrication at Extreme Pressures with Mineral Oil Films. J. Appl. Phys., vol. 22, no. 4, Apr. 1951, pp. 474–483.
59. Smith, F.W.: The Effect of Temperature in Concentrated Contact Lubrication, ASLE Trans., vol. 5, no. 1, Apr. 1962, pp. 142–148.
60. Plint, M.A.: Traction in Elastohydrodynamic Contacts. Proc. Inst. Mech. Eng. (London), vol. 182, pt. 1, no. 14, 1967, pp. 300–306.
61. Loewenthal, S.H.: Spin Analysis of Concentrated Traction Contacts. ASME Paper 84-DET-99, 1984.
62. Poritsky, H.; Hewlett, C.W., Jr.; and Coleman, R.E., Jr.: Sliding Friction of Ball Bearings of the Pivot Type. J. Appl. Mech., vol. 14, no. 4, Dec. 1947, pp. A-261 to A-268.
63. Lutz, O.: Grundsatzliches uber stufenlos verstellbare Walzgetriebw. Z. Konstruktion, vol. 7, 1955, p. 330; vol. 9, 1957, p. 169; vol. 10, 1958, p. 425.
64. Wernitz, W.: Walz-Bohrreibung-Bestimmung der Bohrmomente und Umfangskrafte bei Hertzscher Pressung mit Punktberuhrung.

Vol. 19 of Schriftenreihe Antriebstechnik, Fr. Vieweg und Sohn, Braunschweig, 1958.
65. Maas, H.: Untersuchung uber die in elliptischen Hertzscher Flachen ubertragbaren Umfangskrafte, Dissertation, Technical University of Braunschweig, 1959.
66. Thomas, W.: Reibscheiben-Regelgetriebe (Linienberuhrung), Vol. 4 of the Schriftenreihe Antriebstechnik, Fr. Vieweg und Sohn, Braunschweig, 1954.
67. Wernitz, W.: Friction at Hertzian Contact with Combined Roll and Twist. Rolling Contact Phenomena, J. B. Bidwell, ed., Elsevier Publishing Co., 1962, pp. 132-156.
68. Magi, M.: On Efficiencies of Mechanical Coplanar Shaft Power Transmissions. Chalmers University of Technology, Gothenburg, Sweden, 1974.
69. Cheng, H.S.; and Sternlicht, B.: A Numerical Solution for the Pressure, Temperature, and Film Thickness Between Two Infinitely Long, Lubricated Rolling and Sliding Cylinders, Under Heavy Loads., J. Basic Eng., vol. 87, no. 3, Sept. 1965, pp. 695-707.
70. Dyson, A.: Frictional Traction and Lubricant Rheology in Elastohydrodynamic Lubrication, Philos. Trans. R. Soc. London A, vol. 266, no. 1170, Feb. 1970, pp. 1-33.
71. Trachman, E.G.; and Cheng, H.S.: Thermal and Non-Newtonian Effects on Traction in Elastohydrodynamic Contacts. Elastohydrodynamic Lubrication: 1972 Symposium, Inst. of Mech. Eng. (London), 1972, pp. 142-148.
72. Poon, S.Y.: Some Calculations to Assess the Effect of Spin on the Tractive Capacity of Rolling Contact Drives. Proc. Inst. Mech. Eng., vol. 185, no. 76/71, 1970-71, pp. 1015-1022.
73. Lingard, S.: Traction at the Spinning Point Contacts of a Variable Ratio Friction Drive. Tribol. Int., vol. 7, no. 5, Oct. 1974, pp. 228-234.
74. Tevaarwerk, J.L.; and Johnson, K.L.: The Influence of Fluid Rheology on Performance of Traction Drives. J. Lubr. Technol., vol. 101, no. 3, July 1979, pp. 266-274.
75. Johnson, K.L.; and Greenwood, J.A.: Thermal Analysis of an Eyring Fluid in Elastohydrodynamic Traction. Wear, vol. 60, no. 2, June 16, 1981, pp. 353-374.
76. Tevaarwerk, J.L.: A Simple Thermal Correction for Large Spin Traction Curves. J. Mech. Des., vol. 103, no.2, Apr. 1981, pp. 440-446.
77. Styri, H.: Friction Torque in Ball and Roller Bearings. Mech. Eng., vol. 62, no. 12, Dec. 1940. pp. 886-890.
78. Trippett, R.J.: A High-Speed Rolling-Element Bearing Loss Investigation. J. Eng. Power, vol. 100, no. 1, Jan. 1978, pp. 40-47.
79. Raimondi, A.A.; and Boyd, J.: A Solution for the Finite Journal Bearing and Its Application to Analysis and Design, pts. I, II, III. ASLE Trans., vol. 1, no. 1, Apr. 1958, pp. 159-209.
80. Crook, A.W.: The Lubrication of Rollers. IV-Measurements of Friction and Effective Viscosity, Philos. Trans. R. Soc. London A, vol. 255, no. 1056, Jan. 17, 1963, pp. 281-312.
81. Greenwood, J.A.; and Tabor, D.: The Friction of Hard Sliders on Lubricated Rubber: The Importance of Deformation Losses. Proc. Phys. Soc. London, vol. 71, pt. 6, June 1958, pp. 989-1001.
82. Lane, T.B.: The Lubrication of Friction Drives. Lubr. Eng., vol. 13, no. 2, Feb. 1957, pp. 85-88.
83. Haseltine, M.W.; et al.: Design and Development of Fluids for Traction and Friction Type Transmissions. SAE Paper 710837, 1971.
84. Hamman, W.C.; et al.: Synthetic Fluids for High Capacity Traction Drives. ASLE Trans., vol. 13, no. 2, Apr. 1970, pp. 105-116.
85. Loewenthal, S.H.; and Parker, R.J.: Rolling-Element Fatigue Life with Two Synthetic Cycloaliphatic Traction Fluids. NASA TN D-8124, 1976.
86. Loewenthal, S.H.; and Rohn, D.A.: Regression Analysis of Traction Characteristics of Two Traction Fluids. NASA TP-2154, 1983.
87. Walowit, J.A.; and Smith, R.L.: Traction Characteristics of a MIL-L-7808 Oil. ASME Paper 76-Lubs-19, May 1976.
88. Hewko, L.O.: Contact Traction and Creep of Lubricated Cylindrical Rolling Elements at Very High Surface Speeds. ASLE Trans., vol. 12, no. 2, Apr. 1969, pp. 151-161.
89. Jones, W.R., Jr.; et al.: Pressure-Viscosity Measurements for Several Lubricants to 5.5×10^8 Newtons Per Square Meter (8×10^4 psi) and 149°C (300°F). ASLE Trans., vol. 18, no. 4, Sept. 1975, pp. 249-262.
90. Wernitz, W.: Friction Drives. Mechanical Design and Systems Handbook, H. A. Rothbart, ed., McGraw-Hill Book Co., 1964, pp. 14-1 to 14-22.